

Molecular Characterization of the Mitochondrial Presequence Translocase

Dissertation
for the award of the degree
”Doctor rerum naturalium”
of the Georg-August-Universität Göttingen

within the doctoral program
Biomolecules: Structure - Function - Dynamics
of the Göttingen Graduate School for Neurosciences,
Biophysics, and Molecular Biosciences (GGNB)

submitted by

Niels Denkert

from Kiel, Germany

Göttingen, 2017

Members of the Thesis Committee:

Prof. Dr. Michael Meinecke (first reviewer)

Department of Cellular Biochemistry, University Medical Center Göttingen

Prof. Dr. Claudia Steinem (second reviewer)

Department of Organic and Biomolecular Chemistry, University of Göttingen

Prof. Dr. Ralph Kehlenbach

Department of Molecular Biology, University Medical Center Göttingen

Additional Reviewers:

Prof. Dr. Peter Rehling

Department of Cellular Biochemistry, University Medical Center Göttingen

Prof. Dr. Stefan Jakobs

Department of NanoBiophotonics, Max Planck Institute for Biophysical Chemistry Göttingen

Dr. Alexander Stein

Group of Membrane Protein Biochemistry, Max Planck Institute for Biophysical Chemistry Göttingen

Date of oral examination: 24.II.2017

Affidavit

I hereby declare that this thesis has been written independently and with no other sources and aids than quoted.

Furthermore, I confirm that this thesis has not yet been submitted as part of another examination process neither in identical nor in similar form.

Niels Denkert
Göttingen, 08. October 2017

- *to Wibke* -

- *to my parents* -

- *to Maja, Fritz and Karl* -

List of Publications

Parts of this thesis have been previously published in the following article:

Niels Denkert*, Alexander Benjamin Schendzielorz*, Mariam Barbot, Lennart Verseemann, Frank Richter, Peter Rehling and Michael Meinecke. 2017. Cation selectivity of the presequence translocase channel Tim23 is crucial for efficient protein import. *eLife* 6:e28324

*: these authors contributed equally

The following article is not part of this thesis:

Mariam Barbot, Daniel C. Jans, Christian Schulz, **Niels Denkert**, Benjamin Kroppen, Michael Hoppert, Stefan Jakobs and Michael Meinecke. 2015. Mic10 Oligomerizes to Bend Mitochondrial Inner Membranes at Cristae Junctions. *Cell Metabolism* 21, 756–763

Contents

Contents	xi
List of Figures	xv
List of Tables	xvii
Acronyms	xix
1 Introduction	1
1.1 Protein Import into Mitochondria	2
1.2 Mitochondrial Protein Translocases	6
1.2.1 Translocase of the Outer Membrane (TOM)	6
1.2.2 Sorting and Assembly Machinery (SAM)	9
1.2.3 Carrier Translocase (TIM22)	13
1.2.4 Presequence Translocase (TIM23)	16
1.2.5 Oxidase Assembly Machinery (OXA)	20
1.3 Molecular and Channel Properties of Tim23	23
2 Aims of this Thesis	27
3 Materials and Methods	29
3.1 Materials	29
3.2 Methods - Molecular Biology	33
3.2.1 Polymerase Chain Reaction	33
3.2.2 DNA Sequencing	33
3.2.3 DNA Concentration Determination	34
3.3 Methods - Cell Biology	34
3.3.1 <i>E. coli</i> Strains and Medium	34

3.3.2	Generation and Transformation of Chemically Competent <i>E. coli</i> Cells	35
3.3.3	Protein Expression and Inclusion Body Purification	36
3.3.4	Affinity Chromatography	37
3.3.5	Size-Exclusion Chromatography	38
3.4	Methods - Protein Biochemistry	39
3.4.1	Sodium dodecyl sulfate polyacrylamide gel electrophoresis (SDS-PAGE)	39
3.4.2	Protein Visualization on SDS-PAGE	40
3.4.3	TCA Precipitation	41
3.5	Methods - Liposome Techniques	41
3.5.1	Liposome Preparation	41
3.5.2	Protein Incorporation into Liposomes	42
3.5.3	Liposome Flotation Assay	42
3.5.4	Sodium Carbonate Extraction	43
3.6	Methods - Electrophysiology	44
3.6.1	General Principle of Electrophysiology	44
3.6.2	Reversal Potential and Ion Selectivity	45
3.6.3	Conductance	47
3.6.4	Assembly of the Chamber	48
3.6.5	Electrical Setup and Software	49
3.6.6	Fusion of Proteoliposomes	50
3.6.7	Data Reconstruction with <i>R</i>	50
3.6.8	Mean-Variance Analysis	52
4	Results	53
4.1	In-depth Characterization of the Tim23 Channel	53
4.1.1	Expression and Purification of Tim23	53
4.1.2	Electrophysiological Characterization of Tim23 Wild Type	56
4.2	Tim50 _{core} Regulates Tim23 and Hands Over Preproteins	66
4.2.1	Voltage-Regulation by Tim50 Subdomains	66
4.2.2	Presequence Handover to Tim23 by Tim50	67
4.3	Conserved TMS2 Residues Constitute Ion Filter	70
4.3.1	Design and Expression of Tim23 Mutants	70
4.3.2	Electrophysiological Screening of Tim23 mutants	72
4.3.3	Yeast Growth and Complex Integrity of Tim23 Mutants	78

4.3.4	Presequence Titration of Cox4 to Tim23 ^{NI50A} and Wild Type	83
5	Discussion	87
5.1	Tim23 Kinetics Change upon Presequence Interaction	88
5.2	Tim50 ^{core} Regulates Tim23 and Hands Over Preproteins	89
5.3	Tim23 ^{NI50A} is Impaired in Presequence and Preprotein Translocation	92
6	Summary and Conclusion	97
	Bibliography	99
	Appendix - R scripts	119
6.1	R: Reconstruction of .abf Using SMUCE	119
6.2	R: Reconstruction of .abf Using JULES	127
6.3	R: Mean-Variance Analysis from Dwelltime-List	133
	Acknowledgments	135
	Curriculum Vitae	

List of Figures

1.1	Cell overview with mitochondrion	2
1.2	Protein translocation into mitochondria	4
1.3	Protein translocation through TIM23	17
3.1	General principle of density gradient flotation	43
3.2	Circuit sketch of an ion channel in a biological membrane	45
3.3	Sketch of electrophysiological setup and vesicle fusion	50
4.1	Purification of Tim23 to homogeneity	55
4.2	Tim23 incorporation into liposomes	55
4.3	Voltage ramp of a Tim23 wild type	57
4.4	Triple-pore formed by recombinant Tim23	58
4.5	Voltage-dependent open probability of Tim23	60
4.6	Voltage ramp at asymmetric buffer conditions	61
4.7	Traces after Cox4 activation	62
4.8	Gating and dwell times before and after Cox4 activation	64
4.9	Dwell time histogram before and after Cox4 activation	65
4.10	Voltage regulation of Tim23 by Tim50 subdomains	67
4.11	Voltage ramps with preprotein after Tim50-induced closure	69
4.12	Current traces with preprotein after Tim50-induced closure	69
4.13	Sequence alignment of Tim23	71
4.14	TMS2 helical wheel projection	72
4.15	Open probability of Tim23 mutants	74
4.16	Voltage ramps at asymmetric buffer conditions of Tim23 mutants	75
4.17	Protein levels, complex and membrane integrity of mutant mitochondria	80
4.18	Import of various substrates into wild type and mutant mitochondria	82

4.19	General characterization of Tim23 ^{N150A}	84
4.20	Tim23 ^{N150A} and wild type reaction to Cox4 presequence	86

List of Tables

3.1	Lipids	29
3.2	Consumables	30
3.3	Plasmids	30
3.4	Primers	31
3.5	Centrifuges and rotors	31
3.6	Buffers	32
3.7	PCR-thermocycle setup	33
3.8	<i>Escherichia coli</i> strains	34
3.9	SDS-PAGE gel matrix and buffer composition	40
3.10	Reconstruction <i>stepR</i> -parameters	52
4.1	Conductance states and reversal potentials of Tim23 mutants	77
4.2	Growth of yeast expressing Tim23 mutants	79
4.3	Voltage-dependent open probability of stimulated Tim23 ^{N150A}	85

Acronyms

SI units and SI-derived units were used in this thesis without further declaration.

AAC	ADT/ATP carrier
ADP	adenosine diphosphate
ATP	adenosine triphosphate
BAM	bacterial β -barrel assembly machinery
CL	cardiolipin
Cox4	presequence of the cytochrome c oxidase subunit 4
DDM	n-Dodecyl β -D-maltoside
DMSO	dimethylsulfoxide
DTT	dithiothreitol
E. coli	Escherichia coli
EDTA	ethylenediaminetetraacetic acid
ER	endoplasmic reticulum
ERMES	ER-mitochondria encounter structure
IM	inner membrane
IMS	intermembrane space
IPTG	isopropyl β -D-1-thiogalactopyranoside
LB	lysogeny broth
LUV	large unilamellar vesicles
Mdm	mitochondrial distribution and morphology protein
MEGA-9	acyl-N-methylglucamine 9
MIA	mitochondrial intermembrane space assembly
MICOS	mitochondrial contact site and cristae organization system

Mim	mitochondrial import protein
NMR	nuclear magnetic resonance
OD	optical density
OM	outer membrane
Omp	outer membrane protein
PAM	presequence translocase-associated motor
PBD	presequence binding domain
PC	phosphatidylcholine
PE	phosphatidylethanolamine
PI	phosphatidylinositol
PiC	phosphate carrier
POTRA	polypeptide-transport associated domain
PS	phosphatidylserin
PTFE	polytetrafluoroethylene
rpm	rounds per minute
<i>S. cerevisiae</i>	<i>Saccharomyces cerevisiae</i>
SAM	sorting and assembly machinery
SDS-PAGE	sodium dodecyl sulfate polyacrylamide gel electrophoresis
TCA	trichloroacetic acid
TEMED	Tetramethylethylenediamine
TIM	translocase of the inner mitochondrial membrane
TOM	translocase of the outer membrane
VDAC	voltage-dependent anion channel
WT	wild type

Chapter 1

Introduction

All cells are surrounded by biological membranes to shield and confine the cellular interior. In eukaryotic cells, biological membranes even separate functional compartments or organelles: confined environments that provide specific chemical conditions or harbor macromolecules and protein machineries to fulfill highly specialized tasks within the cells, like DNA replication and transcription, adenosin triphosphate (ATP) generation, lipid or protein biogenesis or fatty acid oxidation.

Biological membranes take on a very important role for the cell and its organelles. They limit diffusion of proteins, ions, toxic byproducts or protons, enable specific and directed transport of these solutes, harbor localized protein machineries and enable transient or permanent electrochemical gradients. As most functions of organelles are fulfilled by the organellar proteome, protein translocation over these membranes is of special importance for cell viability. While most protein importing organelles are of relatively simple constitution and maintain only few protein translocation systems, mitochondria and chloroplasts differ due to their unique, multi-membrane compartmenting structure (see

figure 1.1). In yeast and mammals, protein import into mitochondria is arguably the most complex of all protein sorting mechanisms.

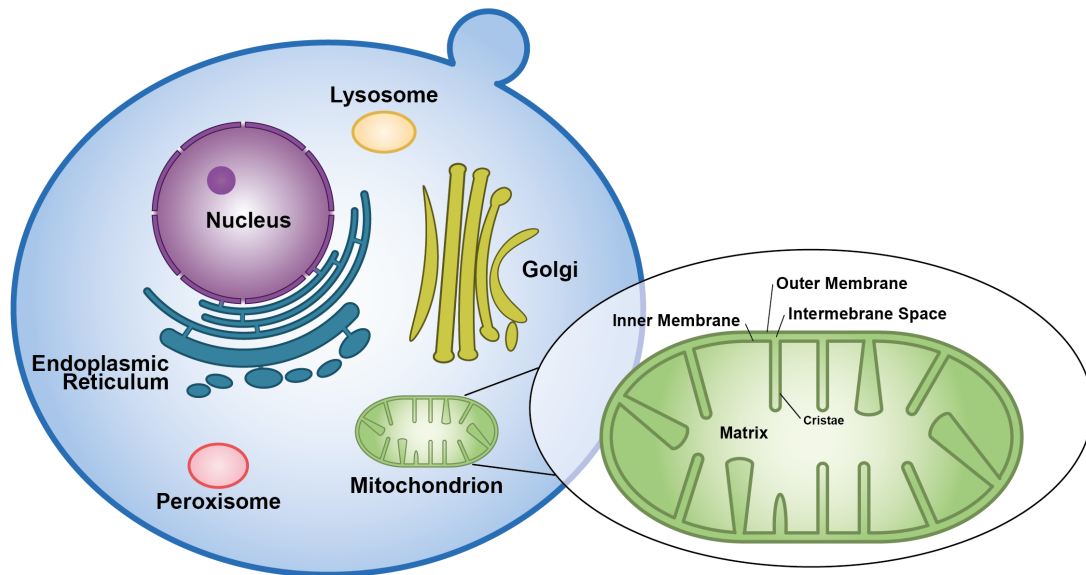


Figure 1.1: Sketch of a typical yeast cells with various organelles. Zoom into mitochondrion shows multi-membrane ultrastructure.

1.1 Protein Import into Mitochondria

Mitochondria are essential cellular organelles of all eukaryotic cells that play a pivotal role in many physiological processes. Their best known role is the involvement in oxidative phosphorylation, the most important ATP-generating metabolic pathway, making mitochondria vital for cell growth and viability¹. The organelle also harbors protein machineries involved in breaking down fatty acids via β -oxidation² and play a significant role in biosynthesis of lipids^{3;4}. The mitochondrial iron-sulfur cluster assembly machinery not only matures Fe/S proteins within the organelle, but also contributes to biogenesis of cytosolic and

nuclear Fe/S proteins, making mitochondria essential even when respiration is not required, e.g. yeast is grown on fermentable media. Another critical involvement of mitochondria is in not cell growth but cell death, by setting the stage for early steps of the intrinsic apoptotic pathway: the release of cytochrome *c*⁵ and SMAC⁶, triggering the caspase-9 cascade⁷.

Historically, the mitochondrion originates from endosymbiotic α -proteobacteria which left it with a double-membrane envelope and an own, albeit reduced, genome. After massive gene transfer to the nucleus^{8;9}, the mitochondrial genome nowadays only encodes for e.g. thirteen proteins in humans¹⁰ or eight proteins in the budding yeast *Saccharomyces cerevisiae* (*S. cerevisiae*)^{11;12}, accounting for about 1% of the total mitochondrial proteome in general¹³. These proteins mainly are components of respiratory chain complexes, e.g. subunits of the cytochrome *c* oxidase, of the ATP synthase and, in humans, of the nicotinamide adenine dinucleotide (NADH) dehydrogenase.

Similar to gram-negative bacteria or chloroplasts, which originate from endosymbiotic uptake of cyanobacteria, mitochondria possess two distinct membranes, dividing the organelle into four different subcompartments: The outer membrane (OM), the intermembrane space (IMS), the inner membrane (IM) and the matrix (see figure 1.1). Together, all four subcompartments are targets for import of over one thousand precursor proteins^{13;14}. In the last two decades, multiple pathways that work alone, in strictly consecutive or even in very complex cooperative manner have been revealed (see figure 1.2). At the hearts of these pathways protein-conducting channels have been discovered. Originally thought to be rare cases for translocation and insertion machineries, it is now accepted that such channels rather represent normality at least in mitochondria

and were also discovered in other eukaryotic organelles¹⁵⁻¹⁸ and in bacteria^{19;20} to constitute protein translocases. A vital property of mitochondria, required for

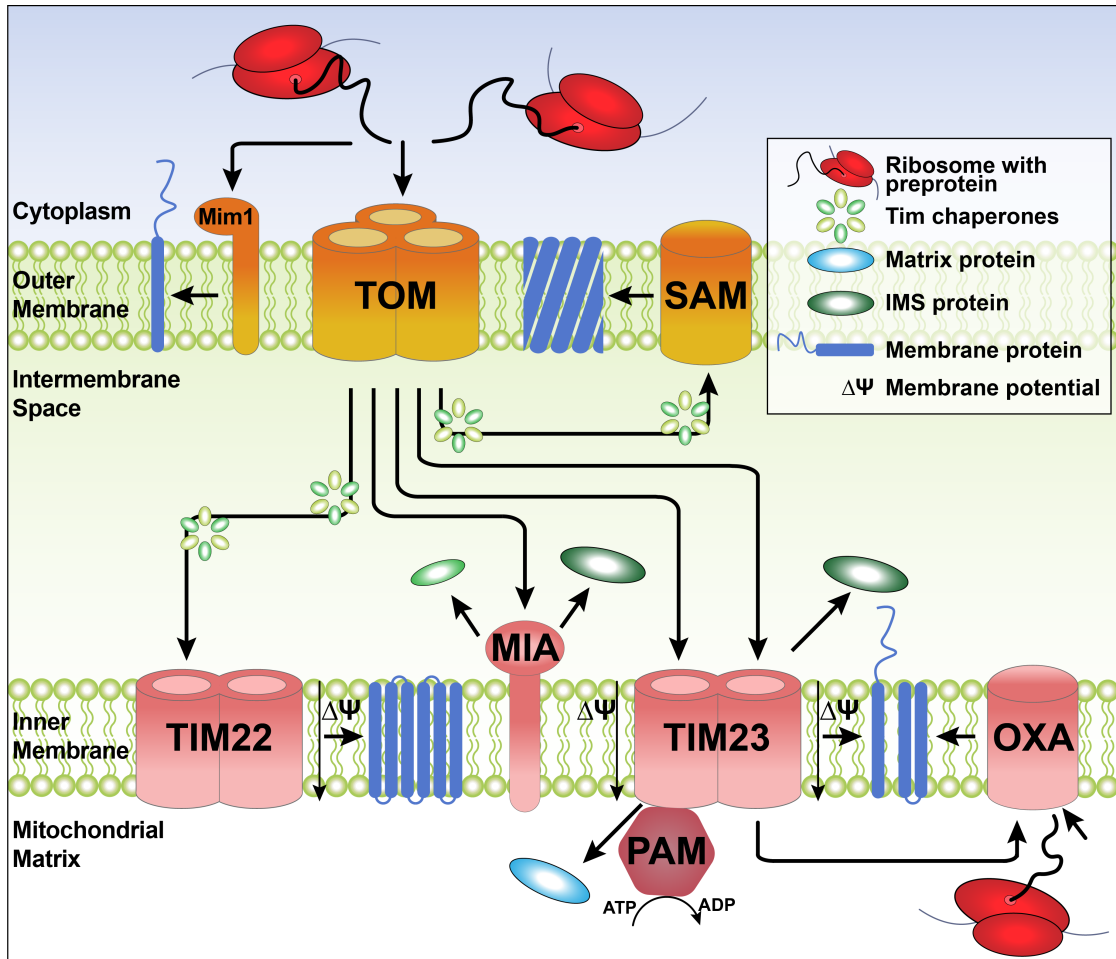


Figure 1.2: Protein import into mitochondria follows multiple pathways from the cytoplasm to the respective subcompartment.

multiple functions, is the transmembrane potential across the inner membrane, created by an electrochemical gradient due to proton pumping from matrix to intermembrane space by respiratory chain complexes¹. The electrochemical gradient is used by protein translocation systems and by the ATP generating system of the inner membrane.

The history of mitochondrial protein import research is a history of frequent revisions and of recurrent revolutions. Originally, mitochondrial protein import was believed to be performed by a single, streamlined pathway involving a translocase of the outer membrane (TOM)²¹⁻²³ and a translocase of the inner membrane (TIM)²⁴⁻²⁸, importing unfolded proteins with an N-terminal presequence. Following this idea of a solitary pathway, the two translocases had to be responsible for translocation into all four subcompartments of the mitochondrion: outer membrane and intermembrane space, inner membrane and matrix. While the presequence translocase of the inner membrane (TIM23) was indeed capable of both translocation into the matrix and lateral release into the inner membrane, the model of a solitary pathway had to be corrected shortly after. Studies regarding import of the inner membrane ADP/ATP carrier (AAC) family proteins revealed the essential involvement of Tim22²⁹, a protein organized in high molecular weight complexes. Not only did these Tim22-containing complexes show no association with TIM23, but import of AAC proteins was found to be fully independent of the presequence translocase. A new insertion pathway had been discovered: the carrier translocase of the inner membrane TIM22. For a long time afterwards, the trinity of protein translocases in mitochondria was mostly accepted and models were sought after how TOM itself could release membrane proteins into the outer membrane^{30,31}.

The triple-translocase model was challenged with the discovery of the sorting and assembly machinery (SAM)^{32,33} and the mitochondrial import protein Mim1^{34,35} in the outer membrane. The small 13 kDa protein Mim1 inserts α -helical transmembrane proteins like the TOM receptor Tom20^{36,37} into the OM independently of the TOM complex. It receives its substrates from the cytosol and can even accommodate multi-helical proteins^{38,39}. SAM on the other hand

is primarily inserting β -barrel proteins, like the TOM core component Tom40, and receives its substrates from the IMS side for which it cooperates with the TOM complex and soluble TIM-chaperones. These soluble chaperones and many other IMS-proteins contain characteristic -CX₃C- or -CX₉C- cysteine motifs and IMS sorting signals^{40;41}. In the IMS, they are recognized by the mitochondrial intermembrane space assembly (MIA), consisting of the disulfide relay system Mia40/Erv1. MIA catalyzes the formation of intramolecular disulfide bonds and facilitates oxidative folding⁴²⁻⁴⁴. Membrane proteins encoded in the mitochondrial genome highlight the necessity of another protein insertion or translocation pathway in the inner membrane. Comparably early, the machinery for insertion of mitochondrially encoded proteins was identified in the OXA complex^{45;46}. Interestingly, the OXA machinery has been revealed to be much more than just the insertase for mitochondrially encoded substrates, as it is also involved in insertion of TIM23 substrates⁴⁷ and even of TIM22 substrates⁴⁸.

1.2 Mitochondrial Protein Translocases

1.2.1 Translocase of the Outer Membrane (TOM)

The very first step for most mitochondrial import substrates after translation is the passage through the abundant mitochondrial entry gate, the TOM complex²². In *S. cerevisiae*, the 450 to 500 kDa TOM complex consists of seven proteins⁴⁹⁻⁵²: Tom40 is a 42 kDa β -barrel protein, forms the essential core of the complex²² and is present with two or three units per complex⁵³⁻⁵⁵. Tom20 and Tom70 are the loosely associated receptors for presequence and carrier precursor proteins, respectively; Tom22 is the tightly associated central receptor,

handling preproteins both at the cytosolic exterior and in the intermembrane space. Tom22 is critical for complex formation, as deletion dissociates the TOM complex, heavily impairing mitochondrial biogenesis^{32;56}. Tom5/6/7 are small proteins and mainly linked to assembly and maintaining stability of the complex.

Translated on cytosolic ribosomes, preproteins destined for mitochondrial import are recognized by membrane bound receptors. Precursors with a positively charged presequence, ultimately enabling import by TIM23, are initially recognized in their secondary structure⁵⁷ by the TOM receptor Tom20 and handed over to the general complex receptor Tom22⁵⁷. Carrier protein precursors with multiple internal targeting signals, on the other hand, are recognized by Tom70 before being handed over to Tom22. It has been reported that some carrier protein precursors are not translocated in a completely unfolded state but in a loop topology with the internal targeting signal leading ahead⁵⁸. After recognition by the central receptor, the respective preproteins are threaded through the pores formed by Tom40 and, after emerging from the channel, are again taken over by Tom22 on the IMS side. From there on, they are taken over and directed to other translocases by the respective targeting signal receptors. In the case of positively charged presequences, the release of preproteins from Tom22 is induced by Tim21, a subunit of the TIM23 complex⁵⁹, while inner membrane carrier preproteins as well as outer membrane β -barrel preproteins are recognized by small Tim chaperones in the IMS and further directed to TIM22 or SAM, respectively⁶⁰.

Initially, the protein conducting pore was found and characterized in isolated full TOM complexes after solubilization using the mild detergent digitonin²². It

showed striking similarity to the peptide-sensitive channel (PSC) that was found ten years earlier²¹, indicating that these two channels are indeed identical. Later, the same pore characteristics were found in the smaller core complex isolated via a slightly harsher detergent n-Dodecyl β -D-maltoside (DDM), lacking Tom70 and Tom20 compared to the previously described intact complexes⁴⁹. Furthermore, similar characteristics could be attributed to Tom40 isolated from *Neurospora crassa*⁵³, Tom40 from *S. cerevisiae* and to both NcTom40 and ScTom40 heterologously expressed in *E. coli*^{23;61}. Initially, there was some disagreement on the number of pores and conductance states (see Becker et al.⁶¹ for an experimental elucidation of the problem), though in the end a conclusive picture could be drawn: The TOM complex contains a water-filled translocation channel, the β -barrel protein Tom40 which forms a cation-selective pore ($P_+ : P_- \approx 10 : 1$) with a main conductance $G_{\text{main}} = 370$ to 390 pS and a subconductance gating state $G_{\text{sub}} = 150$ pS (in 250 mM KCl). The pore diameter was assessed using different techniques like electron tomography, computational modeling or calculation from the conductivity of the channel. The independent experiments all led to a diameter of 2.1 to 2.6 nm for one pore unit, wide enough to import preproteins with two secondary structured stretches in parallel.

Surprisingly, the water-filled pore itself is capable of binding import substrates like the positively charged presequence of cytochrome c oxidase subunit 4 (Cox4) even without receptor units and, upon binding of substrates, exhibits a significant increase in channel activity. The full TOM complex shows similar behavior, though at a 40- to 60-fold increased sensitivity^{23;61}. Recombinant Tom40 also exhibited a sensitivity to higher voltages regardless of sign that resulted in a reduced open probability, proving that a voltage sensor is also part of the channel protein and not exclusively located in other subunits of the TOM complex²³.

High-resolution electrophysiology was further used together with detailed kinetic analysis⁶² to investigate substrate peptide interaction with isolated *NcTom40*. They revealed that pure peptide binding and full peptide translocation can be distinguished by temporal parameters of Tom40's substrate response⁶³ and that the energy profile of peptide translocation through the channel can be extracted from temperature-dependent interactions⁶⁴.

While the purified TOM complex was found to mostly constitute twin- or triple-pores²², the TOM core complex formed mainly twin-pores, no triple-pores, but a significant portion of single-pores. This distribution was recently confirmed and explained by the presence of two different populations of TOM complexes *in vivo*, with a lack of receptors in the twin-pore conformation⁶⁵. The single-pore appearance was also found for recombinantly expressed and reconstituted Tom40 from yeast⁶¹. Very recently, the structure of the TOM core complex was solved using electron microscopy⁵⁵. The complex isolated with dodecyl-maltoside exhibits the twin-pore formation without Tom20 or Tom70, in line with the assumption that the milder detergent digitonin might be required to isolate the complex also in the triple-pore formation^{49;54;65}. Bausewein et al.⁵⁵ speculate that the triple-pore might represent a TOM-SAM supercomplex instead, though this assumption is not in agreement with previous model-free crosslink-data⁶⁵.

1.2.2 Sorting and Assembly Machinery (SAM)

The second translocase in the outer membrane is constituted by SAM, also referred to as *topogenesis of the outer mitochondrial membrane β -barrel proteins* (TOB) complex. This complex is a relic of the endosymbiotic origin of mitochondria and shows homology to the bacterial β -barrel assembly machinery (BAM)

which inserts β -barrel proteins from the periplasm into the outer bacterial membrane. In yeast mitochondria, five different β -barrel proteins are known, all substrates of the SAM pathway: The outer membrane entry gate Tom40; the insertase of the SAM complex, Sam50, itself; the voltage-dependent anion channel (VDAC) which is related to Tom40; and the two mitochondrial distribution and morphology proteins Mdm10 and Mdm34. The SAM complex of *S. cerevisiae* consists of three proteins: the β -barrel protein Sam50³³, a member of the Omp85-family, the β -signal receptor Sam35⁶⁶, both essential, and the non-essential Sam37 which promotes release of the precursor proteins. Each protein is present with one unit in the 140 kDa core complex⁶⁷.

One of SAM's substrates, the β -barrel protein Mdm10, is partially associated with the SAM complex⁶⁷. This association was initially thought to just originate from Mdm10's nature as a SAM substrate, though the most abundant substrate VDAC was not co-isolated with SAM. Mdm10 was known to participate in mitochondrial fusion and fission⁶⁸ and is, as well as Mdm34, a component of the ER-mitochondria encounter structure (ERMES)⁶⁹. Mdm10 was also reported to play a crucial role in biogenesis of Tom40 and thus of the TOM complex itself, while biogenesis of VDAC was not impaired in *mdm10* Δ deletion strains of *S. cerevisiae*⁷⁰. Another temporary SAM constituent was found to be Tom5, one of the small TOM subunits, that plays a vital role in assembly of Tom40 at SAM⁷¹ but is not necessary for binding Tom40 in the first place, even indicating a two-step procession of β -barrel precursors at the SAM complex. In an earlier study of the same group, Mim1, which also interacts with TOM and SAM, was reported to be crucial for Tom40 biogenesis⁷², though Mim1's involvement was later linked only to Tom5 biogenesis⁷¹, a common substrate of the Mim1-pathway. Surprisingly, a significant part of α -helical OM proteins is indeed not imported via Mim1 but in-

stead utilizes SAM proteins and even Mdm10 to be inserted^{73;74}. These substrates usually contain a transmembrane segment in their C-terminal half, like Tom22, or are tail-anchored at their extreme C-terminus.

SAM substrates are recognized by Sam35 by a β -signal which was first identified for ScTom40. It resides in the last transmembrane β -strand of the protein⁷⁵, consistent with the targeting signal of prokaryotic β -barrels insert by BAM⁷⁶, and follows the semi-conserved sequence *Po-X-G-X-X-Hy-X-Hy* (*Po*: polar, *G*: glycine, *Hy*: hydrophobic). Based on these findings, a more complex, circular β -signal, containing the semi-conserved sequence, was identified that also contains all information for targeting the preprotein to mitochondria⁷⁷.

The moment preproteins with such a β -signal enter the IMS through TOM, they are recognized by small Tim chaperones⁷⁸⁻⁸¹. They are six-bladed α -propeller complexes formed either by the essential proteins Tim9 and Tim10 or by Tim8 and Tim13, as a trimer of dimers in triangular conformation^{82;83}. These chaperones are thought to shield the hydrophobic stretches of the preproteins from the aqueous IMS environment during shuttling from TOM to SAM or TIM22. After recognition at the SAM complex, the preproteins are handed over to the substrate receptor Sam35, where the preproteins are subsequently passed on to Sam50 and then released into the outer mitochondrial membrane, assisted by Sam37. It was originally assumed that the Tim chaperones take over emerging preproteins from TOM and then shuttle them to the independent SAM complex^{67;84-86} as a soluble chaperone-substrate complex. However, no soluble intermediates of β -barrel preproteins could be found in the IMS. Instead, a recent study reported the importance of the central TOM receptor Tom22 in not only import but oxidation and thus folding of β -barrel proteins at the SAM complex⁶⁰. Using intact complex

investigations, the authors of that study identified a transient 650 kDa TOM-SAM supercomplex that mediates the handover of preproteins from one complex to the other and is linked by Tom22 on the cytosolic side.

Mdm10 was not found to be part of this supercomplex, although its formation was studied using a Tom40-probe which should recruit Mdm10 to SAM at some point as seen before⁶⁷. One could speculate that Mdm10's recruitment to SAM for Tom40 biogenesis might happen in a later stage, after supercomplex disassembly. Previous studies found that a core component of the mitochondrial contact site and cristae organizing system (MICOS), Mic60 (Fcj1/Mitofilin), binds both TOM and SAM complexes independently⁸⁷⁻⁹². While it might be tempting to speculate that simultaneous binding of both complexes by Mic60 represents an early stage of supercomplex formation, this seems unlikely as binding of SAM to Mic60 was shown to depend on an IMS-facing polypeptide-transport associated (POTRA) domain of Sam50⁸⁷, while supercomplex formation of SAM and TOM still happens after deletion of said POTRA and thus is independent of that POTRA domain⁶⁰.

The essential SAM component Sam50 has two noteworthy structural features: The β -barrel itself, predictably composed of 16 β -strands^{93;94}, and the N-terminal POTRA domain that is conserved in the Omp85-family, though with various number of copies per protein⁹⁵. The POTRA domain was initially proposed to function as a chaperone or as a receptor as it binds precursors, with partial deletion of the domain leading to growth defects⁹⁶. Only shortly thereafter though, an extensive study⁷⁵ showed that deletion of the whole POTRA domain does not inhibit yeast growth or protein import and assembly by SAM at all, concluding that POTRA does not act as the main receptor domain. Instead, in a combined electrophysiological and biochemical approach the authors investigated the channel properties of the SAM complex and of Sam50 alone under

various conditions. They found that both Sam50 and the full SAM complex exhibit very similar electrophysiological characteristics: The channel is mildly cation-selective ($P_+ : P_- \approx 4 : 1$) and is gating frequently between an open and a semi-open state with a conductance difference $\Delta G = 160$ pS (250 mM KCl). Upon addition of a shortened substrate, the β -signal of Tom40, Sam50 alone showed no alteration while the full SAM complex exhibits reduced gating frequency, remains mainly in the open state and even opens up to much higher conductance. Surprisingly, these increased conductance differences are multiples of the minimal conductance, i.e. the channel can open to 320 pS and rarely even to 640 pS, which might indicate that upon substrate binding the complex does not only undergo simple rearrangement but even that other, previously dormant units of Sam50 now contribute to channel formation.

1.2.3 Carrier Translocase (TIM22)

The carrier translocase TIM22 is one of two inner membrane translocases that handle substrates previously imported by TOM. It inserts multi-spanning transmembrane proteins into the inner membrane in a strictly membrane potential dependent manner^{29;79;97}. Substrates for TIM22 are mainly metabolite carriers like the ADT/ATP carrier (AAC) or the phosphate carrier (PiC), each carrying three pairs of transmembrane α -helices. TIM22 also imports protein translocases of the Tim17/22/23 homology family, with four α -helices each. In *S. cerevisiae*, the 300 kDa TIM22 core complex is formed by the central translocation channel Tim22^{97;98}, the chaperone-receptor Tim54⁹⁹, Tim18^{100;101}/Sdh3¹⁰², both required for complex assembly, and the peripheral inner membrane protein Tim12^{103;104} that interacts with the chaperones Tim9/10. Of the four integral

core components only Tim22 is essential for yeast growth, while deletion of the other proteins lead to more or less severe growth defects^{98;102}. Additional to the integral components, the peripheral membrane protein Tim12 was reported to be associated with the TIM22 complex via a large IMS-domain of Tim54^{103;104}, though it first forms a soluble complex with the chaperones in the IMS before becoming membrane-bound¹⁰⁵.

Similar to β -signal proteins, preproteins with multiple targeting signals are recognized by Tim9-Tim10 or Tim8-Tim13 chaperone complexes^{82;83} at the IMS side of the TOM complex. There, the Tim9-Tim10 chaperone complex promotes import of metabolite carrier proteins like SiC or AAC, while import of ScTim23 additionally requires the Tim8-Tim13 chaperone complex^{82;106}. After the chaperone-cargo complex is formed in the IMS, it is recognized by Tim12¹⁰⁵ and further directed to TIM22. Here, the soluble cargo-Tim9-Tim10-Tim12 complex is recruited to the membrane via interaction between Tim12 and Tim54, which leads to stable association of the peripheral membrane protein Tim12 with the TIM22 complex and the carrier preprotein is inserted by the central channel protein Tim22. Binding or tethering of the chaperone-cargo complex to TIM22 is independent of the mitochondrial membrane potential, while the initial insertion of α -helices into a pore of Tim22 requires a low polarization ($\Delta\Psi > 60$ mV) of the inner membrane. The final insertion and subsequent release into the membrane occurs only in the presence of both a targeting signal and a higher membrane potential ($\Delta\Psi > 120$ mV)^{97;107}.

In an early study, Tim22 was identified as water-filled channel, the core of the TIM22 complex, and characterized electrophysiologically⁹⁸. Recombinantly expressed ScTim22 constitutes a cation selective channel with a maximum ob-

served conductance change of $G_{\text{main}} = (540 \pm 18)$ pS under symmetrical buffer conditions with 250 mM KCl. Interestingly, the channel gates in eight steps of $G_{\text{sub}} = (67 \pm 5)$ pS from open to closed and exhibits direct conductance transitions covering multiples of G_{main} with frequencies much higher than expected for incidental simultaneous gating of independent pores. This indicates that the main conductance change G_{main} indeed corresponds to gating of one functional subunit of a coupled channel. At asymmetric buffer conditions, Tim22 reveals a varying cation preference of $P_+ : P_- \approx 15 : 1$ in the smallest conductance state and $P_+ : P_- \approx 4 : 1$ in the fully open state. Isolated TIM22 complexes though exhibited a significantly reduced ion preference ($P_+ : P_- > 2.4 : 1$), indicating a possible reducing contribution by other complex constituents.

The channel is voltage-activated, i.e. at low membranes potential the channel is present in a closed conformation but starts to open at elevated voltages regardless of sign. Prolonged exposure to higher membrane potentials, on the other hand, again induces closure of Tim22, similar in principle to Tom40. While an open, substrate-susceptible TIM22 is a reasonable requirement for membrane potential dependent protein import, *staying* open would compromise the energized state of the inner membrane.

A follow-up study revealed the twin-pore nature of TIM22, using electron microscopy and electrophysiological investigations¹⁰⁷. In electron micrographs, TIM22 appears as a twin-pore similar to the TOM core complex. Isolated TIM22 complexes fused to a planar lipid bilayer reveal a channel with identical pore conductances compared to recombinantly expressed Tim22, but appearing only in multiples of two. The possibility of two independent channels, e.g. an artifact of complex isolation or reconstitution, was refuted by the presence of direct conductance changes of $\Delta G_{\text{TIM22}} = 2 \cdot G_{\text{max, Tim22}}$, with a much higher fre-

quency than expected for independent pores. Interestingly, both native complex and recombinant protein are excitable using a combination of an uncharged targeting signal (internal signal peptide of the phosphate carrier) and a high transmembrane potential, leading to strongly increased gating activity of each channel. While this shows that the Tim22 protein contains both a targeting signal recognition mechanism and a voltage sensor, and does not require the full complex for this, the voltage threshold required for activity increase is much lower for the full complex ($\Delta\Psi_{\text{min,TIM22}} \approx 70 \text{ mV}$) than for the recombinant protein ($\Delta\Psi_{\text{min,Tim22}} \approx 140 \text{ mV}$).

1.2.4 Presequence Translocase (TIM23)

Designated mitochondrial matrix proteins and non-carrier inner membrane proteins are imported via the TIM23 pathway (see figure 1.3). These substrates typically bear positively charged, N-terminal presequences making up $\approx 70\%$ of the mitochondrial proteome¹⁰⁸. The presequences are cleaved after import by mitochondrial peptidases in the matrix or the IMS¹⁰⁹. Some substrates, like the cytochrome b_2 ¹¹⁰, are even released back to the IMS after being processed by an IMS peptidase¹¹¹.

In *S. cerevisiae*, the TIM23 core complex consists the channel-forming eponymous protein Tim23^{24;28;112}, its homolog Tim17²⁶ (both also homolog to Tim22), the main presequence receptor Tim50¹¹³⁻¹¹⁵ and Mgr2¹¹⁶. TIM23 exists in two different forms in the inner mitochondrial membrane to accommodate its dual function: Integral inner membrane proteins are inserted by the TIM23^{SORT} complex, containing Tim21 as an additional integral component¹¹⁷. For import of mitochondrial matrix proteins on the other hand, TIM23 recruits the presequence

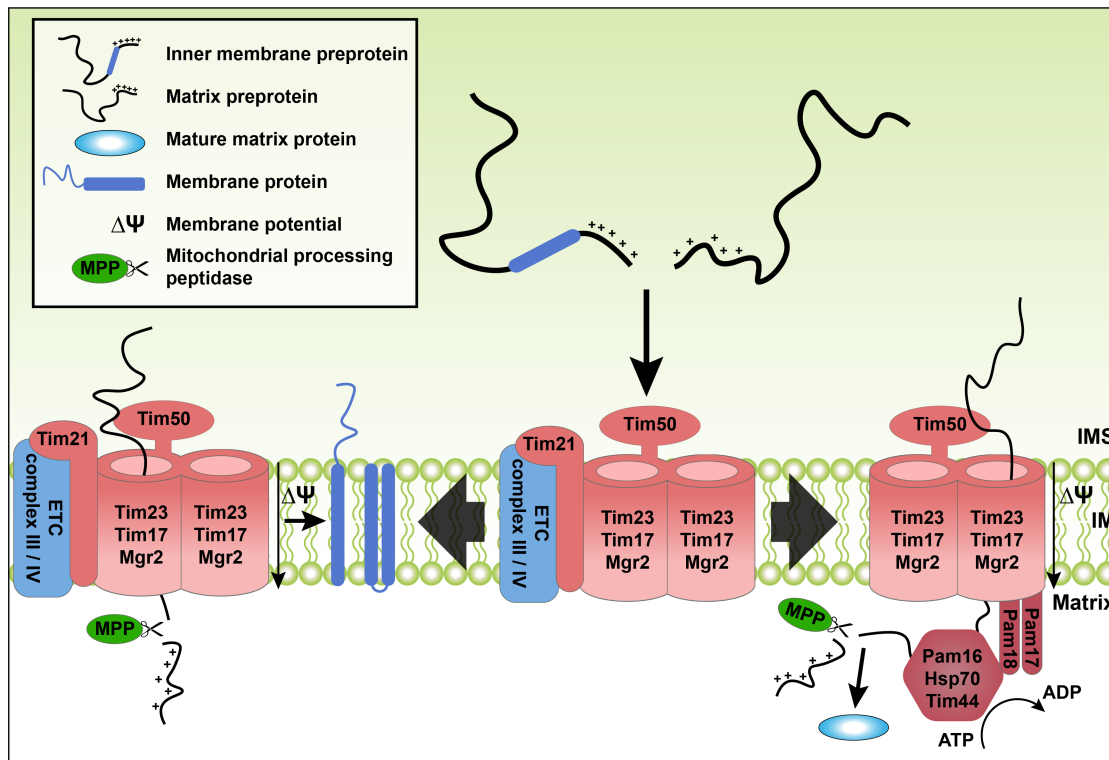


Figure 1.3: Protein import through TIM23 requires dynamic switching of the complex between two different conformations: Preproteins with a presequence and hydrophobic sorting signals are inserted into the inner membrane via the Tim21-containing TIM23^{SORT}, assisted by electron transfer chain complexes III and IV. Preproteins with a presequence but without sorting signals are translocated into the matrix with the help of the PAM motor complex.

translocase-associated motor (PAM) on the matrix side^{59;118}. PAM consists of the chaperone heat-shock protein 70 (Hsp70), the membrane-anchored co-chaperone Pam18, the scaffold proteins Pam16 and Tim44, and the nucleotide exchange factor Mgel.

Upon emergence from TOM to the IMS, preproteins are bound by the central receptor Tom22. Tom22^{IMS} was found to also interact with Tim23^{IMS}¹¹⁹ and Tim21^{IMS}^{59;120}, effectively linking the inner to the outer membrane. The preprotein is handed over to the TIM23 complex via the main receptor Tim50. The IMS domain of Tim50 contains two presequence-binding subdomains: Tim50^{core}, which also interacts with TIM23^{IMS}, and the essential Tim50^{PBD}¹²¹. Both Tim50^{IMS} and Tim23^{IMS} can bind presequences, though binding affinity was orders of magnitude lower for Tim23 in comparison^{122;123}, indicating that indeed binding to Tim50 is the first step in preprotein reception. During early steps of recognition and handover, protein domain interactions are competing in a complex manner. Tim50^{PBD} is able to interact with both Tim50^{core} and presequences with overlapping sites¹²⁴, presumably to enable preprotein handover between the two subdomains of Tim50. Further, Tim50^{IMS}- and presequence-binding to Tim23^{IMS} are mutually exclusive^{121;125}, i.e. IMS domains of Tim50 and Tim23 dissociate upon presequence handover to the channel protein. Now that the preprotein has reached Tim23^{IMS}, it is inserted into the pore in an unknown manner and then electrophoretically threaded through the inner membrane.

If the preprotein contains a sorting signal, typically a hydrophobic stretch after the presequence^{51;126}, translocation through TIM23^{SORT} proceeds until the hydrophilic presequences emerges on the matrix side. Here, most presequences are proteolytically processed by the mitochondrial processing peptidase (MPP)^{127;128}.

The protein is laterally released into the lipid bilayer through a yet unknown lateral gate. Mgr2^{116;129} and Tim17^{116;130} both interact with preproteins during lateral sorting of inner membrane proteins, with Mgr2 acting as the quality control of lateral protein release¹²⁹. Interactions with preproteins and involvement in lateral release lead to the speculation that Mgr2 and Tim17 form or contribute to the lateral gate of TIM23^{59;129;131}. Mgr2 and Tim21 are also critical for recruitment of respiratory chain complexes to TIM23^{SORT}^{116;132}, which is speculated to ensure a sufficient membrane potential in close proximity to TIM23¹³³.

The mitochondrial membrane potential $\Delta\Psi$ is the sole energy source of membrane protein insertion by TIM23¹¹⁷. Dissipation of $\Delta\Psi$ leads to complete collapse of protein import for most TIM23 substrates, though interestingly, some preproteins lacking a classical cationic presequence are still imported by TIM23 at a basal rate¹³⁴. Even more so, deletion of the only cationic amino acid in the targeting signal of such a preprotein, subunit *e* of the F₀F₁-ATP synthase, leads to complete independence of its import from the membrane potential.

Designated matrix preproteins interact with Tim50 when they reach TIM23. Tim21 then dissociates from Tim50^{IMS} and consequently from TIM23¹²³, which in turn recruits Pam17 to the complex¹¹⁸. After handover of the preprotein to Tim23, it is threaded through the channel in a $\Delta\Psi$ -dependent manner. When it emerges on the matrix side, the PAM protein Tim44 can bind the presequence after its recruitment by Tim17 and Tim23¹³⁵. Upon preprotein binding, Tim44 recruits the ATP-loaded main chaperone Hsp70¹³⁶, which in turn then binds to the emerging presequence^{137;138}. ATP-hydrolysis by Hsp70 is stimulated by the J-proteins¹³⁹ Pam16/18^{140;141} that are recruited to TIM23 via interaction with Tim17^{IMS}⁵⁹. Conversion of ATP leads to tightening of Hsp70 around the presequence¹⁴² which pulls the preprotein a short distance into the matrix. Then, Hsp70^{ADP} and the other

PAM proteins dissociate from the complex and fresh Hsp70^{ATP} and co-chaperones bind to TIM23 and the presequence. This subsequent recharging of PAM maintains continuous presequence import¹⁴³ into the matrix.

1.2.5 Oxidase Assembly Machinery (OXA)

The oxidase assembly machinery (OXA) has a unique position among all mitochondrial protein translocation pathways. It has been identified as the only mitochondrial export machinery to handle mitochondrial encoded proteins⁴⁵ through a highly-conserved pathway. The OXA complex acts as an insertase of the inner membrane by directly binding mitochondrial ribosomes and inserting the nascent protein chain into the IM in a co-translational manner⁴⁶. OXA is constituted by the membrane proteins Oxal, Mbal and Mdm38. Oxal is the core protein of the complex, contains five transmembrane α -helices and spans the inner membrane in a N_{Out}-C_{In} topology. It is a member of the YidC/Alb3/Oxal family¹⁴⁴ which is a small family of insertases with YidC and Alb3 being found in bacteria and chloroplasts, respectively. The individual function of each OXA protein appears not to be easily attributed as each component seems to participate in multiple processes in protein insertion and even beyond that. First of all, each of the three proteins was shown to bind mitochondrial ribosomes and they were speculated to act cooperatively with each other¹⁴⁵⁻¹⁴⁹. Early investigations of Mbal function showed that it can compensate for import defects in yeast strains with Oxal-mutants¹⁵⁰ and a very recent study bolstered the view that Mbal is not just a passive ribosome receptor but actively aligns the ribosome exit tunnel with the insertion complex¹⁵¹. Mdm38 on the other hand fulfills two major functions that are spatially distinct on the protein level: The transmembrane part acts as an K₊/H₊ antiporter¹⁵²⁻¹⁵⁴ while the matrix exposed part has a ribosome binding domain with structural

similarity to 14-3-3 proteins¹⁴⁹. Both proteins also exhibit a regulatory function on translation of mRNAs and can compensate for each other in that, while loss of both proteins together leads to severe aberrant synthesis of respiratory chain proteins¹⁴⁸.

Substrates for the OXA pathway like *ScCox2p* can employ a cleavable targeting signal which is recognized by *Oxa1*¹⁵⁵ and processed by the inner membrane peptidase (IMP) for maturation and insertion of the substrate, while other substrates, e.g. the human *HsCox2*, do not have a cleavable leader sequence. OXA inserts not only mitochondrially but also some nuclear encoded inner membrane preproteins in a pathway referred to as conservative sorting. There, the precursor proteins make their way through TOM and TIM23 and are then not or only partially released to the IM by TIM23's sorting mechanism. Instead, they are fully or partially translocated to the matrix where they are taken over by OXA to insert the remaining transmembrane segments¹⁵⁶. This pathway provides two different modes of action: chaperone-mediated release of transmembrane segments into the matrix by TIM23 and subsequent insertion by OXA ("conservative sorting") or segment-wise insertion into the membrane directly by TIM23 ("stop-transfer"). Initially, both modes were thought to be conflicting models of protein insertion but were then proven to work in a complementary manner in during insertion of multispanning membrane proteins, as shown for the ATP binding cassette (ABC) transporter *Mdl1*^{47;157}. Another prominent substrate of this pathway is *Oxa1* itself which is translated in the cytosol, imported via TOM and TIM and inserted via existing OXA complexes⁴⁵. Interestingly, OXA was recently found to participate in biogenesis of another type of inner membrane proteins, the ATP/ADP carrier protein *Aac2* which is actually inserted via TIM22⁴⁸. While the specific role of *Oxa1* in this context is still unknown, the authors suggested a function in folding

newly inserted carrier proteins.

Recently, some light was shed on the molecular mechanism of protein insertion by OXA as an aqueous pore was identified in native OXA complexes¹⁵⁵. For this purpose, Oxal was isolated from three different sources, purified from *S. cerevisiae*, recombinantly expressed in *E. coli* and isolated as native OXA complexes, and subjected to planar lipid bilayer electrophysiology. This revealed a dynamic, cation-selective pore with a main conductance state $G_{\text{main}} = 530$ pS, a minimal subconductance state $G_{\text{sub,min}} = 75$ pS and multiple conductance states in between, partially depending on the sign of the applied voltage. Oxal has a calculated diameter of ≈ 1.9 nm and comes in minimal units of four pores. Incorporated channels reacted to α Oxal antibodies by near-complete blockage, while incubation of Oxal-channels with the presequence of the substrate ScCox2 led to a drastic increase in activity of the channel. Investigations further confirmed prior findings^{158;159} that Oxal is present as a homo-tetramer or, as two of four pores are functionally coupled, as a dimer of dimers. After the discovery tetrameric Oxal forming a water-filled pore in the inner mitochondrial membrane, crystal structures of the bacterial Oxal-homolog YidC emerged^{160;161}. These structures show YidC in a monomeric state, a configuration that would not suggest channel activity. Instead the authors proposed that YidC forms a hydrophilic groove in the inner leaflet of the bilayer. This groove recruits the hydrophilic stretch of a substrate and transfers it to the extracellular space in an unknown manner whilst releasing the hydrophobic domain into the bilayer^{144;160}.

This obviously also challenged the idea of Oxal being a water-filled channel in an oligomeric state, as both proteins share a high degree of sequence similarity. While crystal structures provide a plethora of new and helpful information, also towards understanding the molecular mechanism of a protein, they naturally are

snapshots of a specific static state and often do not allow deeper insights into the protein dynamics. Even if the implications from the crystal structure were transferred from YidC to Oxal, one could speculate that the monomeric, crystallized form might represent an idle state whose oligomerization *in vivo* needs to be induced to form the import-competent complex. It can also be speculated that two hydrophilic grooves, as found in YidC, together constitute one coupled double-pore, as found for Oxal complexes. It is tempting to imagine possible ways to merge electrophysiological data with crystal structures from putative, especially from non- β -barrel pores. While typical β -barrel channels often have stable shapes, fixed number of β -strands and were shown to form oligomers of pre-existing pores, but not assemble the pores by oligomerization^{162;163}, the same cannot be said for α -helical transmembrane proteins like Oxal or Tim23.

1.3 Molecular and Channel Properties of Tim23

Tim23 has been subject of multiple molecular and electrophysiological investigations, trying to shed light on molecular mechanisms and the origin of channel properties. The protein consists of four α -helical, C-terminal transmembrane segments¹⁶⁴ and an unstructured, N-terminal domain facing the intermembrane space¹⁶⁵, which enables interaction with presequences²⁸. The IMS domain is able to homodimerize in the presence of a membrane potential, but dissociates upon binding of presequences²⁸, although the N-terminal IMS domain of Tim23 was found in an NMR study to exist purely as a monomer¹⁶⁵. Later, it was revealed that the dimerization requires a functional first transmembrane segment (TMS1)¹⁶⁶, possibly explaining the previous discrepancy. Interestingly, the third (TMS3) and fourth (TMS4) transmembrane segment were found dispensable for protein import¹⁶⁶, though it is unclear if they just do not take part in pore formation or

if their contribution to the channel lining could be rescued by e.g. the homolog Tim17.

Tim 23 is the main channel-forming protein of the complex¹⁶⁷, was identified as a component of the inner membrane import machinery nearly 25 years ago^{24;26} and found to constitute the aqueous pore in the *multiple conductance channel* (MCC)¹¹². It forms a triple pore when constituted alone¹⁶⁷ and a twin pore in the full complex¹⁶⁸. Tim23 gates with a main conductance change $G_{\text{main}} = (450 \pm 11)$ pS and the subconductance change $G_{\text{sub},1} = (140 \pm 15)$ pS, with a single-pore diameter of 6.5 Å to 12 Å¹⁶⁷, which is wide enough to accommodate two parallel α -helices without tertiary structure. Although the actual protein constitution of the pore within the TIM23 complex is unknown, both Tim17, containing four indispensable transmembrane α -helices, and Mgr2, with two α -helices, were found to mediate preprotein release into the bilayer and thus could be contributors towards pore constitution. According to basic calculations, eight to ten α -helices could together form an aqueous channel with a size comparable to the Tim23 pore^{131;169}, without the need for Tim23-dimer formation.

The Tim23 channel is voltage-activated, but closes upon prolonged exposure to higher voltages. As with TIM22, this is in line with the need for an open channel to insert presequences while keeping the electrochemical barrier intact. The voltage-sensitivity is increased by the IMS domain of the receptor Tim50, drastically lowering the threshold for voltage-induced closing¹⁷⁰. Even without other complex constituents, recombinant Tim23 recognizes preproteins with its N-terminal IMS domain and reacts with fast gating (*flickering*) to site-specific presequence addition in electrophysiological studies^{117;167;170}. The voltage sensor of Tim23 is proposed to be formed by a leucine zipper motif in the IMS domain, re-

sponsible for voltage-regulated dimerization of the domain²⁸, though the voltage sensor can not be exclusively located in the N-terminal IMS domain, as a truncated, C-terminal version of Tim23 was found to also exhibit voltage-dependent channel activity^{167;171}. Similar to the full length protein, the truncated version also closed at high membrane potentials, indicating the presence of an membrane-based part of the voltage sensor.

The Tim23 channel is, compared to potassium channels, mildly cation-selective and prefers potassium ions over chloride ions with $P_{K^+} : P_{Cl^-} \approx 16 : 1$. Variations of the buffer-constituting cation revealed that the determining factor for ion permeability is dehydration energy¹⁷¹, i.e. the likelihood of the ion to shed the hydration shell to move through the channel¹⁷². An alternative determination factor is ion size, i.e. the ability to strongly bind to negative charges along the channel lumen. It was concluded that negatively charged amino acids in both IMS domain and channel lumen together constitute the ion filter of Tim23. Interestingly, the TIM23 complex shows slightly weaker cation selectivity $P_{K^+} : P_{Cl^-} \approx 11 : 1$ compared to recombinant Tim23, highlighting that net contribution of other complex subunits to the ion filter is small. The nonetheless present difference in selectivity could be attributed to Tim17 or Mgr2, putatively forming a part of the pore in fully assembled complexes.

Using a broad library of cysteine mutants of Tim23¹⁶⁴, interaction of Tim23 residues with preproteins during import was investigated via cross-link analysis. In line with the later finding that TMS3 and TMS4 are dispensable, the substrate was successfully cross-linked to the IMS domain and the first two helices of Tim23¹⁷³. As TMS2 showed a specifically high cross-link efficiency, it was further characterized using a sophisticated, environment-sensitive fluorophore

labeling approach. The attached fluorophore changes its spectral properties depending on the polarity of its environment. It revealed that the TMS2 faces two different environments, the aqueous channel and the lipid or protein phase. The highly conserved, lumen-facing residues were further shown to switch to a more non-polar environment after preprotein incubation, indicating the TMS2 is in very close proximity to the substrate during translocation. In a follow-up study, the TMS2 of Tim23 was found to undergo structural rearrangements upon dissipation of membrane potential. In an energized membrane TMS2 forms a straight α -helix, while upon depolarization the helix breaks into two smaller helices, presumably around residue I162, at the IMS-facing end of the helix¹⁷⁴.

Taken together, multiple studies have been conducted to elucidate molecular characteristics and electrophysiological properties of Tim23. It was found to react to membrane potentials with increased gating and successive closing, enhanced by the voltage regulator, while membrane depolarization leads to helix-kinking and opening of the channel. The cation-selective Tim23 channel also closely interacts with positively-charged substrates via the channel lumen, and exhibits fast channel flickering upon incubation with presequences.

Chapter 2

Aims of this Thesis

Protein biogenesis of mitochondria is an essential requirement for not only mitochondrial fitness but also for cell viability. Despite its own genome and protein synthesis, the overwhelming majority of proteins is imported from the cytosol to one of the four distinct subcompartments of mitochondria, following multiple pathways. At the heart of these pathways lie protein-conducting, aqueous nanopores which cooperate in a complex orchestra.

One of the translocases of the inner membrane, TIM23, handles over 70% of all mitochondrial proteins and transports them either to the mitochondrial matrix or the inner membrane. While TIM23 requires a complex interplay of multiple subunits, switches between two different conformations to accommodate either type of substrate and might constitute the channel itself from two or three subunits, the basic properties of the water-filled pore originate from one subunit, the eponymous Tim23.

While its pore characteristics have been analyzed to some extent, studies on structural implications and molecular localization of specific channel mechanisms are scarce and suffer from the difficulties of handling hydrophobic

membrane proteins *in vitro*.

The aim of this study is to investigate the molecular origin of basic pore properties, interaction with regulators and substrates, and their implication for channel function. To this end, high-resolution single channel electrophysiology was employed to monitor channel behavior and interaction effects, combined with site-directed mutagenesis to study the impact of specific regions of the pore on its electrophysiological characteristics.

Chapter 3

Materials and Methods

3.1 Materials

Standard chemicals and laboratory consumables were purchased from Th. Geyer (Renningen, Germany), Carl Roth (Karlsruhe, Germany), Sarstedt (Nümbrecht, Germany), Sigma Aldrich (Taufkirchen, Germany). Oligonucleotides were purchased from Metabion (Planegg, Germany). Special chemicals and materials used in this study that were not purchased from Carl Roth are listed in table 3.2.

Table 3.1: Lipids used in this study

Abbrev.	Name	Purchased from
PC	L- α -phosphatidylcholine (Egg, Chicken)	Avanti Polar Lipids
PE	L- α -phosphatidylethanolamine (Egg, Chicken)	Avanti Polar Lipids
PS	L- α -phosphatidylserine (Brain, Porcine)	Avanti Polar Lipids
PI	L- α -phosphatidylinositol (Liver, Bovine)	Avanti Polar Lipids
CL	L- α -Cardiolipin (Heart, Bovine)	Avanti Polar Lipids
SIV-PC	L- α -Phosphatidylcholine (soybean, Type IV-S)	Sigma Aldrich

Table 3.2: Special consumables not purchased from Carl Roth

Product	Supplier
Chloroform	Merck, DE
Deoxynucleotide triphosphate mix	5 PRIME, DE
Deoxyribonuclease I (DNase I)	Sigma Aldrich, US
Dimethyl sulfoxide (DMSO)	Thermo Scientific, US
DpnI	Thermo Scientific, US
Glisseal-HV Laborfett	VWR, US
Histodenz	Sigma Aldrich, US
Lysozyme	Sigma Aldrich, US
Mark12 Unstained Standard	Thermo Scientific, US
N-Nonanoyl-N-methylglucamin (MEGA-9)	Glycon, DE
PageRuler Prestained Protein Ladder	Thermo Scientific, US
Parafilm	Bemis, US
Phusion DNA Polymerase	Thermo Scientific, US
Pierce ECL Western blotting substrate	Thermo Scientific, US
Proteinase inhibitor pills (EDTA-free)	Roche Applied Science, DE
PTFE-Film	GoodFellow GmbH, DE
Spectra/Por Standard RC Tubing 3.5 kDa	Spectrum Labs Inc, US
Triton X-100	Sigma Aldrich, US
Wizard SV Miniprep DNA Purification Kit	Promega, DE
Wizard SV Gel and PCR Clean-Up Kit	Promega, DE

Table 3.3: Plasmids used in this study

Plasmid	Encoded protein	Vector	Marker	Origin
MM_87	ScTim23	pET10N	Amp	Truscott et al. ¹⁶⁷
MM_103	ScTim23-N150A	pET10N	Amp	this study
MM_104	ScTim23-G153A	pET10N	Amp	this study
MM_105	ScTim23-Y159A	pET10N	Amp	this study
MM_117	ScTim23-A152G	pET10N	Amp	this study
MM_118	ScTim23-L155A	pET10N	Amp	this study
MM_119	ScTim23-N160A	pET10N	Amp	this study
MM_120	ScTim23-N163A	pET10N	Amp	this study
MM_189	ScTim23-D174A	pET10N	Amp	this study
MM_190	ScTim23-K190A	pET10N	Amp	this study
MM_191	ScTim23-G153L	pET10N	Amp	this study
MM_192	ScTim23-G153C	pET10N	Amp	this study
MM_196	ScTim23-A156G	pET10N	Amp	this study
MM_197	ScTim23-A156L	pET10N	Amp	this study
MM_198	ScTim23-A156F	pET10N	Amp	this study

Table 3.4: Primers used in this study

Primer	Encoded Mutation	Direction	Sequence
MM13F	Tim23-N150A	Forward	AGAGGTCCTTCTTAGGTGCTAAT
MM13R	Tim23-N150A	Reverse	GAGAATCCCCGCATTAGCACC
MM14F	Tim23-G153A	Forward	TTCTTAGGTAATAATGCGGCGATT
MM14R	Tim23-G153A	Reverse	GAGAATCGCCGCATTATTACC
MM15F	Tim23-Y159A	Forward	GCGTTGAGCGCCAATATCATC
MM15R	Tim23-Y159A	Reverse	TGTAGAATTGATGATATTGGCGCT
MM32F	Tim23-L155A	Forward	GGTAATAATGCGGGGATTGCCGCGTTGAGCTACAATATC
MM32R	Tim23-L155A	Reverse	GATATTGTAGCTCAACGCGGCAATCCCCGCATTATTACC
MM33F	Tim23-A152G	Forward	CTTCTTAGGTAATAATGGGGGGATTCTCGCGTTG
MM33R	Tim23-A152G	Reverse	CAACGCGAGAATCCCCCATTATTACCTAAGAAG
MM34F	Tim23-N163A	Forward	GCGTTGAGCTACAATATCATCGCTTCTACAATAGATGCACTAAG
MM34R	Tim23-N163A	Reverse	CTTAGTGCATCTATTGTAGAAGCGATGATATTGTAGCTCAACGC
MM36F	Tim23-N160A	Forward	GATTCTCGCGTTGAGCTACGCTATCATCAATTCTACAATAG
MM36R	Tim23-N160A	Reverse	CTATTGTAGAATTGATGATAGCGTAGCTCAACGCGAGAATC
MM108F	Tim23-D174A	Forward	TGCACTAAGAGGCAAACATGCCACCGCGGCTC
MM109R	Tim23-D174A	Reverse	GAGCCCGCGGTGGCATGTTTGCCTCTTAGTGCA
MM110F	Tim23-K190A	Forward	TCACGGGCGCTTTGTTTCGCGTCTTCAAAAGGTTTG
MM111R	Tim23-K190A	Reverse	CAAACCTTTTGAAGACGCGAACAAGCGCCCGTGA
MM112F	Tim23-G153L	Forward	CTTAGGTAATAATGCGTTGATTCTCGCGTTGAGCTAC
MM113R	Tim23-G153L	Reverse	GTAGCTCAACGCGAGAATCAACGCATTATTACCTAAG
MM119F	Tim23-A156L	Forward	GTATAATGCGGGGATTCTCCTGTTGAGCTACAATATCATC
MM120R	Tim23-A156L	Reverse	GATGATATTGTAGCTCAACAGGAGAATCCCCGCATTATTAC
MM135F	Tim23-A156G	Forward	GTATAATGCGGGGATTCTCGGGTTGAGCTACAATATCATC
MM136R	Tim23-A156G	Reverse	GATGATATTGTAGCTCAACCCGAGAATCCCCGCATTATTAC

Table 3.5: Centrifuges and rotors used in this study

Centrifuge	Rotor	Manufacturer
Sorvall RC12BP	H-12000 BioProcessing	Thermo Scientific, US
Eppendorf 5810 R	A-4-62 swinging bucket	Eppendorf AG, DE
Sorvall RC6	F10S-6x500y mL	Thermo Scientific, US
	JA-10	Beckman Coulter Inc., US
	JA-20	Beckman Coulter Inc., US
Optima L-90K UC	Sw60 Ti swinging bucket	Beckman Coulter Inc., US
Eppendorf 5415 R	F45-24-11	Eppendorf AG, DE
Optima MAX-XP UC	TLA-55	Beckman Coulter Inc., US

Table 3.6: Buffers used in this study

Buffer	Buffer composition
Inclusion body purification buffers	
Lysis buffer	100 mM NaCl, 50 mM Tris-HCl, 10 $\mu\text{g mL}^{-1}$ Dnase I, 5 mM MgCl ₂ , 1 pill/50 mL cOmplete protease inhibitor cocktail without EDTA pH 8.0
Triton X-100 buffer	100 mM NaCl, 1 mM EDTA, 10 mM DTT, 2% Triton X-100, 50 mM Tris-HCl, pH 8.0
TEN buffer	100 mM NaCl, 1 mM EDTA, 10 mM DTT, 50 mM Tris-HCl, pH 8.0
TN buffer	100 mM NaCl, 50 mM Tris-HCl, pH 8.0
Chromatography buffers	
HisTrap buffer A	8 M urea, 150 mM NaCl, 10 mM Tris-HCl, 50 mM Imidazole, pH 8.0
HisTrap buffer B	8 M urea, 150 mM NaCl, 10 mM Tris-HCl, 500 mM Imidazole, pH 8.0
Size-exclusion buffer	8 M urea, 150 mM NaCl, 10 mM Tris-HCl, pH 8.0
General experiment buffers	
Liposome buffer	150 mM NaCl, 20 mM MOPS-Tris, pH 7.0
Electrophysiology buffer 1	250 mM KCl, 20 mM MOPS-Tris, pH 7.0
Electrophysiology buffer 2	20 mM KCl, 20 mM MOPS-Tris, pH 7.0
Other buffers	
Competent cell buffer 1	30 mM KAc, 10 mM CaCl ₂ , 50 mM MnCl ₂ , 100 mM RbCl, 15% glycerol, pH 5.8
Competent cell buffer 2	10 mM RbCl, 75 mM CaCl ₂ , 15% glycerol, 10 mM MOPS, pH 6.5
TAE buffer	20 mM Acetic acid, 40 mM Tris, 20 mM EDTA, pH 7.6

3.2 Methods - Molecular Biology

3.2.1 Polymerase Chain Reaction

Polymerase chain reaction (PCR)¹⁷⁵ was employed to perform site-directed mutagenesis. Primer pairs were designed to contain the desired base mutation in their center and purchased from Metabion (DE). For PCR, a 50 μ L PCR reaction mix was set up, containing: 100 ng DNA template, 0.2 μ M each forward and reverse primer, 3% DMSO, 0.2 μ M dNTP mix, 1 U Phusion DNA polymerase and 1x Phusion HF buffer. The PCR mix was subjected to 20 cycles of Denaturing - Annealing - Elongation (see table XY). The methylated template DNA was digested with 1 μ L DpnI and 5 μ L of the digested PCR product was transformed into 50 μ L *E. coli* XLI-Blue cells for plasmid amplification (see section 3.3.2).

3.2.2 DNA Sequencing

Plasmid DNA was sequenced, after amplification and isolation, by GATC Biotech AG (DE).

Table 3.7: Thermocycle setup for polymerase chain reactions

Step	Temperature	Time	
Lid	99 °C		
Initial Denaturing	98 °C	30 s	
Denaturing	98 °C	50 s	20x
Annealing	55 °C	30 s	
Elongation	68 °C	10 min	
Final Elongation	68 °C	10 min	
End	4 °C		

3.2.3 DNA Concentration Determination

DNA concentration was determined spectrophotometrically with a NanoDrop 2000 (Thermo Scientific, US) and its built-in *Nucleic Acid* method. The calculation uses on a modified version of the Lambert-Beer law (equation 3.1 which yields the concentration C_{DNA} by measuring the absorbance A at 260 nm, baseline-corrected by absorbance at 340 nm, with the path length d and an extinction coefficient ϵ .

$$C_{\text{DNA}} = (A \cdot \epsilon) / d \quad 3.1$$

3.3 Methods - Cell Biology

3.3.1 *E. coli* Strains and Medium

In this study, three different *E. coli* strains were used (table 3.8). ScTim23 was expressed in BL21 (DE3) cells. Plasmid amplification for all plasmids was carried out in XLI-Blue cells.

All *E. coli* strains were grown on LB (lysogeny broth) with 10 g NaCl, 5 g yeast extract and 10 g tryptone per liter of culture. For LB-Agar solid medium, the LB was supplemented with 15 g L⁻¹ Agar-Agar. Cells containing ScTim23 pET10N vector were grown in medium complemented with 100 mg L⁻¹ Ampicillin.

Table 3.8: *Escherichia coli* strains used in this study

Strain	Genotype	Supplier
XLI-Blue	<i>recA1 endA1 gyrA96 thi-1 hsdR17 supE44 relA1</i>	Stratagene
BL21 (DE3)	F ⁻ <i>ompT h_B (r_B⁻ m_B⁻) gal dcm λ(DE3)</i>	Novagen

3.3.2 Generation and Transformation of Chemically Competent *E. coli* Cells

E. coli cells were made chemically competent according to a previously published protocol¹⁷⁶. Briefly, a 1 L culture of *E. coli* BL21 (DE3), XLI-Blue or Rosetta (DE3) cells was grown without antibiotics to an optical density at 600 nm (OD) of 0.6 at 37 °C and cooled down on ice for 15 min. After centrifugation at 2700 g for 15 min at 4 °C, the cells were resuspended in 200 mL ice-cold competent cell buffer 1 and pelleted again at the same speed. After resuspension in 30 mL of the final competent cell buffer 2 the cells were aliquoted, frozen in liquid nitrogen and stored at -80 °C for further usage.

Transformation of competent cells was achieved by adding 100 ng plasmid DNA or 20 µL ligation PCR mix to 50 µL competent cells, thawed on ice, and incubation for minimum 5 minutes on ice. The mix was subjected to a heat-shock at 42 °C for 45 s and incubated on ice for minimum 2 minutes before 300 µL pre-warmed LB medium was added. The cells were recovered by shaking them for one hour at 37 °C and 450 rpm and subsequently plated on LB-Agar plates containing the appropriate antibiotics specified by the plasmid (100 µg mL⁻¹ Ampicillin for the pET10N-vector). The plates were left at 37 °C until bacterial colonies were visible.

For plasmid amplification after mutagenesis (see chapter section 3.2.1), XLI-Blue cells were transformed with the respective plasmid and plated on LB-Agar plates supplemented with 100 µg mL⁻¹ Ampicillin. Multiple colonies were picked and each grown in 10 mL LB medium with antibiotics for 12 – 24 hours. The cells were collected in 50 mL tubes by centrifugation (Centrifuge 5810 R, A-4-62 rotor, 4000 rpm or 3200 g, room temperature, 5 min). Cells were resuspended,

lysed and plasmids were isolated and purified, using *Wizard Plus SV Minipreps DNA Purification System* (Promega, DE) according to the manufacturers protocol.

3.3.3 Protein Expression and Inclusion Body Purification

Tim23 wild type and mutants containing an N-terminal His-Tag were expressed in *E. coli* BL21 (DE3) cells as described before^{167;177}. To this end, the pET10N plasmid carrying Tim23 wild type or mutant expression gene was transformed into *E. coli* BL21 (DE3) cells which were plated on LB-Agar plates supplemented with Amp (100 µg/mL). After incubation for 24 h at 37 °C, single colonies were picked to inoculate a preculture of 10 mL LB (+Amp) for 6 h, which in turn was used to inoculate a 250 mL overnight culture of LB+Amp to an OD600 (optical density at $\lambda = 600$ nm; OD600 is proportional to cell density) of 0.05. The next morning, autoclaved LB medium in flasks (2 L medium per 5 L flask, typically 12 L total culture volume) was supplemented with Amp, inoculated with the overnight culture to an OD600 of 0.05 and left in an incubator shaker until the culture reached an OD600 of 0.6 - 0.8, which corresponds to the log or exponential growth phase, characterized by uninhibited cell growth i.e. doubling¹⁷⁸. Then, IPTG was added (1 mM) and expression was induced for 3 h at 37 °C before all cells were collected by centrifugation (Sorvall RC12BP with H-12000 rotor, 4000 rpm or 5300 g, 18 °C, 20 min). The cell pellets were resuspended in 50 mL of cell resuspension buffer per 2 L of original culture and again collected via centrifugation (Sorvall RC6 with F10S rotor, 5000 rpm or 4200 g, 20 min, 4 °C). The cell pellet was typically frozen at this step.

As Tim23 is a highly hydrophobic membrane protein, it must be isolated and purified from inclusion bodies. To this end, the pellet was resuspended in lysis

buffer (10 mL/g wet cells) and the cells were lysed by three passes at 1000 bar through a cooled EmulsiFlex-C3 (Avestin Inc., US). The cell lysate was supplemented with deoxycholic acid and lysozyme, stirred with a magnetic bar for 30 min at room temperature (to enable DNase activity) and centrifuged (Sorvall RC6 with F10S rotor, 5000 rpm or 4200 g, 60 min, 4 °C) to remove soluble proteins and bacterial cytoplasm. Next, membrane fractions and membrane-inserted proteins were removed by resuspension in 75 mL Triton X-100 buffer, stirring for 30 min at 4 °C and centrifugation (Sorvall RC6 with F10S rotor, 5000 rpm or 4200 g, 30 min, 4 °C). The inclusion body pellet was then further washed by resuspension in 75 mL TEN buffer, stirring for 1 h at 4 °C and centrifugation (as before). Ethylenediaminetetraacetic acid (EDTA) and dithiothreitol (DTT) were removed by resuspension in 75 mL TN buffer and centrifugation (as before), before the pellet was stored at -20 °C.

3.3.4 Affinity Chromatography

The protein was solubilized from inclusion bodies using high molar concentrations of urea, a chaotropic salt, and purified via His-tag affinity chromatography. Unlike protein tags, e.g. Glutathion-S-Transferase (GST), which require proper folding of the tag, peptide tags like polyhistidine tags enable affinity chromatography purification even for denatured proteins, though specificity is typically greater with GST-tag. The imidazole moiety of polyhistidine tags binds preferentially to complexed divalent metal ions, e.g. Ni²⁺-NTA or Co²⁺-NTA, with NTA being crosslinked to an agarose matrix¹⁷⁹. Proteins without polyhistidine tags do not bind at all or not tightly to the Ni²⁺-NTA and can be washed off even with low concentrations of imidazole, while the proteins of interest can be eluted from

the Ni²⁺-NTA by high concentrations of imidazole. This technique is typically used with either agarose beads as a matrix to enable purification in reaction tubes or with chromatography columns, either self-packed or commercially prepacked, to be used with chromatography setup, e.g. ÄKTA systems. In this study, affinity chromatography was used with prepacked HisTrapFF 1mL or 5mL columns (GE Healthcare, UK), operated on an ÄKTA Prime Plus system (GE Healthcare, UK).

Prior to use, all chromatography buffers were sterile filtered through 0.22 µm filters and degassed. The pellet was resuspended in buffer containing 50 mM imidazole to reduce unspecific binding of contaminations. The resuspension was stirred for 60 min at room temperature and then centrifuged (Sorvall RC6 with JA-20 rotor, 12000 rpm or 17400 g, 20 min, room temperature) in a pre-warmed rotor. Urea is temperature sensitive at very high concentrations. Using the rotor right from the fridge would lead to precipitation of urea and thus of the protein of interest. Alternatively, instead of urea guanidine hydrochloride can be employed at 6 M concentrations¹⁷⁷ and used at 4 °C as it is not temperature sensitive. The supernatant was filtered through 0.45 µm filters and loaded to the column with a flow rate of 0.5 mL/min to allow binding. The column was washed with 20 column volumes (CV) of HisTrap buffer A at 1 mL/min and the bound protein was eluted from the column with 4 CV of HisTrap buffer B, containing 500 mM imidazole, at 1 mL/min and fractionated in 1 mL steps.

3.3.5 Size-Exclusion Chromatography

Proteins pre-purified using affinity chromatography were further subjected to size-exclusion chromatography, where particles, like proteins, are not separated by binding affinity but by their size, more precisely their hydrodynamic

volume¹⁸⁰. The size-exclusion matrix used in this study was made of crosslinked agarose with covalently bound dextran to form a porous matrix. While the smallest particles can enter the various nanometer-sized pores in the matrix, bigger particles pass by most pores and cavities. This leads to a much higher elution time for smaller particles that are trapped in the pores, whereas bigger particles just pass by the porous cavities. In this study, a HiLoad 16/600 Superdex 200 pg (GE Healthcare, UK) operated on an ÄKTAPrime Plus system (GE Healthcare, UK) and was used to separate Tim23 proteins from contaminations and aggregates, with a constant flow rate of 1 mL/min. Before the separation run, the column was equilibrated with 1 CV of ddH₂O and 1.5 CV of size-exclusion buffer. After injection, not exceeding a sample volume of 2 mL, the sample was eluted with 1 CV of sizeexclusion buffer and fractionated in 2 mL steps.

3.4 Methods - Protein Biochemistry

3.4.1 Sodium dodecyl sulfate polyacrylamide gel electrophoresis (SDS-PAGE)

Proteins were separated and detected using discontinuous Tris-Glycine SDS-PAGE^{181;182}. Here, the negatively charged detergent SDS denatures proteins and binds to them approximately proportional to the protein mass with ≈ 2 molecules of SDS per amino acid. Application of an electric field across the gel leads to migration of the, now negatively charged, proteins towards the anode. The polyacrylamide gel matrix acts as a sieve, with smaller molecules passing through the pores easier than bigger molecules, effectively separating smaller from bigger proteins.

The SDS polyacrylamide gels used in this study were cast with a stacking gel

Table 3.9: SDS-PAGE gel matrix and buffer composition

Matrix	Composition
Stacking gel	12.5% (30/0.8) acrylamide / bis-acrylamide, 0.1 % SDS, 386 mM Tris/HCl pH 8.8, 0.1% APS, 0.08% TEMED
Running gel	5% (30/0.8) acrylamide / bis-acrylamide, 0.1% SDS, 126 mM Tris/HCl pH 6.8, 0.1% APS, 0.2% TEMED
Running buffer	0.1% SDS, 191 mM glycine, 25 mM Tris
Loading buffer	2% SDS, 10% glycerol, 1% β -mercaptoethanol, 0.01% bromphenol blue, 60 mM Tris/HCl pH 6.8

above the actual running gel. The stacking gel had a low polyacrylamide concentration, and thus a higher porosity, and a pH of 6.8 and was used to focus the proteins to a single band after loading. With a higher polyacrylamide concentration, the porosity of the matrix becomes the limiting factor for protein migration, thus separating the proteins by size. For initial denaturing, the protein sample of interest was incubated with 1x Loading buffer (from 5x stock). To estimate molecular weight of protein bands, either *Mark12 unstained marker* (Novex) or *PageRuler prestained marker* (Thermo Scientific) were loaded on the gel as well.

3.4.2 Protein Visualization on SDS-PAGE

Proteins were visualized on gels after SDS-PAGE using Coomassie Brilliant Blue. For a lower detection sensitivity, the gel was immersed in Coomassie stainer, containing 25% ethanol, 10% acetic acid and 0.1% Coomassie Brilliant Blue R-250, heated in a microwave and incubated for 30 min on a shaker. Stainer was then discarded and replaced with destainer, same composition but without Coomassie Brilliant Blue, again heated and incubated for 30 min on a shaker. Destainer was replaced as needed for further destaining.

To reach a higher detection sensitivity or to visualize lipids on a gel, a colloidal

Coomassie stain¹⁸³ was used, containing 0.12% Coomassie Brilliant Blue G-250, 10% ammonium sulfate, 10% phosphoric acid, and 20% methanol. The gel was immersed in the stain and incubated on a shaker for minimum one hour, typically over night, and then washed multiple times with ddH₂O. While normal Coomassie stain stains the whole gain and has to be thoroughly destained, background staining of colloidal Coomassie stain is minimal and can be washed with normal water.

3.4.3 TCA Precipitation

Protein samples with a too high volume or a too low concentration for SDS-PAGE had to be precipitated and redissolved in loading buffer. To this end, the sample were incubated with 15% trichloroacetic acid (TCA) for 30 min on ice and centrifuged (Centrifuge 5415 R, 13,200 rpm or 16,100 g, 4 °C, 30 min). The supernatant was carefully discarded, the pellet was washed with 1 mL ice-cold acetone and again centrifuged at the same conditions. Supernatant was again discarded and the samples were dried on air over night. SDS loading buffer was added to dried precipitation pellets. Due to the acidic precipitant, the redissolved pellet in loading buffer might turn yellow (due to pH-sensitive bromphenol blue) and was brought back to a higher pH by addition of 2 µL 1 M Tris.

3.5 Methods - Liposome Techniques

3.5.1 Liposome Preparation

For liposome formation, PC, PE, PI, PS and CL (see table 3.1) were first prepared in chloroform and then mixed in the desired molar ratios, i.e. either 70:15:15

PC:PE:CL or 45:20:15:5:15 PC:PE:PI:PS:CL, in glass test tubes. The lipid mixture in chloroform was dried under a nitrogen stream for 5 min followed by desiccation in vacuum for 2 h. The dried lipid film was fully resuspended with liposome buffer (150 mM NaCl, 20 mM MOPS/Tris, pH 7.0) for a final mass concentration of 10 mg mL⁻¹. The lipid suspension was then subjected to at least seven freeze-thaw cycles, i.e. freezing in liquid nitrogen followed by thawing in cold water and vortexing for 3 min. To reach size-uniformity of the liposomes, the suspension was extruded 31 times through polycarbonate membranes with a pore size of 200 nm (Whatman). The assembled extruder setup was washed with 3x MeOH, 2x ddH₂O, 2x liposome buffer, 5 passes each.

3.5.2 Protein Incorporation into Liposomes

The Tim23 protein was incorporated into liposomes in a detergent mediated manner as described before¹⁶⁷. For that, both extruded liposomes and Tim23 protein in Urea were incubated with 80 mM MEGA-9 (non-ionic detergent, critical micelle concentration $cmc \approx 20$ mM, dialyzable) for 30 min, then mixed in 1:50 protein to lipid (w/w) ratio and incubated for another 45 min. The mixture was then dialyzed in membrane tubes with 3.5 kDa cutoff (Spectrum Labs) in 5 L liposome buffer to remove both Urea and MEGA-9, first for 2 h at room temperature followed by overnight dialysis at 4 °C.

3.5.3 Liposome Flotation Assay

To assess protein co-migration with liposomes, density gradient flotation was employed using nonionic Histodenz as we described before¹⁷⁷. With this technique, membrane-unbound proteins can be separated from liposomes and membrane-bound proteins. While liposomes, both empty and with incorporated

protein, migrate to areas of lower density, unbound protein stays in the loading fraction (see figure 3.1). The base layer, 700 μL 46% Histodenz mixed with 100 μL proteoliposomes, was loaded in the bottom of a polycarbonate test tube and discreet layers of 20%, 10%, 5% and 0% in liposome buffer with 900 μL each were cast on top. The density gradient was centrifuged in a swinging bucket rotor (Optima L-90K UC with Sw60 Ti rotor, 55k rpm or 210,000 – 400,000 g, 4 $^{\circ}\text{C}$, 1 h) and then fractionated in 500 μL steps from top to bottom. The fractions were TCA-precipitated and subjected to SDS-PAGE.

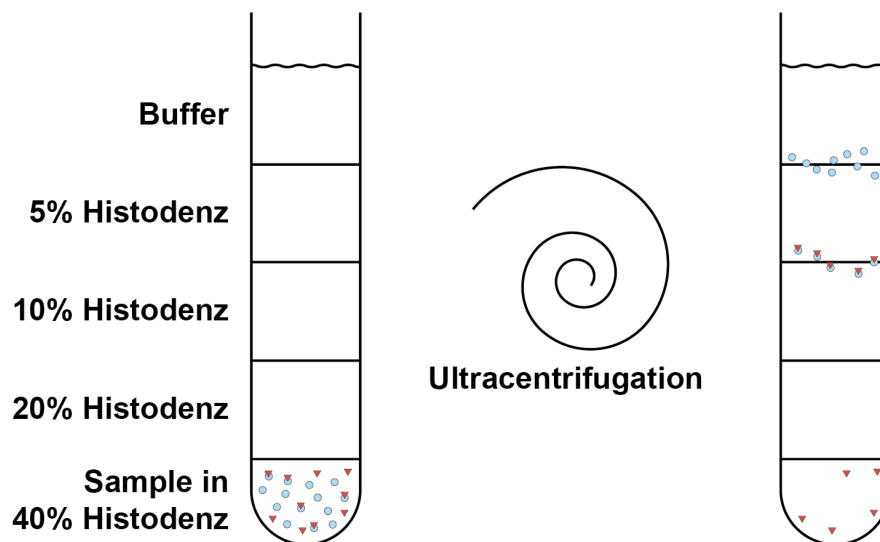


Figure 3.1: General principle of density gradient flotation as employed in this thesis. Liposomes and proteoliposomes migrate to low-density interfaces while unbound protein or unincorporated protein stays in the loading fraction.

3.5.4 Sodium Carbonate Extraction

To test if proteins are only attached or truly inserted into liposomes, proteoliposomes were diluted in 200 mM sodium carbonate (Na_2CO_3). This leads to detachment of peripherally attached proteins from the membrane due to distur-

bance of electrostatic interactions and unfolding of the protein¹⁸⁴. Proteoliposomes were used in a modified flotation assay with 900 μL 50% Histodenz mixed with 100 μl proteoliposomes as base layer, followed by 1 ml 20% Histodenz and 2.5 ml 0% Histodenz. After centrifugation, the liposomes were carefully extracted from the interface between 20% and 0% layers with a pipette. The floated liposome samples were diluted in 10x 200 mM sodium carbonate, incubated on ice for 30 min and then centrifuged at 186,000 g for 45 min at 4 °C. Pellet and supernatant were separated, the supernatant was TCA-precipitated and both samples were subjected to SDS-PAGE.

3.6 Methods - Electrophysiology

3.6.1 General Principle of Electrophysiology

For electrophysiological considerations, reduced membrane systems and even whole cells can be brought down to an equivalent circuit diagram, that of a *leaky capacitor*¹⁸⁵. In a minimal system, as used in this thesis, the circuit consists of a series connection of resistor $R_{\text{Electrolytes+Electrodes}}$, representing the resistance of both the electrical setup (headstage and electrodes) and the electrolytes, with a parallel connection of C_{membrane} and R_{membrane} , capacitance and resistance of the impermeable lipid bilayer, and R_{channel} , resistance (or inverse conductance $1/G$) of an incorporated ion channel (figure 3.2A). $R_{\text{EL+EL}}$ is small compared to R_{channel} and can therefore be neglected in a series connection, while R_{membrane} is big compared to R_{channel} and can be neglected in a parallel connection, leaving a reduced circuit (figure 3.2B). Current flux through a capacitor depends on changes of applied potential, thus directly after setting a constant holding potential U , the capacitor C_{membrane} is conducting for a few hundred milliseconds until exponen-

tial decay reduces the respective current to near zero. Then, all current I is flowing through $R_{channel}$, enabling direct calculation of the channel's conductance G via Ohm's first law:

$$U = R \cdot I = \frac{I}{G} \Leftrightarrow G = \frac{I}{U} \quad 3.2$$

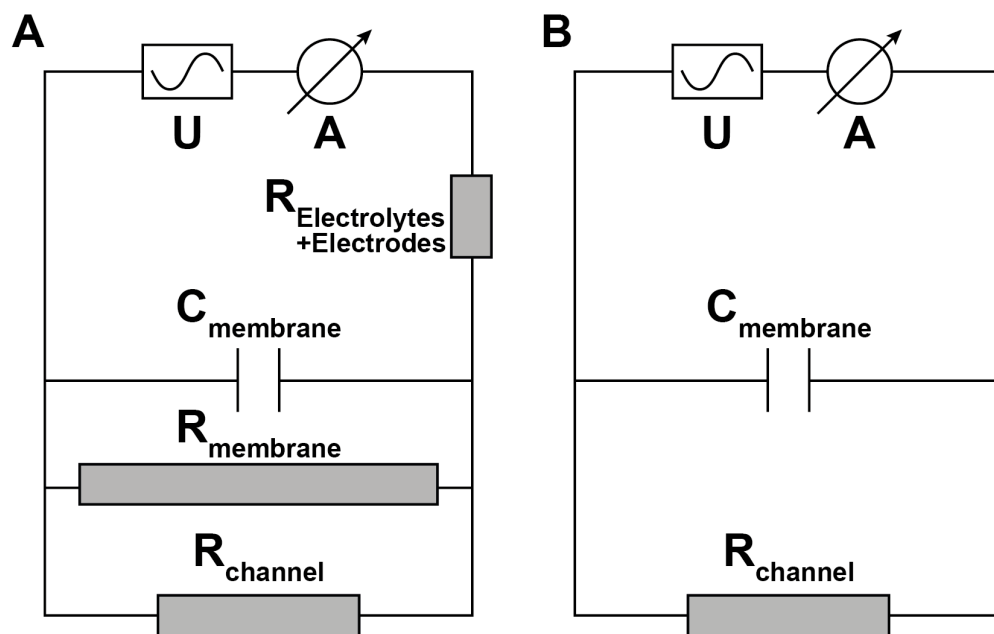


Figure 3.2: Complex (A) and reduced (B) circuit sketch of an ion channel in a biological membrane.

3.6.2 Reversal Potential and Ion Selectivity

In eukaryotic cells, the plasma membrane and many organellar membranes are nearly impermeable for ions and only allow ion passage through dedicated ion transporter. This restricted ion movement leads to an ion concentration gradient over the membrane. The concentration difference results in an electrochemical membrane potential which strives to equilibrate the ion concentration on both

sides of the membrane again. The potential that needs to be applied over the membrane to stop all ion flux through the membrane is termed *reversal potential*¹⁷². If only one ion species, e.g. Na⁺, is transported over the membrane and contributes to the asymmetry, the resulting equilibrium potential can be calculated using the Nernst equation

$$U_{rev} = \frac{RT}{zF} \cdot \ln \frac{C_1}{C_2}, \quad 3.3$$

where R is the universal gas constant ($R = 8.314 \text{ J K}^{-1} \text{ mol}^{-1}$), T is temperature, z is ion charge, F is Faraday's constant ($F = 96485.332 \text{ C mol}^{-1}$) and $C_{1/2}$ is ion concentration on each side of the membrane.

If multiple anions and cations contribute to the electrochemical potential, it is not sufficient to only sum up the Nernst potentials (equation 3.3) for each ion as the ions may have different permeabilities through the membrane. At asymmetric salt concentrations, both anions and cations strive to equilibrate, and if the channel is not ion selective, all anions and cations migrate with the same rate, resulting in zero net current. Though, if the channel discriminates between ions, one type of ions has a higher permeability through the channel than the other, resulting in a higher ion flux for the preferred type which can be measured as a nonzero current at zero voltage. The reversal potential required to zero any current flux depends on the salt concentrations and the relative ion preference of the channel and can be calculated from the respective ion concentrations and their permeability, using the Goldman or Goldman-Hodgkin-Katz voltage equation^{186;187}

$$U_{rev} = \frac{RT}{F} \cdot \ln \left(\frac{\sum P_C [C]_{outer} + \sum P_A [A]_{inner}}{\sum P_C [C]_{inner} + \sum P_A [A]_{outer}} \right), \quad 3.4$$

where $[C] / [A]$ is the concentration of cations or anions, $P_{C/A}$ are the permeability

of cations or anions and *inner/outer* refers to the side of the membrane.

In this study, we use a potassium chloride buffer with known, different salt concentrations on trans and cis sides of the channel. We can solve the equation for the relative ion selectivity to

$$P_{K^+} : P_{Cl^-} = \frac{[Cl^-]_{trans} - \exp\left(\frac{U_{rev}F}{RT}\right) \cdot [Cl^-]_{cis}}{\exp\left(\frac{U_{rev}F}{RT}\right) \cdot [K^+]_{trans} - [K^+]_{cis}}, \quad 3.5$$

where P_{K^+/Cl^-} are the permeability of potassium or chloride ions, $[K^+]/[Cl^-]$ are the respective ion concentrations, *cis/trans* correspond to the two sides of the bilayer, F , R , T are constants as declared before and U_{rev} is the measured reversal potential.

3.6.3 Conductance

As introduced in section 3.6.1, ion flux through an open channel results in a recordable current I_{open} that depends on the applied voltage. After partial or full closure of a channel, the current is reduced to a $I_{intermediate}$ or I_{closed} . It has to be noted that I_{closed} can be non-zero, originating either from the membrane if it is not fully impermeable or from the channel if it allows a residual current even in its closed conformation.

Using Ohm's law (equation 3.2), dividing recorded current by applied voltage, yields the channels conductance at that specific voltage. This is an indicator of how big the pore or multiple pores are. The diameter of a cylindrical pore can be calculated according to Hille¹⁷² from the approximate length L of the cylinder, the resistivity ρ of the buffer and the recorded and calculated conductance G of the

channel. L can take on e.g. 0.5 nm for a very short constriction zone or 5 nm for a membrane-spanning cylinder. Resistivity ρ is approx. 50 Ω cm for unrestricted electrophysiology buffer 1 (250 mM KCl, 20 mM MOPS-Tris, pH 7.0), whereas electrolytes exposed to strong electrical fields within a pore exhibit a much higher resistivity and a correction factor of 5 was determined for such a narrow channel¹⁸⁸. The pore size can then be calculated:

$$d = 2 \cdot G \cdot \rho \cdot \left(\frac{1}{4} + \sqrt{\frac{1}{16} + \frac{L}{G \cdot \rho \cdot \pi}} \right) \quad 3.6$$

Current recordings of a channel were also analyzed with regards to the occupation of open or closed states. To this end, the open probability P_{open} was calculated by dividing the mean current I_{mean} , typically recorded over the course of a minute, by the maximum current I_{max} of a trace. Extracting the maximum current of a current recording can pose a difficulty if the channel is never fully open during the recording, possibly due to substrate or "stress" effects leading to closure.

3.6.4 Assembly of the Chamber

All electrophysiological experiments in this thesis were carried out using the planar lipid bilayer setup^{189;190}. A very detailed method review describing the vertical bilayer setup used in this thesis, with only minor alterations regarding the electrical setup (see section 3.6.5), was published recently¹⁹¹.

Briefly, the bilayer chamber consists of two half-chambers with a circular aperture on each side. One aperture per half-chamber was closed with a glass plate and fixated with Parafilm and a tight PTFE ring. One half chamber was inserted with the glass front first into the metal cage. On the other side of the half chamber, Glisseal vacuum grease was applied to the flat front and a Polytetrafluoroethylene (PTFE) film with a needle-tip sized hole was glued to one half chamber. The hole

was created by carefully puncturing the PTFE film with a needle and trimmed with three pulses of a self-made spark gap. The other half chamber was greased without a PTFE film and inserted grease front first into the metal cage. There, the non-glass fronts of both half-chambers face each other and are sealed, upon contact, by the vacuum grease and the PTFE film after closing and carefully tightening the setup with a metal screw ring. Magnetic stir bars of 5 mm length are inserted in each half-chamber to allow buffer mixing with the magnetic stirrer underneath the metal cage.

Now, Type IV-S L- α -Phosphatidylcholine (SIV-PC) in decane (redissolved after drying from chloroform in a dessicator, 3 mg lipid in 50 μ L decane) is painted on the small hole in the PTFE film with a syringe and left for 20 min incubation time. The bilayer was created by first adding 3 mL of electrophysiology buffer 1 to each half-chamber and then repeatedly raising and lowering the buffer level over the lipid film to remove decane and excess lipids layer-wise. A lipid bilayer can be distinguished from a non-bilayer film by eye as described in Bartsch et al.¹⁹¹ or by its electrical properties, i.e. capacitance of a bilayer is much smaller than that of a non-bilayer film.

3.6.5 Electrical Setup and Software

Ag/AgCl electrodes were created by soldering silver wire (diameter 1 mm) to gold connectors and immerse the wire of the electrodes in 12% NaClO for minimum 3 h; alternatively, the Ag-electrodes can be chlorinated by immersing the wire and the ground in 1 M KCl and applying a voltage of 5 V over the electrode for 10 min. To eliminate liquid junction potentials, the electrodes were inserted into glass tubes and embedded in a 2 M KCl-Agar bridge. Electric recordings were performed with Ag/AgCl electrodes connected to a CV-5-IGU headstage and fur-

ther to a Geneclamp 500B current amplifier (both Axon Instruments, now Molecular Devices, US), with the trans-electrode used as reference electrode and the cis-electrode grounded. Currents were digitized using a Digidata 1440A AD/DA converter and recorded with a PC using the software AxoScope 10.3 for constant holding potentials or Clampex 10.3 for voltage ramps (Molecular Devices, US).

3.6.6 Fusion of Proteoliposomes

Proteoliposomes were added close to the bilayer in the *cis* compartment of the chamber. A salt gradient over the membrane was established with high salt in *cis* and low salt in *trans* compartment, to enable osmotically-driven fusion^{192;193} of proteoliposomes with the bilayer (figure 3.3). If fusion rates are low, CaCl_2 can be added to *cis* compartment to 10 to 20 mM. After fusion, the buffer in each chamber was perfused with 20 chamber volumes (60 ml) of standard 250 mM KCl buffer to set exact salt concentrations.

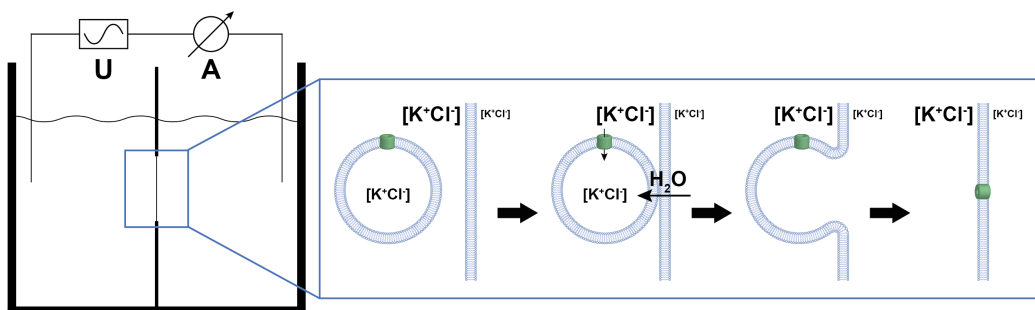


Figure 3.3: Sketch of electrophysiological setup and of channel insertion by osmotically-driven fusion of proteoliposomes to the lipid bilayer.

3.6.7 Data Reconstruction with R

As manual analysis of electrophysiological recordings can be prone to unintended bias (e.g. how to assess electrical noise to identify the *true* starting and

ending levels of a gating event), a sophisticated data analysis tool was further developed in collaboration with Inder Tecuapetla-Gómez (Institute for Mathematical Stochastics, University of Göttingen, DE), based on an estimator of stepwise constant functions, *SMUCE*, implemented in the R-package *stepR*¹⁹⁴. In brief, the *SMUCE* reconstructs the underlying clean data by taking into account the estimated filter effect, removing white noise from the presumed pre-filtered data and finally fitting constant segments to the denoised data. The reconstruction allows to easily identify and analyze conductance changes, dwell times and the general dynamic behavior of ion channels. A major advantage of *SMUCE* compared to previous techniques of data reconstruction is that *SMUCE* does not require any a priori information about the channel characteristics, e.g. Markov model parameter, to perform at least on the same level as established methods. With the core algorithm from *stepR*, we created a full reconstruction routine with RStudio (RStudio Inc., US) that automates gating event detection and dwell time calculation (see section 6.1). Routine parameters that were used in this study are displayed in table 3.10. The reconstruction routine exports data analysis in two .txt-files, a dwell time table and a list of gating events, that were further analyzed with OriginPro 8.5 (OriginLab, US).

For analysis of the temporal resolution of Tim23 channels, the very recent estimator JULES¹⁹⁵ was used within our routine instead, keeping the formatting of data export identical (see section 6.2). JULES, related to *SMUCE*, is capable of accurately reconstructing conductance changes, by deconvolution of the data to fully remove the filter effect, that appear smaller than they were before filtering, thus giving information about the "true" conductance levels of very short events (see Pein et al.¹⁹⁵ for a detailed presentation). This routine demands higher computational power than *SMUCE* if used for large amounts of current-voltage traces

and was therefore only used for dwell time analysis.

Table 3.10: Reconstruction *stepR*-parameters

	SMUCE	JULES
Minimum dwell time	$t0 = 2 \text{ ms}$	$t0 = 0 \text{ ms}$
Minimum conductance change	$c0 = 40 \text{ pS}$	$c0 = 15 \text{ pS}$
Fit segment length (points)	$LL = 15000$ i.e. 0.3 s	$n_norm = 50000$ resp. 1 s

3.6.8 Mean-Variance Analysis

A mean-variance analysis is a helpful tool to display and discover complex gating patterns of recorded current traces and is extensively described in Patlak¹⁹⁶. Briefly, pairs of mean and variance for windows with length n are calculated and stored before moving the window forward step-by-step. Starting at the interval $[1, n]$ and storing $(M, V)_1$, next the window $[2, n + 1]$ and the pair $(M, V)_2$ is considered. Analyzing the whole data set with N data points will yield N pairs of mean and variance. The optimal choice of the window length n depends on the kinetics, e.g. gating speed, of the channel. The faster the channel can change its conductance back and forth, the more transitions will be missed or biased using a long window length. Choosing a very short window length, on the other hand, might overvalue artifacts or noise.

Mean-variance analysis in this study was performed using a self-written *R*-script (see section 6.3) and a window length of 2 ms.

Chapter 4

Results

4.1 In-depth Characterization of the Tim23 Channel

4.1.1 Expression and Purification of Tim23

The expression plasmid for N-terminally His-tagged ScTim23 in a pET10N vector was originally created by Kaye Truscott¹⁶⁷. The plasmid was transformed into *E. coli* BL21 (DE3) competent cells and grown in liquid LB medium at 37 °C to an OD of 0.6 – 0.8 before inducing expression for 3 h at 37 °C with IPTG. Recombinantly expressed Tim23 is insoluble and aggregates in inclusion bodies at higher concentrations. These inclusion bodies were isolated from bacterial cell lysate by centrifugation, separated from soluble and membrane fractions via detergent, further washed and finally solubilized in 8 M urea used as a denaturing chaotropic agent (figure 4.1A). Chaotropic agents disrupt hydrogen bonds at very high concentrations, effectively leading to protein unfolding. The solubilized protein was purified by Ni²⁺-NTA affinity chromatography (figure 4.1B) utilizing the N-terminal deca-histidine tag.

To minimize the possibility of sample contamination by bacterial membrane

proteins, which often exhibit channel activity and would mask the signal of Tim23 in electrophysiological experiments, the protein was further purified using size-exclusion chromatography (figure 4.1D), despite its already high purity after Ni²⁺-NTA affinity chromatography. SDS-PAGE analysis of size-exclusion fractions (figure 4.1C) showed that we could purify the protein to homogeneity. Note that the UV_{280nm}-absorption peaks at fractions 57 and 60 did not contain any protein and can be attributed to UV-absorbing oxidized DTT and imidazole, loaded onto the column together with the sample. Typical yield of Tim23 wild type protein expression after purification was \approx 10 mg per liter of culture.

While pore forming toxins or some beta barrel proteins are partly soluble in normal buffer and can insert into lipid bilayers on their own, this does mostly not hold true for more complex membrane proteins like Tim23. To embed this protein into lipid bilayers, it must be incorporated into liposomes first. To this end, large unilamellar vesicles (LUV) with a diameter of 200 nm were preformed from a lipid mixture of PC:PE:PI:PS:CL with 45:20:15:5:15 (mol%) before lipids and protein were, first separate then together, incubated with the mild dialyzable detergent MEGA-9. The mix was dialyzed in 5 L of liposome buffer to remove both urea and MEGA-9, forcing the protein to refold in the lipid bilayer of the liposomes. A density flotation assay was employed to investigate protein incorporation efficiency. The protein co-migrated upwards with the liposomes to a lower density (figure 4.2A), while unbound proteins would have stayed in the loading fraction (fraction 8 & 9). Co-migration of protein with liposomes can occur as integral or peripheral membrane protein. To distinguish between integration and attachment, co-migrated proteoliposomes were subjected to sodium carbonate extraction. Here, the sample is diluted in cold sodium carbonate (Na₂CO₃) to unfold

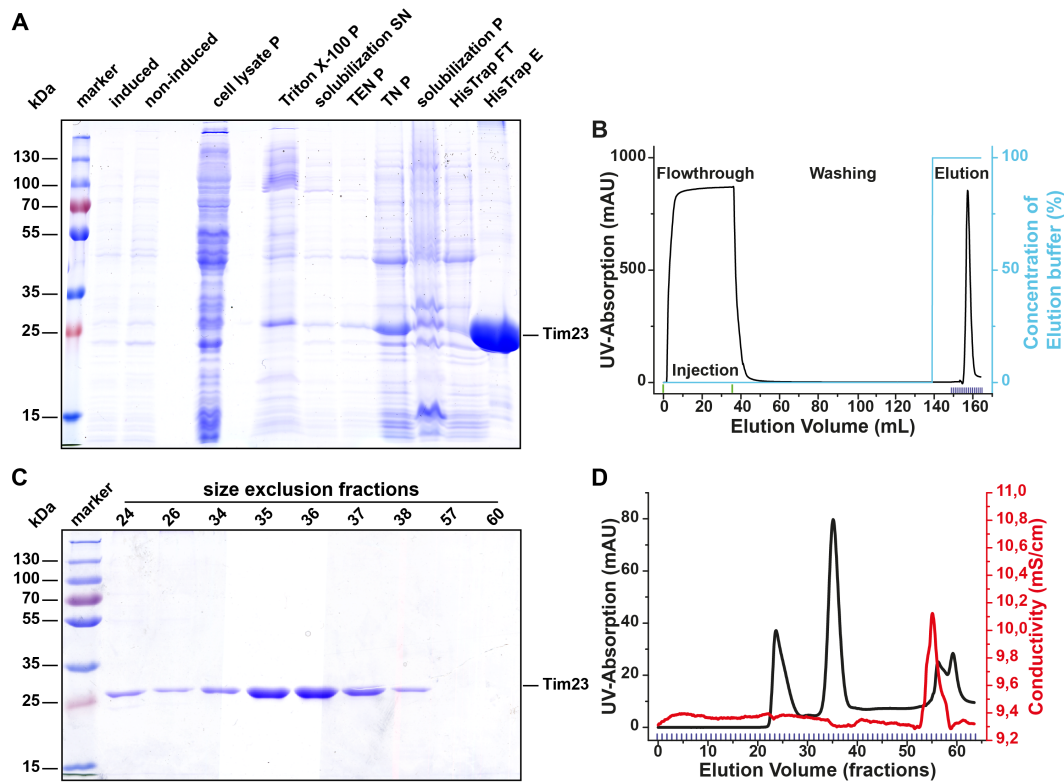


Figure 4.1: Recombinantly expressed ScTim23 was purified to single band purity. (A) Expression and purification steps analyzed by SDS-PAGE. (B) UV_{280nm}-absorption profile of NiNTA-affinity chromatography. (C) Purification using size-exclusion chromatography monitored by SDS-PAGE. (D) UV_{280nm}-absorption profile of size-exclusion chromatography. Meike Wiegand assisted with SDS-PAGE analysis in a lab rotation under my supervision.

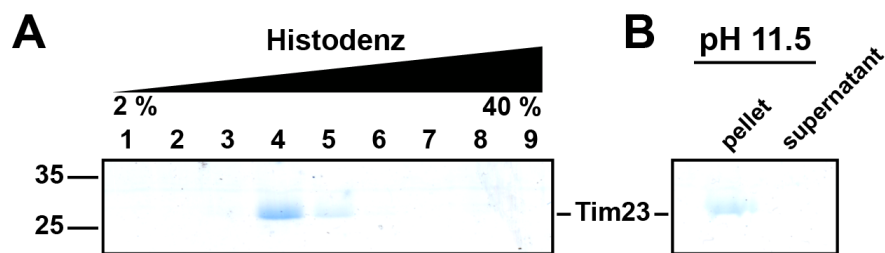


Figure 4.2: Tim23 was successfully incorporated into liposomes. (A) Histodenz density flotation assay analyzed by SDS-PAGE. (B) Ultracentrifuged proteoliposomes after treatment with 200 mM sodium carbonate. Meike Wiegand assisted with SDS-PAGE analysis in a lab rotation under my supervision.

and detach proteins only peripherally attached to a liposome. After ultracentrifugation, Tim23 was found in the pellet together with the liposomes (figure 4.2B) whereas peripherally attached proteins would stay in the supernatant, confirming that Tim23 is indeed incorporated into the liposomes as an integral membrane protein. After successful incorporation into liposomes, Tim23 wild type and mutants were characterized electrophysiologically.

4.1.2 Electrophysiological Characterization of Tim23 Wild Type

The first task in the characterization of molecular mechanisms of Tim23 was to establish a detailed baseline of the channel behavior of recombinant Tim23 wild type. In addition to investigate whether the wild type channel behaves any different from the published channel features^{167;170;171}, it was required to exceed the level of detail present in these previous studies to classify putative incremental mutant effects.

Gating Analysis

The general gating behavior was investigated by recording the current flow through the channel at different voltages. It must be noted that recombinant Tim23 is a lightly rectifying channel, i.e. the conductance depends on the sign of the applied holding potential, and that it typically inserted with the same orientation: Channel conductance is higher at positive than at negative voltages, when the cathode is emerged in the *trans* compartment of the cell (figure 4.3). The *trans* side corresponds to the IMS side of the channel as tested by addition of presequences or voltage regulator Tim50^{167;170} to either side. In this configuration, the native electrochemical potential of the inner mitochondrial membrane corresponds to a holding potential of 150 to 180 mV. To assess the general gat-

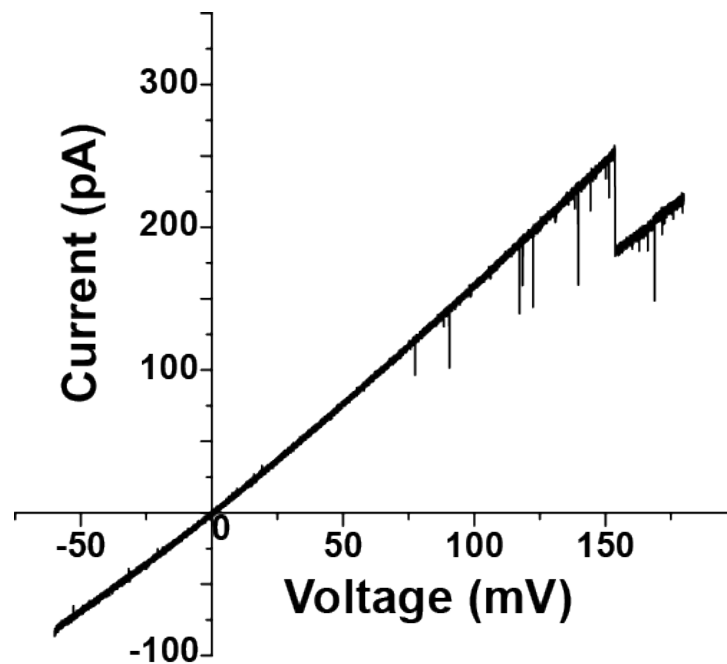


Figure 4.3: Voltage ramp of a Tim23 wild type channel at symmetric buffer conditions.

ing behavior, constant holding potentials ranging from -60 mV to 140 mV were applied to the bilayer incorporated channel in 20 mV steps for 60 s each. Exceeding this holding potential range was found to lead to irreversible closing of one or more pores. The respective channel orientation was determined after each fusion by recording a voltage ramp between -60 and 60 mV and assessing the rectification.

The recorded current traces (see figure 4.4A as example) confirmed that current through Tim23 undergoes changes in three isometric steps (figure 4.4C), indicating the triple pore structure of recombinantly expressed ScTim23 as published earlier¹⁶⁷. All characterized channels contained three or multiples of three pores. Further, all current changes ΔI were extracted from the recordings using the reconstruction algorithm based on *stepR*¹⁹⁴ (see section 3.6.7) and divided by the applied voltage U to obtain conductance changes ΔG . They were displayed in a histogram (figure 4.4B) and further modeled with multiple Gauss fits to ex-

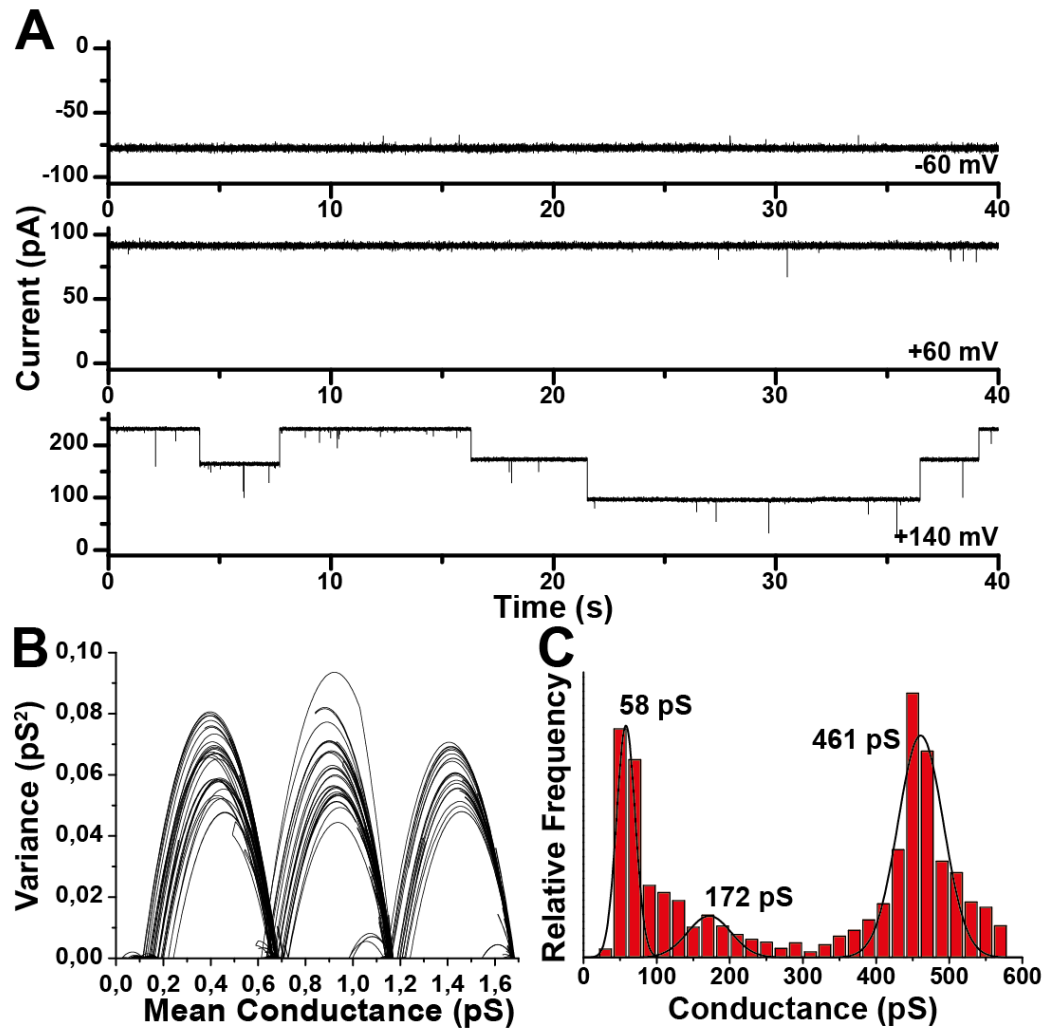


Figure 4.4: Electrophysiological experiments show that Tim23 constitutes a voltage-sensitive triple-pore. (A) Current-recordings at different constant holding potentials. (B) Mean-variance analysis of a single Tim23 trace of 60 s at 120 mV with a window of 2 ms. (C) Gating event analysis of over 2000 gating events from 3 independent experiments.

tract the numeric values for the main conductance state G_{main} and the primary and secondary subconductance states $G_{\text{sub},1}$ and $G_{\text{sub},2}$. The main conductance state $G_{\text{main}} = (461 \pm 31)$ pS (Truscott et al.¹⁶⁷: $G_{\text{main}} = (450 \pm 11)$ pS) corresponds to one full closing or opening of a single pore of three, resulting in a total conductance of $G_{\text{total}} \approx 3 \cdot G_{\text{main}}$. Gating from open to closed or vice-versa appeared to be independent between the pores, i.e. the state of one pore did not obviously affect the state of another pore. The primary subconductance state $G_{\text{sub},1} = (172 \pm 30)$ pS (Truscott et al.¹⁶⁷: $G_{\text{sub},1} = (140 \pm 15)$ pS) and the secondary subconductance state $G_{\text{sub},2} = (58 \pm 13)$ pS are semi-open states a single pore can transition into from the fully open state, but not from the closed state (figure 4.4C).

Voltage-Dependency and Regulation

Increasing the applied holding potential above 100 mV, the channel gradually exhibits a lower open probability $P_{\text{open}} = I_{\text{mean}}/I_{\text{max}}$ (figure 4.5). The voltage sensitivity was further increased by addition of the soluble IMS-domain of ScTim50 to the *trans* side, which lead to a reduction in open probability above 40 mV (figure 4.5, in red), as published before¹⁷⁰.

Ion Selectivity

The presequence translocation channel Tim23 was found to be cation selective in electrophysiological experiments¹⁶⁷, very similar to the other mitochondrial translocases^{23;75;98;155}. For this study, a reversal potential of (47.2 ± 0.4) mV in the presence of a 12.5-fold KCl gradient (250 mM:20 mM) was determined experimentally for incorporated Tim23 wild type (figure 4.6). The corresponding ion selectivity of $P_{K^+} : P_{Cl^-} = 13.3 : 1$ was calculated using the GHK-

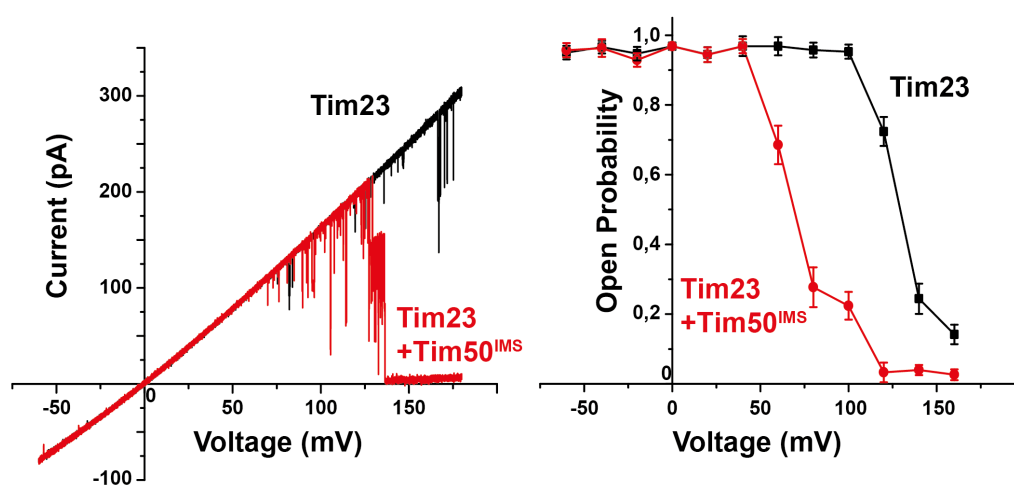


Figure 4.5: Current-voltage ramps (left) and open probabilities (right) of bilayer incorporated Tim23 wild type before (black) and after (red) addition of 700 nM Tim50^{IMS} to the IMS-side of the channel. (n=3, mean \pm SD)

equation (equation 3.4), corresponding well to the published reversal potential of (49.60 ± 3.06) mV¹⁶⁷.

Presequence Activation and Temporal Resolution

Tim23 reacts to substrate addition with fast gating^{117;167;170}. After adding the presequence peptide Cox4 to 300 nM or 500 nM to the IMS side of incorporated Tim23 channels and recording the current traces at $U = 120$ mV, a concentration-dependent increase in gating activity together with premature closing of the channel could be observed figure 4.7. After extracting the reconstructed data from three independent current traces for Tim23 with 0 nM and 500 nM Cox4 using JULES (see section 6.2), the gating events were analyzed in a histogram. The absolute gating frequency (figure 4.8A) confirmed the increase in overall gating event count (relative total increase by factor 18.9 for 500 nM Cox4). Normalization of the histograms showed that the main conductance state around 500 pS was significantly increased, while primary (around 180 pS) and secondary (around 75 pS)

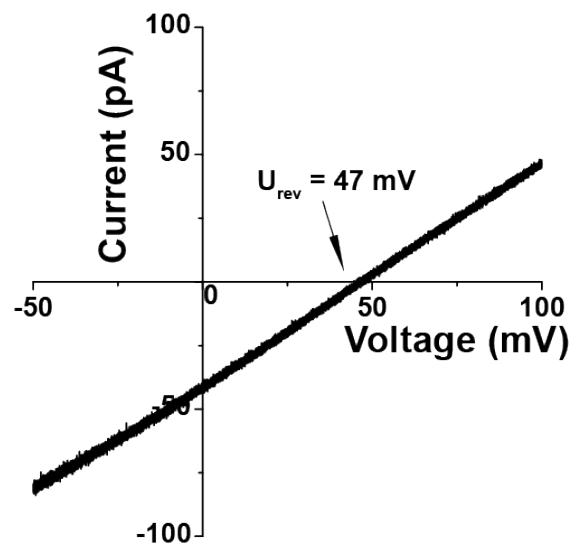


Figure 4.6: Voltage ramp of a Tim23 wild type channel at symmetric buffer conditions.

subconductance states were not increased with the same rate figure 4.8C.

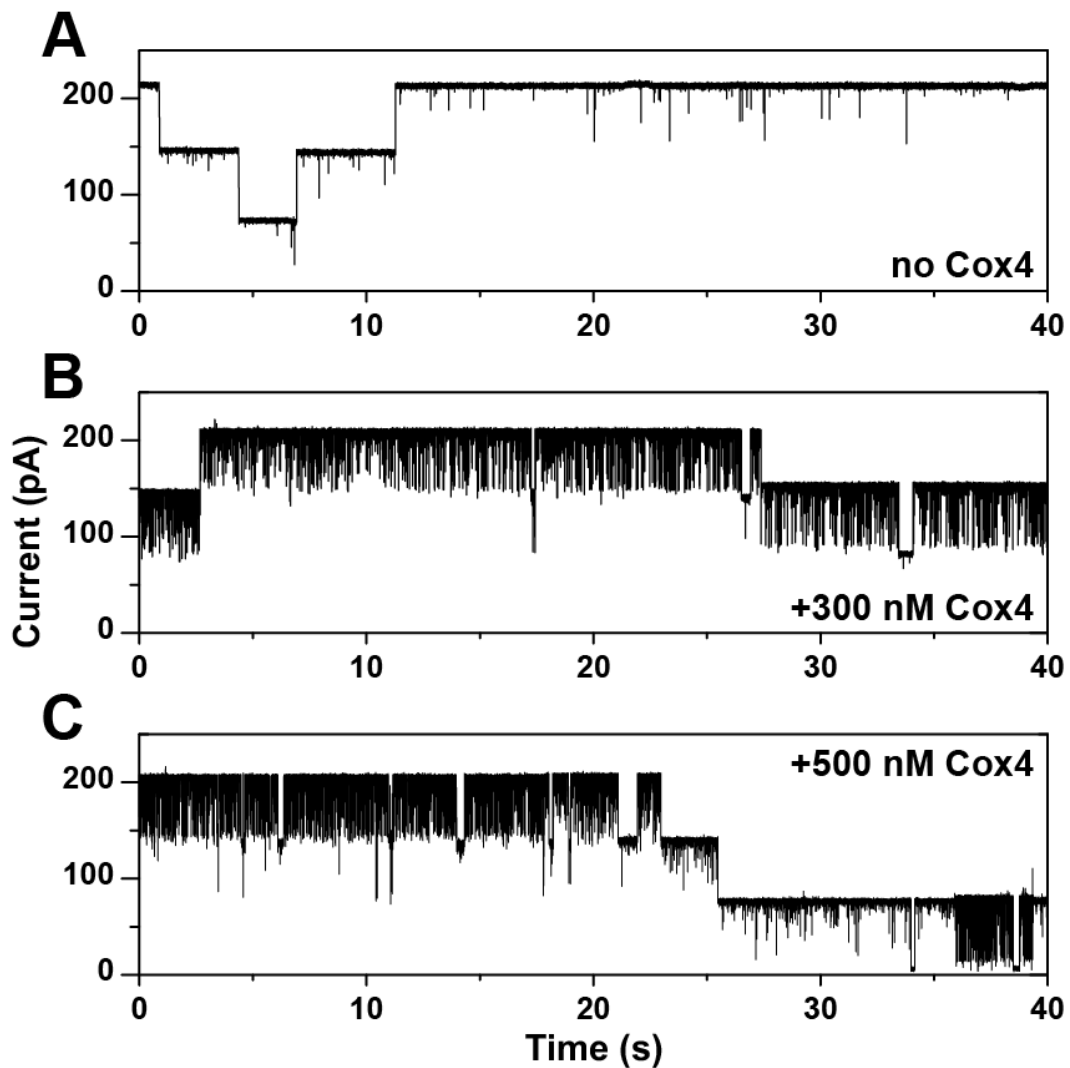


Figure 4.7: Current-recordings of incorporated Tim23 channels at 120 mV, with (A) no, (B) 300 nM or (C) 500 nM Cox4 added to the IMS side of Tim23.

The temporal dimension of Tim23 gating could yield important insight into the channel dynamics. The dwell times, i.e. residence times of the channel at specific conductances, before and after addition of the Cox4 presequence peptide were analyzed. Tim23 not activated with Cox4 showed a primarily open channel that was able to close for very short times. For calculation of the *regular minimal dwell time* per condition, the lowest 1% was excluded. This results in a regular

minimal dwell time of unstimulated Tim23 of 3.2×10^{-5} s (dashed black line in figure 4.8C). In the presence of 500 nM Cox4, gating frequency increased but the open conductance levels decreased slightly in the dwell time analysis, in line with the slight shift of the main conductance state peak in the gating event histogram (figure 4.8A). Despite the significant increase in gating events, the regular minimal dwell time of Cox4-stimulated Tim23 shifted to 5.6×10^{-5} s (dashed red line in figure 4.8C), though the majority of short dwell times (below 5×10^{-4} s) seems to peak not at constant values but proportional to the overall conductance of the occupied state (dash-dotted blue line in figure 4.8C). Even with a less strict view on regular minimal dwell time, short dwell times nearly exclusively occur for partially closed channels for unstimulated and even more so for stimulated Tim23. Data points of Tim23 and Tim23 plus Cox4, above $G = 1$ nS and in the peak area of short dwell times (grey box in figure 4.8C), were extracted and analyzed in a dwell time histogram (figure 4.9A) and fitted with a logarithmic normal distribution with peak center $x_c = (62 \pm 1) \mu\text{s}$ for unmanipulated Tim23 and $x_c = (184 \pm 2) \mu\text{s}$ for Tim23 plus Cox4 (mean \pm SD).

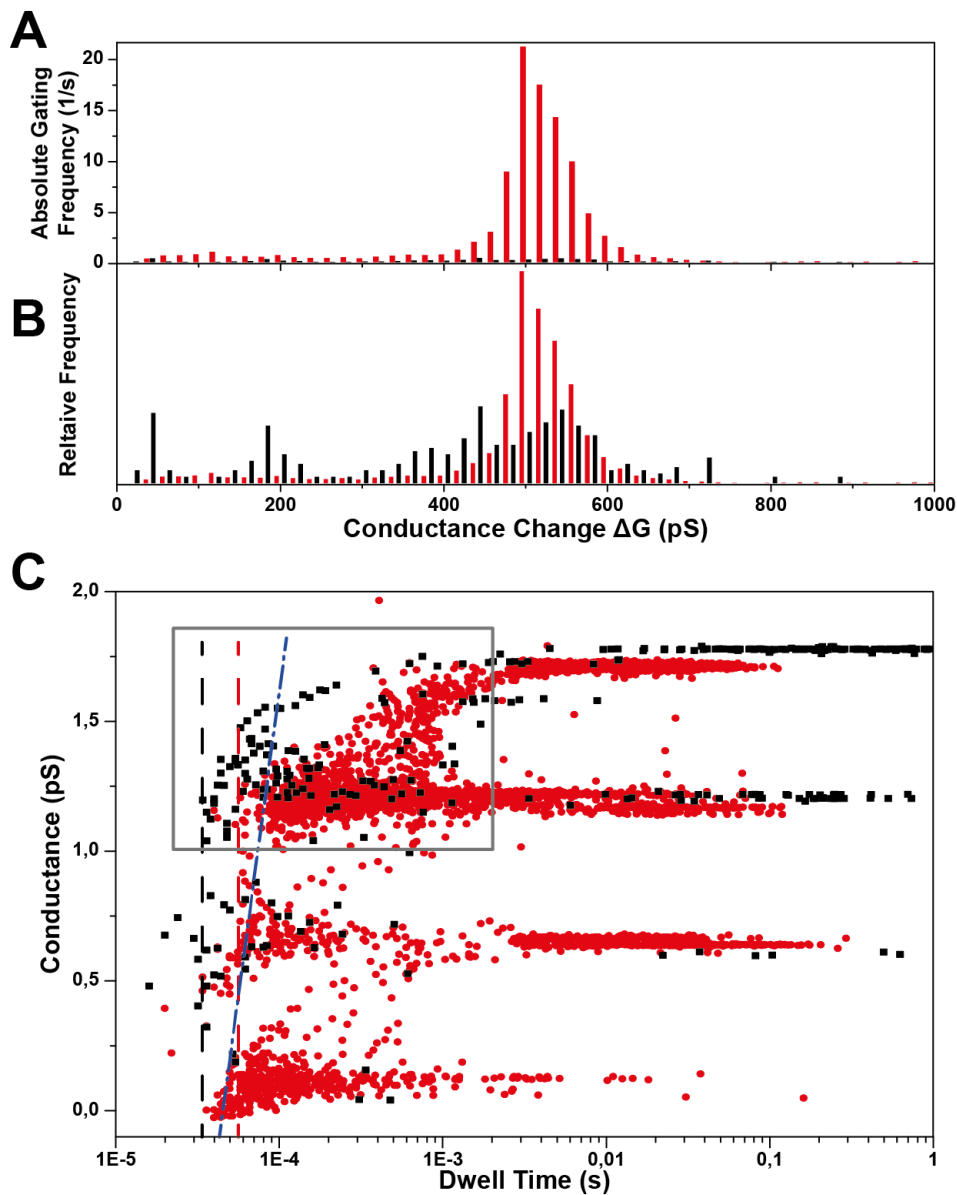


Figure 4.8: Cox4 induced increased gating activity in incorporated Tim23 channels, with no (black) or 500 nM (red) Cox4 added to the IMS side of Tim23. (A) Histogram of gating events per seconds per conductance change ΔG . (B) Histogram of normalized gating frequency. (C) Dwell times at different conductances. Regular minimal dwell time indicated with black dashed line for no Cox4 and red dashed line or blue dash-dotted line for 500 nM Cox4. Grey box marks data used for figure 4.9A. Three independent experiments per condition.

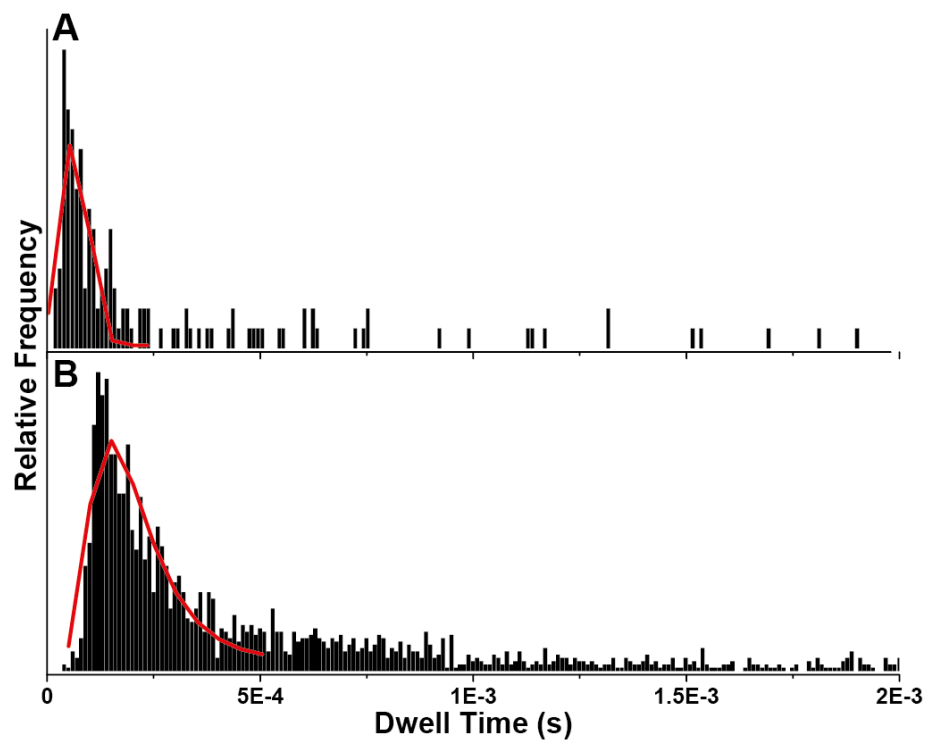


Figure 4.9: Dwell time histogram of the peak area marked in grey in figure 4.8C for Tim23 before (A) and after (B) addition of Cox4. Fit of logarithmic normal distribution in red.

4.2 Tim50_{core} Regulates Tim23 and Hands Over Preproteins

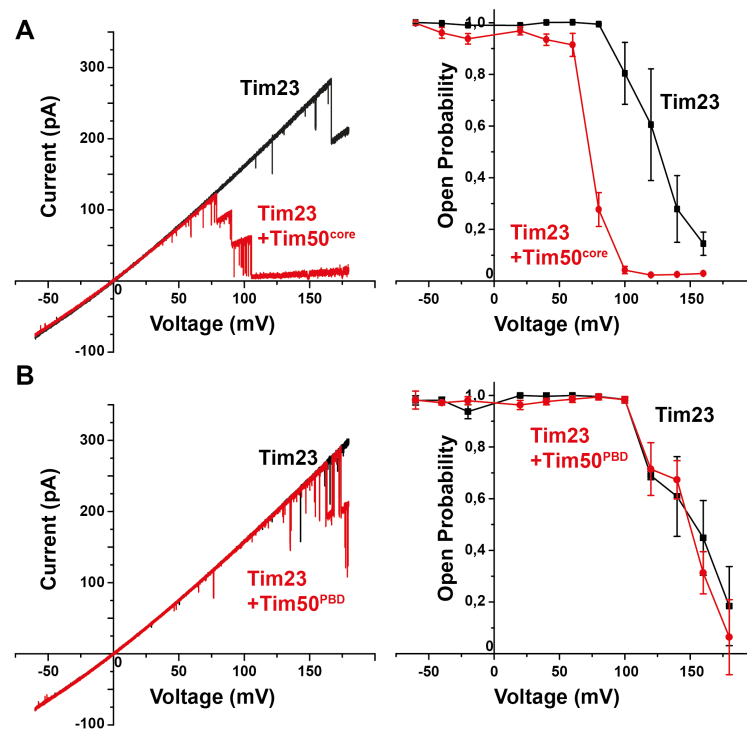
4.2.1 Voltage-Regulation by Tim50 Subdomains

To elucidate on the matter how molecular functions of the Tim50_{IMS} domain are distributed between its subdomains, we investigated the interaction between these subdomains and Tim23 with electrophysiological techniques. All three Tim50 constructs, Tim50^{IMS} (aa 132-476), Tim50^{PBD} (aa 395-476) and Tim50^{core} (aa 132-365), were purified and provided by Christian Schulz and Alexander Benjamin Schendzielorz (both AG Rehling, University Medical Center Göttingen), as described in Schulz et al.¹²¹.

As with wild type Tim23 and Tim50^{IMS} (see section 4.1.2), bilayer-incorporated Tim23 channels were characterized with voltage ramps and three full sets of constant voltage traces (60 s per voltage, from -60 mV to 140 mV in 20 mV steps). Then, Tim50^{core} or Tim50^{PBD} were added to the IMS-side of incorporated Tim23 channels with a final concentration of 730 nM before the buffer in each half-chamber was stirred and left to rest for two minutes each. After resting, a voltage ramp and another full set of traces was recorded.

Voltage ramps and open probabilities showed that Tim50^{core} was able to induce voltage-dependent closure in Tim23 channels (figure 4.10A), while Tim50^{PBD} did not induce any significant change in voltage ramps or open probability (figure 4.10B). Comparison with voltage-regulation by Tim50^{IMS} (figure 4.5) shows that no significant difference between voltage regulation by full IMS- and shorter core domain.

Figure 4.10: Voltage regulation of Tim23 by Tim50 subdomains investigated via voltage ramps and open probabilities. (A) Voltage ramps (left) and open probability (right) of Tim23 before (black) and after (red) addition of Tim50^{core} to the channels IMS side. (B) Voltage ramps (left) and open probability (right) of Tim23 before (black) and after (red) addition of Tim50^{PBD} to the channels IMS side. (n=3, mean±SD)



4.2.2 Presequence Handover to Tim23 by Tim50

After it was confirmed that the regulatory function of Tim50 does not require the presequence binding domain PBD, we attempted to reopen Tim23 channels that were previously closed by Tim50 subdomains by addition of Tim23 substrates. *In situ* additions of the presequence peptide Cox4 to bilayer-incorporated Tim23 did not lead to any reactivation of Tim50-closed channels in previous studies¹⁷⁰. Instead, in that study Tim23 channels were preincubated with Tim50 and Cox4 prior to bilayer fusion, leading to channel-reactivation. Such a preincubation approach does not offer studying the unmanipulated system to detect minor differences, hence we tested the full preprotein $b_2(167)_\Delta$ -DHFR instead of a short presequence peptide to reopen the channel *in situ*.

700 nM of the preprotein added to bilayer-incorporated Tim23 lead to a com-

bination of early closure and increased gating activity (figure 4.11A). When first 730 nM Tim50^{IMS} were added to the IMS side of Tim23 to induce closure before the preprotein was added to the same side, the channel was able to reopen partially (figure 4.11B) in a manner observed for Tim23 + b₂(167)_Δ-DHFR. Repeating the experiment with Tim50^{core} instead of Tim50^{IMS} again induced closure of Tim23 as observed before. Interestingly, the preprotein was again able to induce partial reopening of Tim23 (figure 4.11C) even when Tim50 lacks its PBD. Analysis of current recordings at a constant holding potential of 120 mV confirmed that the preprotein was reactivating Tim23 to a similar extent after Tim50^{IMS}- or Tim50^{core}-induced channel closure.

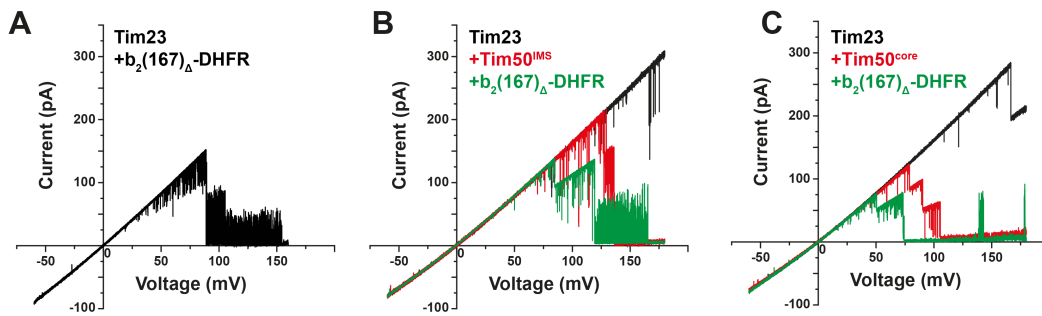


Figure 4.11: Voltage ramps of Tim23 reactivation by $b_2(167)_{\Delta}$ -DHFR after Tim50-induced closure. (A) Voltage ramp of Tim23 channel activation by $b_2(167)_{\Delta}$ -DHFR. (B)+(C) Voltage ramps of Tim23 channel activation by $b_2(167)_{\Delta}$ -DHFR after induced closing with Tim50^{IMS} (B) or Tim50^{core} (C).

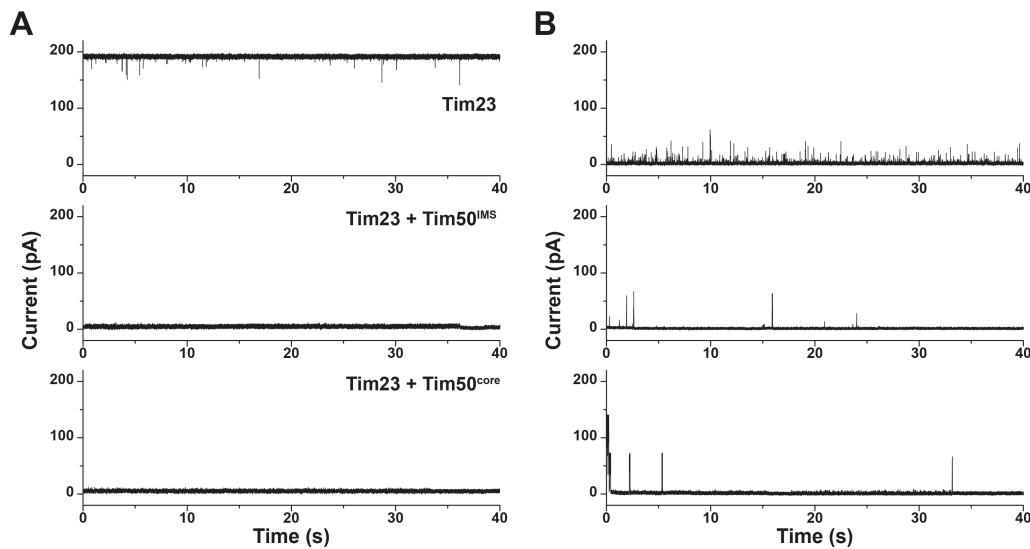


Figure 4.12: Tim23 traces with Tim50-induced closure at constant holding potentials. (A) Current traces of Tim23 at 120 mV without Tim50 (top) or closed by 730 nM Tim50^{IMS} (mid) or Tim50^{core}. (B) Current traces of channels shown in (A), but after addition of 700 nM $b_2(167)_{\Delta}$ -DHFR.

4.3 Conserved TMS2 Residues Constitute Ion Filter

4.3.1 Design and Expression of Tim23 Mutants

To uncover molecular mechanisms that control electrophysiological properties of Tim23 from *S. cerevisiae*, single amino acid residues were mutated in and next to the second transmembrane segment (TMS2) that was shown to closely interact with presequence peptides in transit¹⁷³. Selection of most of these residues was based on a previous identification of amino acids within the second alpha helix (residues 145 – 166) that face an aqueous environment¹⁷³. As these pore-lining residues were also highly conserved among many different species¹⁷⁴ (figure 4.13), we speculated that these residues could constitute specific electrophysiological properties, e.g. voltage sensor, gating hinge or ion filter. The choice of amino acid residues and their distribution on a helical wheel with one side facing the pore interior is depicted in figure 4.14. The residues were mutated to achieve a presumable loss-of-function by substitution with alanine (A), glycine (G). Additionally, G153L was selected as a mutation as it was shown earlier that it constitutes a lethal phenotype when expressed in baker's yeast¹⁹⁷. As A156 was shown to shift from a polar to a non-polar environment in the presence of substrate¹⁷³, the residue was also mutated to more hydrophobic leucine (L) and phenylalanine (F) to shift it from the polar channel lumen even in the rested state, which could impact channel constitution, presequence handling or channel gating. In addition to the TMS2 mutants, two highly conserved, charged residues flanking the third transmembrane segment (TMS3) were mutated. The negatively charged aspartic acid at position 174 at the matrix side and the positively charged lysine at position 190 at the IMS side of TMS3 (residues 175 – 189) were substituted with neutral alanine. These mutations were introduced as a starting point to investigate whether

TIM23_HUMAN	MEGGGGSGNKT-----	12
TIM23_RAT	MEGGGGSSNKST-----	12
TIM23_YEAST	MSWLFGDKTPTDDANAA-----VGGQDTTK-----PKELSLKQS	34
TIM23_DANRE	MDNSTPPPGGFK-----	12
TIM23_NEUCR	MSGLWNTLTGGNKKQQEQQEPAAPAPSAPQTTTTTTSAPSYSPFDASQP	50
	*.	
TIM23_HUMAN	GGLA----GF-FGAGGAGYSHADLAG-VPLTGMNPL-SPYLNVDPRYLVO	55
TIM23_RAT	GGLA----GF-FGAGGAGYSNADLAG-VPLTGMNPL-SPYLNVDPRYLVO	55
TIM23_YEAST	LGFEPNINNIISGPG---GMHVDTARLHPLAGLDKG-VEYLDLEEEQLSS	80
TIM23_DANRE	GGLG----SI-FGGGTPEYSNTELSG-VPLTGMSPL-SPYLNVDPRYLIO	55
TIM23_NEUCR	QGVE----AF-LGSS----SFADPTQLHPLAGLNKETLEYISLEDTPLED	91
	*. : * . . : : **:* . * : : * .	
	TMS1	
TIM23_HUMAN	DTD-EFILPTGANKTRGRFELAFFTIGGCCMTGAAFGAMNGLRLGLKETQ	104
TIM23_RAT	DTD-EFILPTGANKTRGRFELAFFTIGGCCMTGAAFGALNGLRLGLKETQ	104
TIM23_YEAST	LEGSQGLIP-----SRGWTDDL CYGTGAVYLLGLGIGGFSGMMQGLQNI	125
TIM23_DANRE	DTD-EFILPTGANKTRGRFELAFFTIGGCCITGAAFGTLNGLRMGLSETR	104
TIM23_NEUCR	AAG-ASVLP-----SRGFTDDL CYGTGITYLTALTIGGAWGLKEGLQRSA	135
	. : * : * : : * : . : * * : * * .	
	TMS2	
TIM23_HUMAN	NMAWSKPRNVQILNMVTRQGALWANTLGSLALLYSAFGVIEKTRGAEDD	154
TIM23_RAT	SMPWSKPRNVQILNMVTRQGALWANTLGSLALLYSAFGVIEKTRGAEDD	154
TIM23_YEAST	PNSPGKLQNLNTVLNHI TKRGPFLGNNAGILALSINIINSTIDALRGKHD	175
TIM23_DANRE	DMPWSKPRNVQILNMVTRQGASWANTLGSVALLYSVFGVAIEKARGAEDD	154
TIM23_NEUCR	GQP-PKLRNLSVNLNAVTRRGPYLGN SAGVVAICYNLINAGIGYVRGKHDA	184
	. * : : * * : * : * . * . * : * : * * . *	
	TMS3 TMS4	
TIM23_HUMAN	LNTVAAGTMTGMLYKCTGGLRGIARGGLTGLTLTSLYALYNNWEHMKGSL	204
TIM23_RAT	FNTVAAGTMTGMLYKCTGGLRGIARGGLAGLTLTSVYALYNNWEHMKGSL	204
TIM23_YEAST	AGSIGAGALTGALFKSSKGLKPMGYSSAMVAAACAVWCSVKKR-----L	219
TIM23_DANRE	LNTVAAGTLTGMVFKSTGGLKGVARGGLIGLAMSGLYALYNNWDHLKGKS	204
TIM23_NEUCR	ANSILAGALSGMLFKSTRGLKPMMSGGIVATIAGTWAVARRTF-PSPQF	233
	. : : * * : * * : * : * : : . . : . : . . .	
TIM23_HUMAN	LQQSL	209
TIM23_RAT	LQQSL	209
TIM23_YEAST	--LEK	222
TIM23_DANRE	-PSHY	208
TIM23_NEUCR	TNEVD	288

Figure 4.13: Sequence alignment of Tim23 from various species (Homo sapiens, Rattus norvegicus, Saccharomyces cerevisiae, Danio rerio, Neurospora crassa) calculated using ClustalW. Presumed transmembrane segments marked. Consensus: * identity; : high similarity; . low similarity

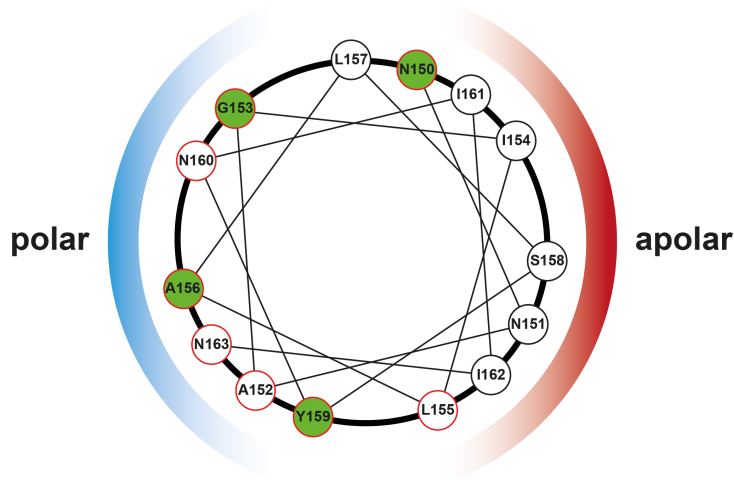


Figure 4.14: Helical wheel projection of Tim23's transmembrane segment 2 residues 150 to 163, with fully conserved residues marked in green. Polar and apolar facing sides are indicated with colored hemispheres, TMS2 residues mutated in this study are circled in red.

charges not inside but flanking the mostly neutral transmembrane helices could constitute or contribute to the channels ion filter.

All mutations were introduced to the wild type *ScTim23* gene on a pET10N vector for recombinant expression in *E. coli* by site-directed mutagenesis. After PCR, transformation into *E. coli* XLI-Blue competent cells, plasmid purification and sequencing, the isolated DNA was transformed into BL21 (DE3) competent cells, expressed and purified as described in section 4.1. Mariam Barbot (AG Meinecke, University Medical Center Göttingen) designed half of the mutants, performed the respective site-directed mutagenesis and expressed two mutants used in this study. Lennart Verseemann (AG Meinecke, University Medical Center Göttingen) assisted with expression and incorporation of several mutants in a lab rotation and his bachelor thesis, both under my supervision.

4.3.2 Electrophysiological Screening of Tim23 mutants

Recombinantly expressed and incorporated mutants of Tim23 were screened for altered electrophysiological properties using the planar lipid bilayer technique. Mariam Barbot (AG Meinecke, University Medical Center Göttingen) contributed

partial electrophysiological characterization of one mutant to this study. Lennart Versemann (AG Meinecke, University Medical Center Göttingen) assisted with the initial screening of several mutants in a lab rotation and his bachelor thesis, both under my supervision, and contributed partial electrophysiological characterization of five mutants to this study.

Gating Hinge

The general gating behavior of TMS2 mutants was studied by applying constant voltages, in 20 mV-steps between -60 mV to 140 mV, to bilayer-incorporated channels and current was recorded for 60 seconds (see figure 4.4A for wild type). Conductance changes were extracted from current recordings ($\Delta G = \Delta I/U$) and plotted in a histogram. From these histograms, the main conductance peak representing the full closing of a single of three pores, and the primary subconductance peak corresponding to the biggest semi-stable state, were modeled with a multiple Gauss fit for each mutant (table 4.1) to extract the main conductance state G_{main} and the primary subconductance state $G_{\text{sub},1}$. Mutant G_{main} and $G_{\text{sub},1}$ do not significantly differ from the wild type levels where $G_{\text{sub},1} = (461 \pm 31)$ pS and $G_{\text{sub},1} = (172 \pm 30)$ pS.

Voltage Sensor

Recombinant Tim23 contains an internal voltage sensor, as evidenced by its strong voltage-dependent gating behavior even in the absence of the *voltage regulator* Tim50^{167;170} (see section 4.1.2). While the IMS domain exhibits a $\Delta\Psi$ -dependent dimerization capability, Tim23 reacts to membrane potentials even in a truncated form, lacking the IMS domain¹⁷¹. This indicates that amino acid residues either in the transmembrane segments or in the loops between helices

contribute to the voltage sensor. To investigate if mutations in the conserved TMS2 residues alter the voltage sensitivity of recombinant Tim23, the open probability P_{open} was calculated from the constant-voltage recordings. In general, no significant difference between wild type and mutant Tim23 was found in how the channels reacted to increased membrane potentials (figure 4.15).

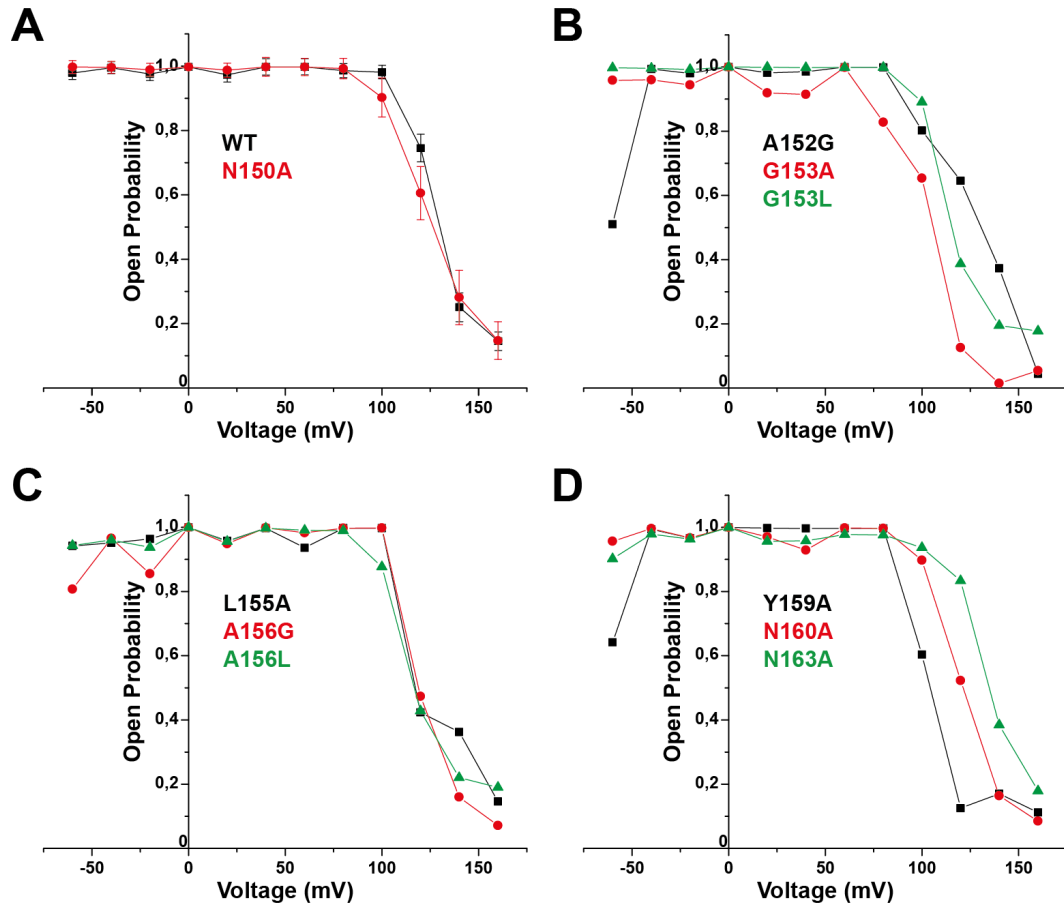


Figure 4.15: (A)-(D) Open probability of Tim23 mutants, and wild type as reference, from three (wild type and N150A) or one full set of constant-voltage traces.

Ion Filter

It is unknown how the ion filter of the channel protein Tim23 is constituted. Previous studies show that the C-terminal transmembrane part of Tim23 still ex-

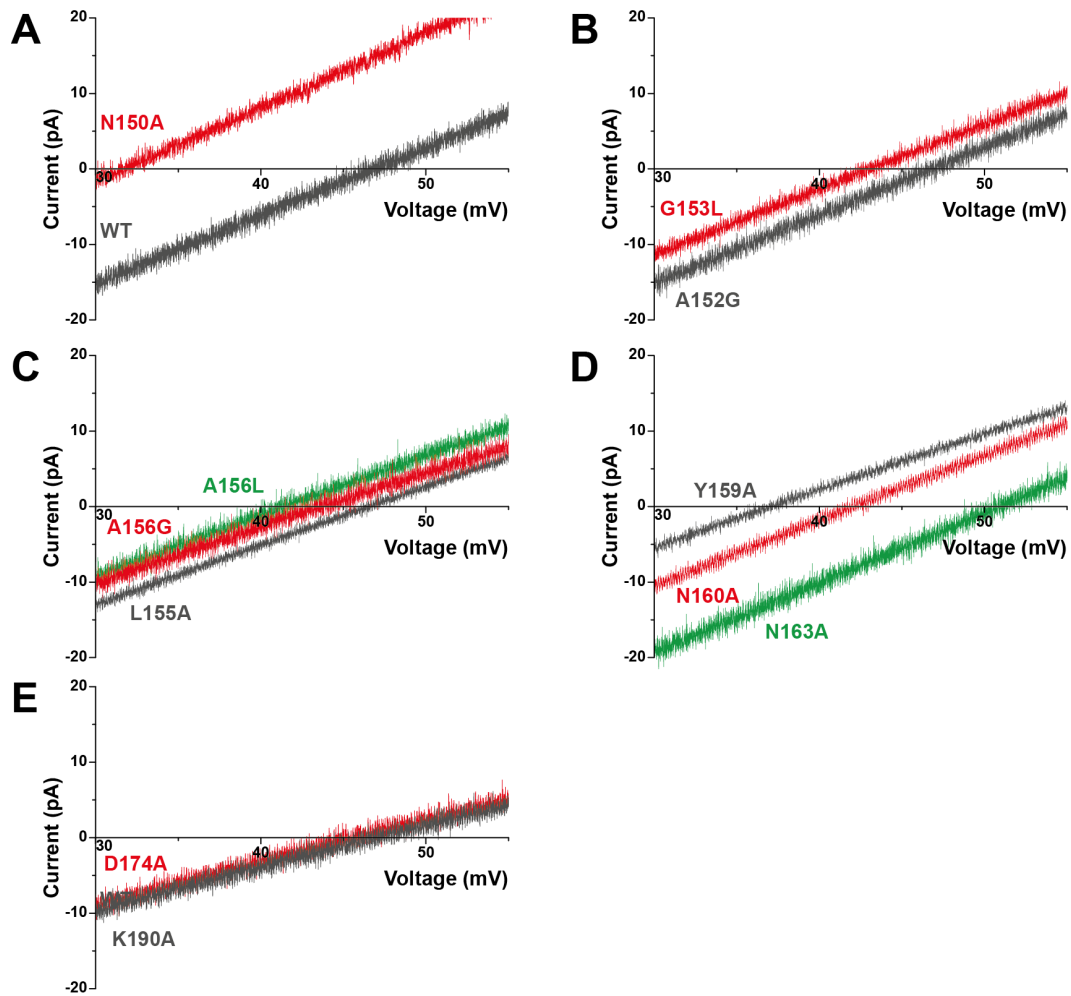


Figure 4.16: (A)-(E) Voltage ramps of Tim23 mutants, and wild type as reference, at asymmetric buffer conditions (250 mM:20 mM, 12.5-fold gradient).

hibits an ion preference, indicating that amino acid residues in the pore-forming transmembrane segments or the inter-helix loops facing IMS or matrix could constitute the ion filter. As with wild type Tim23, the ion selectivity of the mutant channels was assessed by recording a voltage ramp in the presence of a high salt gradient across the membrane, from 250 mM to 20 mM (figure 4.16). The reversal potentials of Tim23 were reduced for mutated residues 150, 153, 156, 159 (all highly conserved among species, see figure 4.13) and 160 (partially conserved among species). The cation preference $P_+ : P_-$ was calculated from the reversal potentials from three independent experiments each and was reduced by $\approx 30-50\%$ for most affected residues and over 65% for Tim23^{NI50A} (table 4.1). Remarkably, charge deletions at residues 174 and 190 flanking TMS3 did not lead to significant alteration of the ion selectivity. On the other hand, they exhibited a noteworthy reduction in fusion rates despite identical incorporation success as monitored by flotation and carbonate extraction, indicating that the charges might be required for proper protein folding or complex assembly. Both mutants were not considered in further studies.

Table 4.1: Main conductance state G_1 (pS), subconductance state G_2 (pS), reversal potential U_{rev} (mV) and the corresponding ion selectivity $P_+ : P_-$ of all investigated Tim23 mutants. Conductance states modeled from histograms using multiple Gauss fits (Peak center \pm SD). Reversal potential modeled from voltage ramps at asymmetric buffer conditions using linear regression (mean \pm SD). Ion selectivity calculated from mean reversal potential 12.5-fold KCl gradient using GHK-Equation.

Tim23 Mutant	G_1 (pS)	G_2 (pS)	U_{rev} (mV)	$P_+ : P_-$
WT	461 ± 31	172 ± 30	47.2 ± 0.4	13,3 : 1
NI50A	465 ± 55	181 ± 47	30.1 ± 0.7	4,4 : 1
AI52G	442 ± 113	168 ± 62	47.6 ± 1.3	13,7 : 1
GI53A	483 ± 50	122 ± 140	40.5 ± 1.8	8,1 : 1
GI53L	498 ± 31	174 ± 42	44.0 ± 1.2	10,4 : 1
LI55A	491 ± 83	209 ± 114	47.3 ± 1.0	13,4 : 1
AI56G	497 ± 60	178 ± 59	39.7 ± 1.6	7,7 : 1
AI56L	469 ± 29	165 ± 145	42.2 ± 1.7	9,1 : 1
YI59A	440 ± 121	198 ± 102	38.0 ± 1.4	6,9 : 1
NI60A	469 ± 126	154 ± 113	42.0 ± 1.2	9,0 : 1
NI63A	472 ± 131	192 ± 123	48.5 ± 1.9	14,8 : 1
DI74A			45.4 ± 1.3	11,5 : 1
KI90A			46.7 ± 2.3	12,7 : 1

4.3.3 Yeast Growth and Complex Integrity of Tim23 Mutants

In a close collaboration with Alexander Benjamin Schendzielorz (AG Rehling, University Medical Center Göttingen), we investigated if the observed alterations in electrophysiological properties, i.e. weakening of the ion filter, had implications for mitochondrial fitness in the yeast *S. cerevisiae*. To this end, the amino-acid substitutions in the second transmembrane segment were first introduced in the yeast plasmid expressing Tim23 wild type by site-directed mutagenesis, with the same primers as were used for mutagenesis of the pET10N-plasmid, and successful mutagenesis was monitored by plasmid sequencing. Half of the mutant plasmids were generated by me, the rest of the mutants and all further yeast handling and yeast experiments were performed by Alexander Benjamin Schendzielorz unless explicitly stated differently. All yeast experiments were performed as described in Denkert et al.¹⁹⁸.

S. cerevisiae cells with a chromosomal deletion of *TIM23* were complemented by a plasmid carrying both wild type *TIM23* and *URA3* genes. In normal medium, the cells survive by expressing Tim23 from the complementing plasmid. Yeast cells were transformed with a pRS413-plasmid containing *HIS3* gene as selective marker and either wild type or mutant *TIM23*. After transformation, yeast cells were plated on medium lacking histidine to select transformants that could grow on -His medium due to the *HIS3* gene. Transformants were further plated on medium containing 5-fluoroorotic acid (5-FOA), leading to *URA3*-induced loss of the *TIM23-URA3*-containing plasmid, to monitor Tim23 mutant ability to compensate for lack of wild type Tim23. Here, Tim23^{G153L} exhibited a lethal phenotype as published before¹⁹⁷. Complementing strains were grown on fermentable glucose and on non-fermentable glycerol at 18 °C, 30 °C or 37 °C. Four strains, ex-

pressing Tim23^{NI50A}, Tim23^{LI55A}, Tim23^{AI56L} or Tim23^{YI59A} respectively, showed a significant growth defect on glycerol at 37 °C, while Tim23^{NI50A} also lead to a mild growth defect on glucose at 37 °C (table 4.2).

To investigate the origin of impaired growth, mitochondria were isolated from yeast cells expressing Tim23 mutants or wild type and mitochondrial protein levels of Tim23 were quantified from independent triplicates and corrected by levels of Por1, an outer mitochondrial membrane porin. The mutants Tim23^{LI55A}, Tim23^{AI56L}, Tim23^{YI59A} or Tim23^{NI60A} have significantly reduced mitochondrial levels of the Tim23 protein figure 4.17A. In addition to reduced Tim23 levels, isolated TIM23 complexes

Table 4.2: *S. cerevisiae* strains expressing mutant forms of Tim23 were analyzed for growth on fermentable (glucose) and non-fermentable (glycerol) medium at different temperatures. Yeast handling was performed by Alexander Benjamin Schendzielorz.

Tim23	Glucose		Glycerol	
	30 °C	37 °C	30 °C	37 °C
WT	+	+	+	+
NI50A	+	-	+	--
A152G	+	+	+	+
G153A	+	+	+	+
LI55A	+	+	+	-
AI56G	+	+	+	+
AI56L	+	+	+	---
YI59A	+	+	+	--
NI60A	+	+	+	+
NI63A	+	+	+	+

from strains expressing Tim23^{AI56L} and Tim23^{YI59A} show reduced levels of both Tim17 and Tim50, determined by co-immunoprecipitation using antibodies against Tim23 (figure 4.17B). The wild type-like integrity of the inner membrane potential in Tim23^{NI50A}-containing mitochondria was confirmed by measuring the dequenching of the $\Delta\Psi$ -sensitive fluorophore DiSC₃(5) (figure 4.17C).

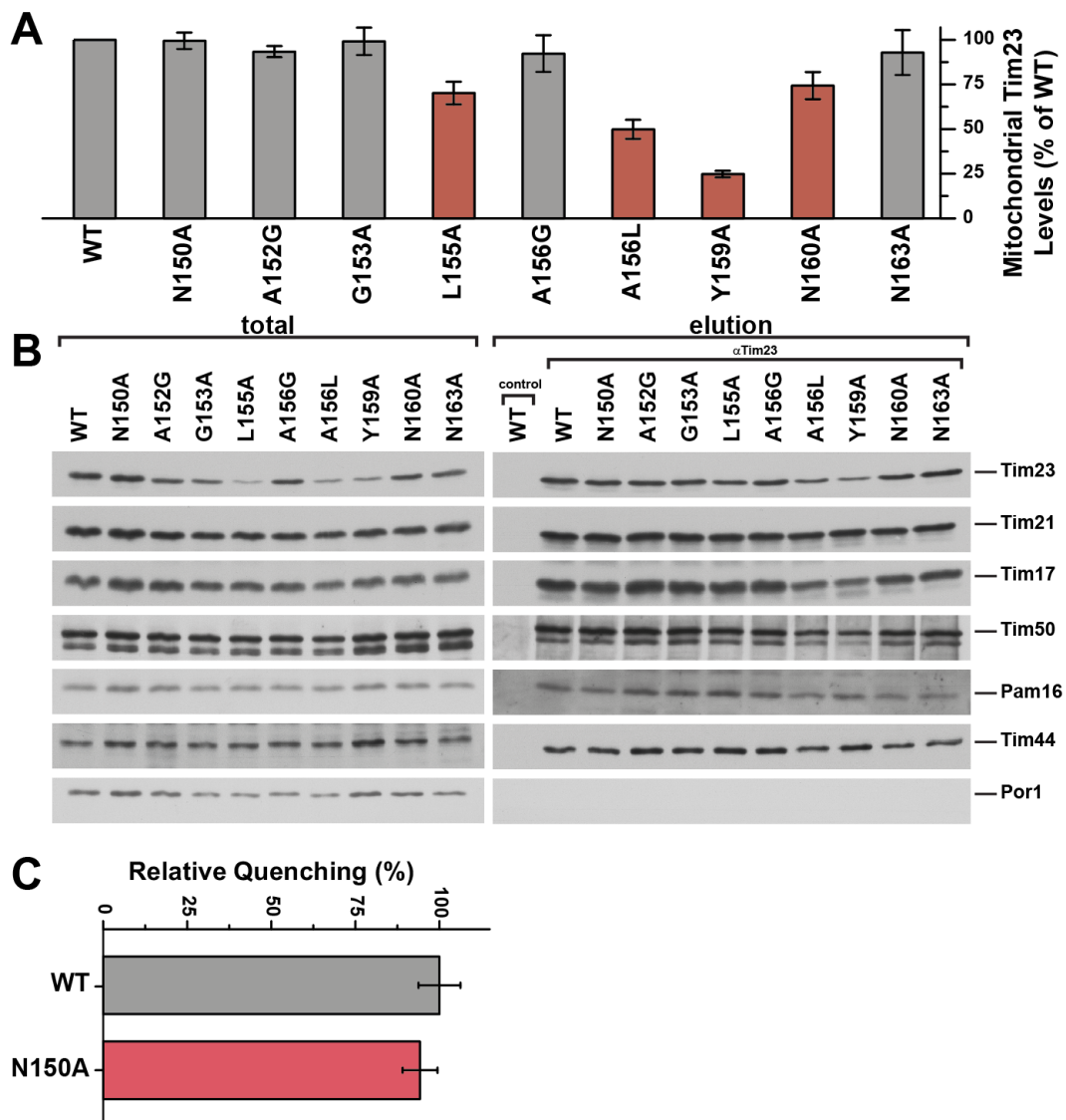


Figure 4.17: Protein levels, complex formation and membrane integrity were monitored for Tim23 mutant containing mitochondria. (A) Tim23 levels in mutant strain mitochondria were assessed by Western blot quantification normalized by Por1 levels from four independent experiments (mean \pm SD). (B) TIM23 complex formation and interaction in mutant mitochondria was analyzed by co-immunoprecipitation with Tim23 antibodies. (C) Relative inner mitochondrial membrane potential was calculated from triplicates by dequenching of $\Delta\Psi$ -sensitive fluorophore DiSC₃(5) for wild type and Tim23^{N150A} mitochondria. Figures were modified from Denkert et al.¹⁹⁸.

It can not be dissected if the growth defects observed for Tim23^{L155A}, Tim23^{A156L} and Tim23^{Y159A} originate exclusively from reduced protein levels and compromised TIM23 complexes or if altered electrophysiological characteristics also reduce mitochondrial fitness, even in intact and proper complexes. Tim23^{N150A}, on the other hand, showed a strong growth phenotype and the strongest reduction in ion selectivity, but was expressed and integrated into yeast mitochondria in wild type levels and maintained the full inner membrane potential.

To examine how Tim23^{N150A} could compromise mitochondrial fitness with wild type-like protein levels, complex integrity and membrane potential, we characterized protein import capabilities of mutant and wild type mitochondria. The matrix-destined substrates F₁β of the F₁F₀-ATP synthase, Cox4 of the cytochrome c oxidase and fusion protein b₂(167)_Δ-DHFR, and the inner membrane sorted fusion protein b₂(220)-DHFR, were translated with [³⁵S]-methionine in rabbit reticulocyte lysate and imported into isolated mitochondria. Tim23^{N150A}-containing mitochondria exhibit a reduced import capability for all substrates, as evidenced by import analysis after 10, 20 and 30 min at 30 °C (figure 4.18A). Import at 30 °C was quantified mid-time after 15 min in independent triplicates and indicated import reductions of Tim23^{N150A} by 30 to 40% of wild type levels. Note that import reduction of b₂(220)-DHFR at later time points becomes even more pronounced, compared to matrix targeted preproteins. Analysis of import kinetics of F₁β and Cox4 at non-permissive temperatures (figure 4.18C) revealed a stronger phenotype at later time points, i.e. a reduction to ≈ 50% of wild type levels after 30 min at 37 °C compared to 70 to 75% at 30 °C.

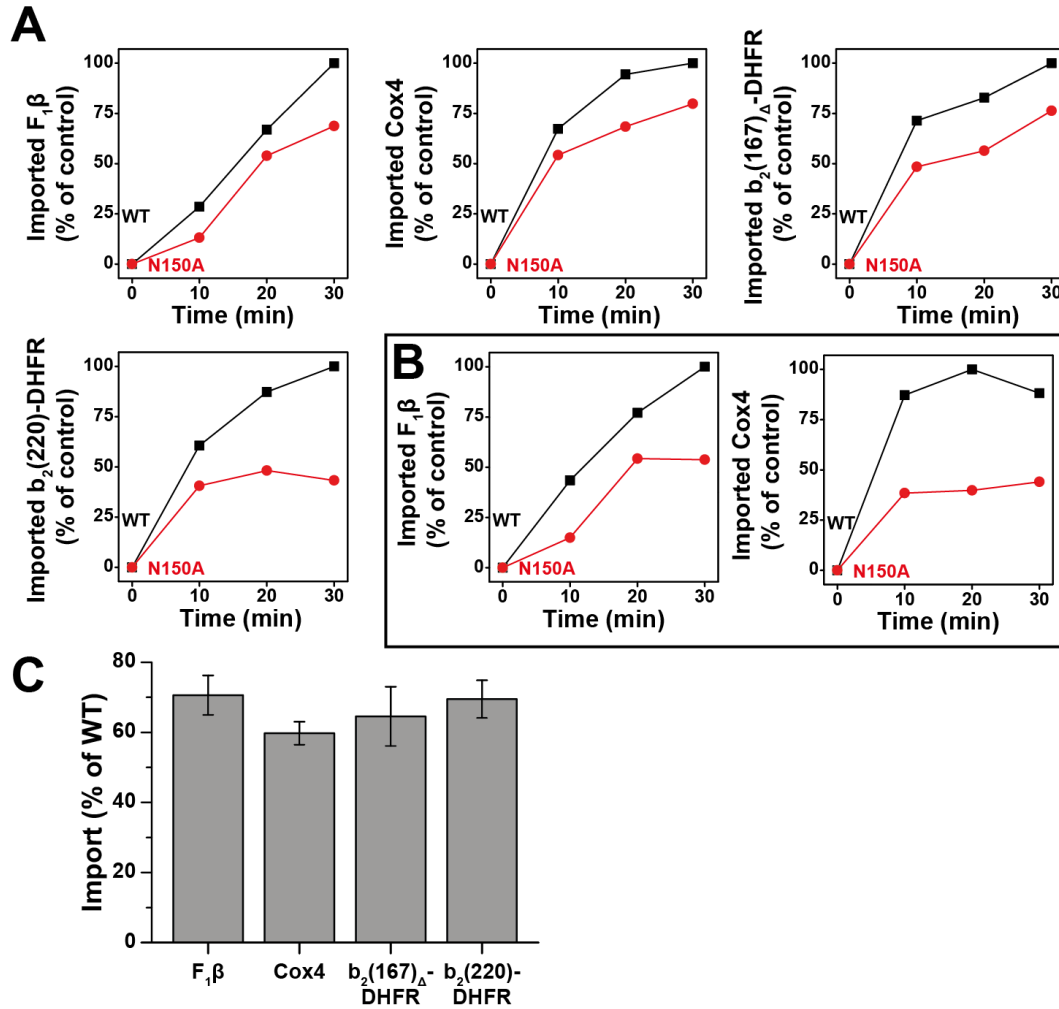


Figure 4.18: Import kinetics of various substrates were determined for wild type or Tim23^{N150A}-containing mitochondria at (A) 30 °C or (B) 37 °C. (C) Import efficiency after 15 min at 30 °C was quantified from independent triplicates ($n=3$, mean \pm SD). Figures were modified from Denkert et al.¹⁹⁸.

4.3.4 Presequence Titration of Cox4 to Tim23^{N150A} and Wild Type

After Tim23^{N150A} was identified as the only studied mutant with reduced ion selectivity, yeast growth defect and proper complex and membrane integrity, we showed that Tim23^{N150A} is importing significantly less preproteins in isolated mitochondria. Considering reduced protein import and the common assumption that cation preference of mitochondrial translocases might be directly connected to cationic presequences, we asked if Tim23^{N150A} exhibits an altered response to model presequences *in vitro*.

Before characterizing the presequence response of Tim23^{N150A}, the mutant was thoroughly characterized to avoid overlooking other alterations possibly responsible for impaired yeast growth or protein import, but neither detailed gating analysis (figures 4.19A to 4.19B) nor voltage-sensitivity with or without Tim50 (figure 4.19D) was altered compared to wild type. The only parameter that changed was the channel's ion selectivity (figure 4.19C).

In section 4.1, it was shown that the most obvious and striking response of Tim23 to the presequences peptide Cox4 is a drastic increase in gating activity. When Cox4 was titrated step-wise to the IMS side of Tim23^{N150A} or wild type and the buffers on each side are first stirred and then left to calm for two minutes, the presequence induced increased gating frequency similar to Tim23 wild type (figures 4.20A to 4.20C), though it appeared that the relative increase is weaker for the mutant channel. For Tim23 wild type, a higher rate of partial closing at elevated voltages was observed for stimulated compared to unstimulated channels. It can not be easily distinguished, if this increased voltage-sensitivity originates from the presequence effect or from stress effects due to prolonged exposure to repeatedly applied holding potentials. When the effects of presequence peptides

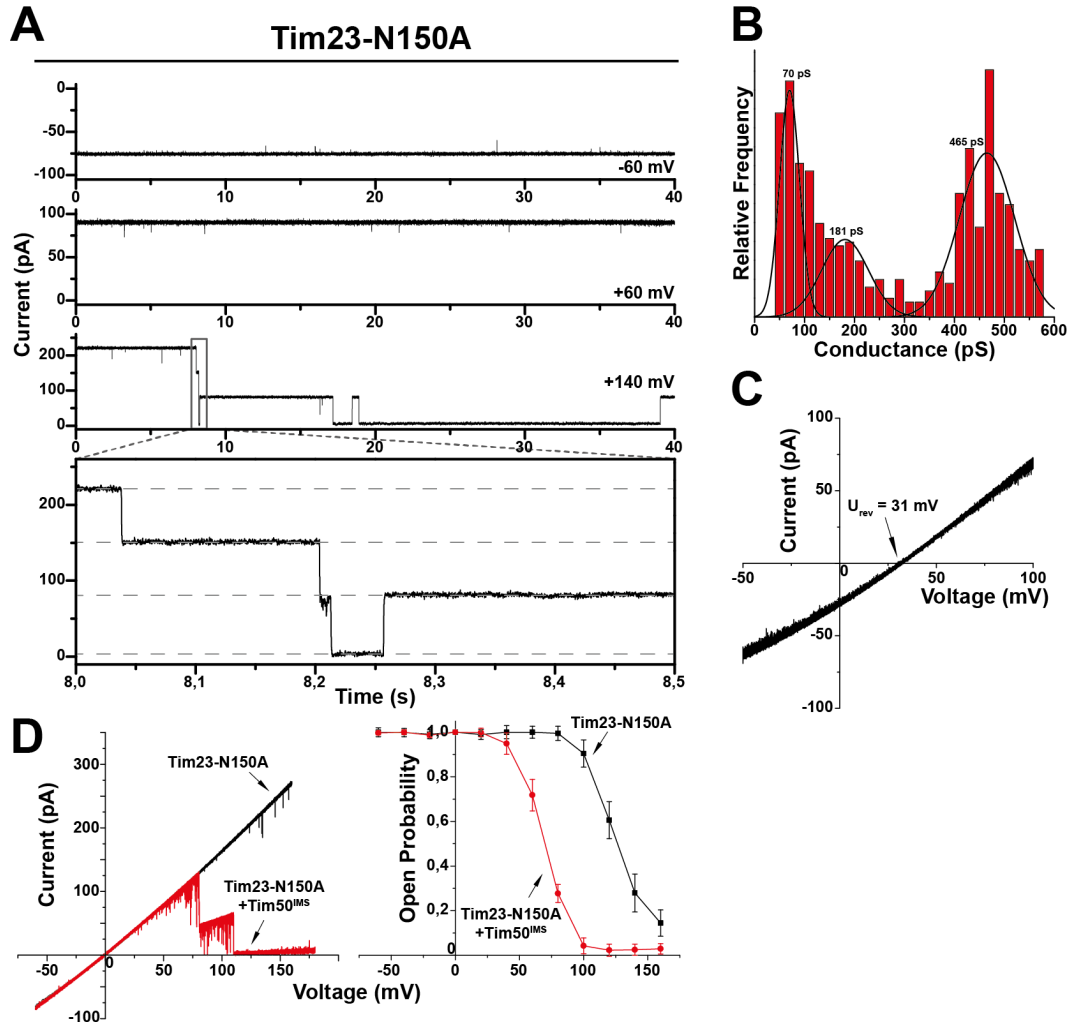


Figure 4.19: General gating analysis of Tim23^{N150A} (A) Constant-voltage recordings of Tim23^{N150A} and different holding potentials. (B) Histogram of over 2000 gating events with main and subconductance states fitted. (C) Asymmetric voltage ramp for reversal potential analysis of Tim23^{N150A}. (D) Current-voltage ramps (left) and open probabilities (right) of bilayer incorporated Tim23^{N150A} before (black) and after (red) addition of 700 nM Tim50^{IMS} to the IMS-side of the channel. (n=3, mean±SD). Figures were modified from Denkert et al.¹⁹⁸.

to gating frequency are to be analyzed in-depth, it is required that all pores of recombinant Tim23 remain open, and thus gating-capable, throughout the experimental process.

In an initial screening, the gating frequency of Tim23^{NI50A} at increasing Cox4 concentrations was analyzed at applied holding potentials of 80 mV, 100 mV and 120 mV figure 4.20D. While the relative gating increase was roughly proportional to the Cox4 concentration for recordings at 80 mV, this does not hold true for more elevated holding potentials. Both at 100 mV and 120 mV, the channel started to close at higher Cox4 concentrations (table 4.3), leading to less open and

Table 4.3: Open probability screening of stimulated Tim23^{NI50A} at different holding potentials.

[Cox4]	Open probability		
0 nM	0,998	0,991	0,984
300 nM	0,993	0,982	0,990
500 nM	0,99	0,982	0,957
700 nM	0,988	0,979	0,875
900 nM	0,97	0,825	0,805
	80	100	120
	Holding potential (mV)		

gating-capable pores and thus underestimation of the gating frequency. Therefore, the quantification of gating activity of Tim23^{NI50A} and wild type were performed at 80 mV only. Here, both Tim23 channel variants showed an increase in activity, roughly proportional to the Cox4 presequence concentration. The relative increase in Tim23 wild type exceeded factor 50 above 500 nM of Cox4, while, for Tim23^{NI50A}, the increase reached a plateau at approximately factor 5 (figure 4.20E). To exclude that this difference, by factor 10, between both channels originates from different gating activities of unstimulated channels, the absolute gating frequency was also analyzed, showing no significant difference between wild type and mutant Tim23 (figure 4.20F).

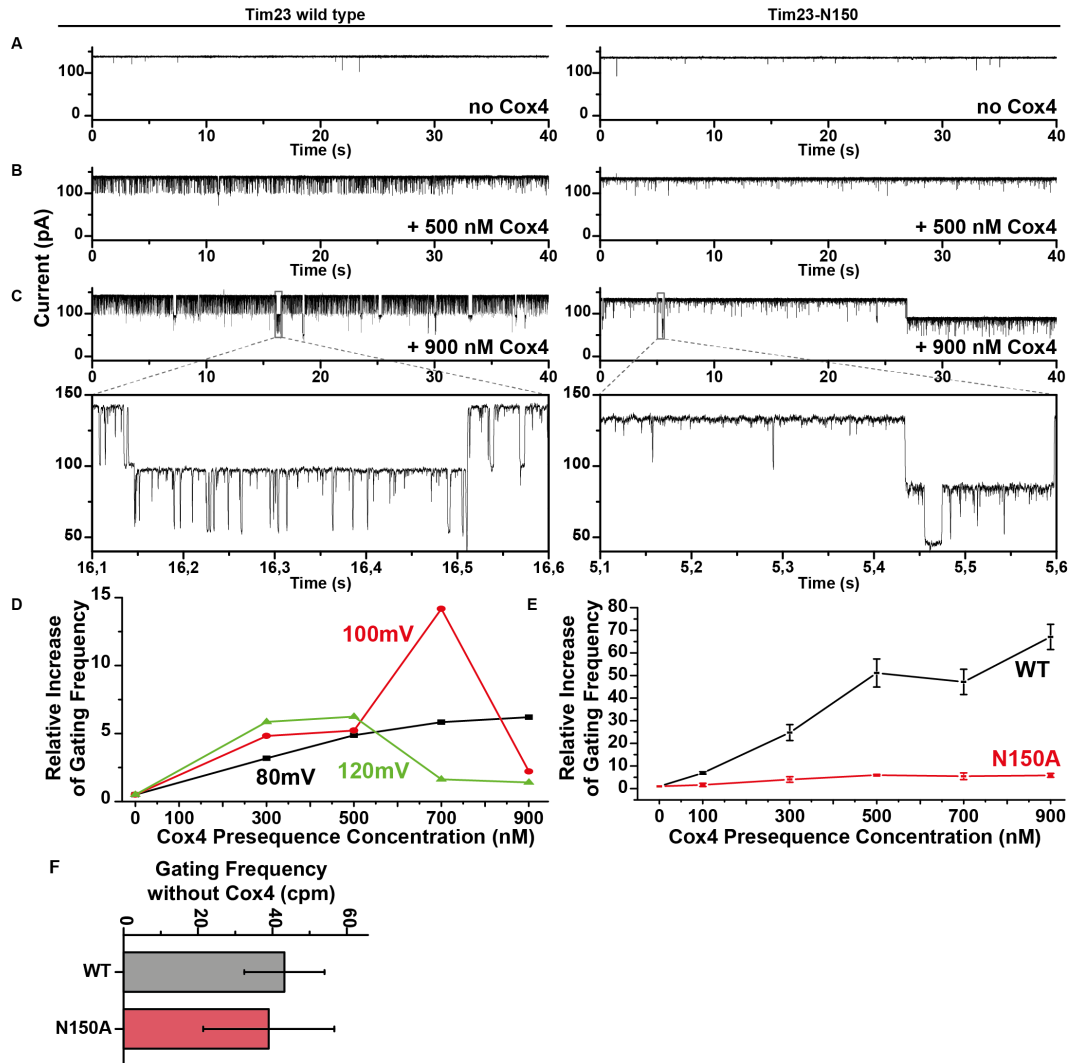


Figure 4.20: Gating frequency analysis of wild type and mutant Tim23 after stimulation with Cox4 presequence. (A)-(C) Constant-voltage recordings of Tim23 wild type (left) and Tim23^{N150A} (right) with no (A), 500 nM (B) or 900 nM (C) Cox4. (D) Voltage dependency of gating frequency development for Tim23^{N150A}. (E) Relative increase in gating frequency depending on Cox4 concentration for wild type (black) and mutant (red) Tim23 from independent triplicates (mean±SD). (F) Absolute gating frequency of unstimulated Tim23 variants (n=3, mean±SD). Figures were modified from Denkert et al.¹⁹⁸.

Chapter 5

Discussion

Tim23 is the eponymous pore-forming unit of the TIM23 translocon, the most complex protein translocation system of mitochondria. Alone, the subunit forms an aqueous pore with defined electrophysiological properties like voltage sensitivity, presequence activation or cation selectivity, that are also present to a similar extent in native TIM23 complexes¹⁶⁷. The molecular origin of Tim23's channel properties is unknown and studies investigating molecular or structural characteristics of the channel-part were often hindered by the difficulty of handling hydrophobic α -helical membrane proteins *in vitro*.

TIM23 utilizes the inner mitochondrial membrane potential $\Delta\Psi$ as the energy source for cationic presequence translocation. The IMS domain of main receptor Tim50 hands over preproteins from the mitochondrial intermembrane space to the channel Tim23, but also acts as the voltage regulator, closing the channel at physiological holding potentials to avoid leakage¹⁷⁰.

In this study, I employed high-resolution single-channel electrophysiology with recombinant Tim23 to investigate channel characteristics in detail, explore origins and implications of these properties using loss-of-function mutations and

dissect interactions with the main receptor Tim50.

Both recombinant Tim23 and isolated TIM23 complexes interact with substrates of the TIM23 pathway bearing positively charged presequences and incubation of the the channel with model peptides leads to stimulation and increased gating activity^{117;167;168;170}. Peptides with similar amino acid composition and identical charge but shuffled order of amino acids were not able to stimulate increased channel activity^{167;168}, indicating that secondary structure and charge alignment plays an important role in presequence recognition by Tim23.

5.1 Tim23 Kinetics Change upon Presequence Interaction

The presequence translocase TIM23 and the pore-forming subunit Tim23 were electrophysiologically characterized to some extent in the past^{117;167;168;170}. To enable reasonable analysis of Tim23 characteristics, e.g. between wild type and mutant channel or truncated forms of regulatory proteins, a detailed baseline of wild type properties had to be established in this thesis. While the general characteristics required for this thesis, like gating behavior, conductance states, ion preference or protein and peptide interactions, were consistent with published results, the aspect of temporal resolution of channel gating was not considered in previous studies.

Recently, studies on Tom40 substrate interaction showed that the process of substrate binding and translocation can be distinguished by analysis of kinetic gating parameters including dwell times of stimulated closing events in the sub-millisecond regime⁶³. A big difficulty in attempting to study channel kinetics at the resolution limit is that unified and consistent analysis and quantification parameters are hard to establish. In this study, sophisticated data reconstruction

tools capable of extracting channel properties like dwell times and conductance changes with unmatched consistency and reliability^{194;195} were employed and refined in collaboration. Using these computationally intensive routines, the time scale of Tim23 channel stimulation by presequence interaction was analyzed by extracting the dwell times, i.e. the time between two conductance changes, of short closing events. Unexpectedly, the minimal dwell time of these events increased after channel stimulation with presequence peptides which induced increased gating activity. Without substrate, regular short-timed events reached dwell times down to 32 μ s. After addition of the Cox4 presequence, the regular minimal dwell time nearly doubled to 56 μ s, although the majority of short events (below 500 μ s) peaked at a much higher dwell time, around 180 μ s.

If presequence incubation of Tim23 merely led to substrate binding to the IMS domain, randomized movement into and from the channel's opening funnel, or presequences being trapped within the channel lumen, the increased gating frequency should follow a similar temporal distribution as unstimulated channels. The data instead shows that presequences block the channel for a rather defined and increased amount of time, suggesting that they traverse the channel from one end to the other. It is tempting to apply this new kind of data analysis to study channel-substrate interaction of presequences with various properties like charge or length.

5.2 Tim50^{core} Regulates Tim23 and Hands Over Preproteins

The voltage regulator and main receptor Tim50 strongly interacts with Tim23 via their IMS domains. Tim50's IMS domain is subdivided into two distinct domains^{121;123;199}, the very C-terminal presequence binding domain (PBD) and the

more N-terminal, globular core domain. Both subdomains bind and properly recognize presequences with similar affinity than the full IMS domain¹²³. PBD and core domain interact with each other¹²⁴, though only the core domain also interacts with Tim23^{IMS}. Still, the core domain can not compensate for PBD-function, as evidenced by the lethal phenotype of Δ PBD-strains¹²¹. Further, Tim50^{IMS}-Tim23^{IMS} and Tim23^{IMS}-presequence interactions are mutually exclusive^{121;125}.

It is suggested that presequence translocation is first initiated by binding to the Tim50^{PBD} when Tim50^{core} is still bound to Tim23^{IMS}, effectively sealing the channel. Next, the presequence-loaded PBD interacts with the core domain and hands over the substrate due to a slightly higher affinity from core domain to presequence¹²³. Although the affinity of Tim23 towards substrates is orders of magnitudes lower¹²², Tim23^{IMS} binds the presequence while dissociating from Tim50^{IMS}. Possibly due to force exertion of the transmembrane potential, the presequence is then threaded into the channel and partially translocated to the matrix before full translocation or membrane sorting is initiated by PAM resp. Tim21/Mgr2.

The question arises why the PBD of Tim50 is essential, i.e. which function of Tim50^{IMS} can not be compensated for by Tim50^{core}. The function of Tim50^{core} was addressed in this study by first investigating the regulatory effect of soluble Tim50^{IMS}, Tim50^{PBD} or Tim50^{core} on voltage-sensitivity of bilayer-incorporated Tim23 channels. Tim50^{PBD} did not induce any premature closing of the channel at elevated voltages, as expected by the lack of interaction between Tim50^{PBD} and Tim23^{IMS}. Tim50^{core}, on the other hand, increased the voltage-sensitivity of the channel to the same extend as Tim50^{IMS}. The data confirms that the voltage regulator property of Tim50 resides in the Tim23-interacting core domain.

Second, the ability of Tim50^{core} to initiate presequence handover to Tim23 without the PBD was investigated. In early studies, the presequence model pep-

tide Cox4 was employed to study channel reactivation after Tim50-induced closing¹⁷⁰. It proved unsuccessful to lift Tim50 from bilayer-incorporated Tim23 by incubation with Cox4 *in situ*, but preincubation of Tim23 proteoliposomes, first with Tim50^{IMS} then with Cox4, lead to reactivation of some Tim23 channels. The downside is that no unmanipulated Tim23 can be characterization with this approach, making it difficult to assess differences between full length and truncated Tim50^{IMS}. In addition, it can never be ruled out that the channel that fused to the bilayer after preincubation was actually not closed by Tim50 before and directly bound Cox4. To compensate for that in this study, the model fusion preprotein b₂(167)_Δ-DHFR was employed instead of Cox4. After Tim50^{IMS}-induced closure of a channel, the full preprotein was able to reactivate Tim23 for very short times, mildly resembling the channel response to the preprotein without Tim50. One has to consider that this preprotein is translocated to the mitochondrial matrix *in vivo* which requires the PAM motor and ATP for full translocation. With only membrane potential, most likely the presequence is threaded through the channel, but the rest of the preprotein is stuck or might slide back. This explains the difference in channel response between presequence and preprotein, where the preprotein mostly leads to closure of the channel with attempts to reopen - the opposite of presequence stimulation.

Strikingly, closure of bilayer-incorporated Tim23 by Tim50^{core} followed by b₂(167)_Δ-DHFR incubation lead to the same reactivation attempts than with Tim50^{IMS}. This suggests that the PBD is not required to initiate presequence hand-over from Tim50 to Tim23.

The question whether the PBD is essential for initial presequence reception from the TOM complex was addressed in a previous study¹²³, where the presequence-triggered dissociation of Tim50 and Tim21 was investigated. Upon

binding of presequences to the main receptor, Tim50 dissociates from Tim21 which in turn leaves the TIM23 complex. Presequence reception was monitored indirectly via Tim50-Tim21 dissociation by cross-linking. The authors manipulated the mitochondria, e.g. by deleting the IMS domain of Tom22 which connects TOM to TIM23, or by gradually substituting Tim50^{IMS} with Tim50^{core}. Both manipulations only slightly reduced the level of dissociation, indicating that neither TIM23 link to TOM nor presence of Tim50^{PBD} are required for initial presequence reception.

It appears that Tim50^{PBD} has an essential function apart from voltage regulation, presequence handover or initial presequence recognition.

5.3 Tim23^{N150A} is Impaired in Presequence and Preprotein Translocation

Remarkably, all mitochondrial protein translocases exhibit an preference for cations in electrophysiological characterizations¹⁸⁹ and many mitochondrial targeting signals contain positive net charges⁵¹. The mitochondrial transmembrane potential $\Delta\Psi$ is required to import presequences and targeting signals via TIM23^{29;117}, not only by inducing structural changes in the translocase^{28;166;174} but also by interacting with the positive charges themselves, pulling them through the channel^{134;200;201}. It was speculated that the cation selectivity of TIM23 is important for presequence recognition and translocation, though experimental evidence was missing.

One contribution to the ion selectivity of Tim23 was identified by chance when the N-terminal IMS-domain of the protein was cleaved of and the remaining C-terminal membrane part was found to still form a channel, though with a

5.3. *TIM23^{N150A} IS IMPAIRED IN PRESEQUENCE AND PREPROTEIN TRANSLOCATION*⁹³

reduced cation preference¹⁶⁷. Another effect on the ion filter was identified when a negative charge was introduced in the transmembrane segment 3 at position 186¹⁶⁷, which lead to significantly weakened ion selectivity and even reduced pre-sequence affinity. On the other hand, it is not surprising that introduction of arbitrary charges in the middle of a transmembrane α -helix lead to alteration of channel properties and especially of a charge-specific process like ion selectivity. The authors of that study speculate^{167;171} that the ion filter might be formed by charges in helix-flanking loops or by pore-facing charges within the channel lumen or a combination of both.

In this study, the origin of pore properties like the ion filter was addressed by introducing presumed loss-of-function mutations in uncharged amino acid residues of the second transmembrane segment (TMS2) of Tim23. These residues were identified as pore-lining and substrate-interacting in previous sophisticated fluorophore-mapping studies^{173;174}. Additionally, for elucidation of the ion filter two highly conserved amino acid residues at positions 174 and 190, flanking the third transmembrane segment, were mutated to alanine to remove their respective charges. In an electrophysiological screening, the only property significantly altered was the ion selectivity of Tim23. Especially pore-facing TMS2-residues with very high sequence identity among species (figure 4.13) contributed to the strong cation preference.

It is remarkable that the charged residues flanking the TMS3 did not contribute to ion selectivity of the channel. This is in line with an experimental determination of Tim23's pore size using the globular non-electrolyte PEG¹⁶⁷, where Tim23 was found to contain wide channel openings at channel entry and exit and a short and narrow constriction zone within the channel. This would indicate that helix-flanking residues are farer from the channel center and are less able to

manipulate ions by pure charge exposure.

Interestingly, uncharged amino acid residues from the matrix end (N150) to the IMS side (N160) of the pore contribute to the ion filter. These results imply that it is not the narrow constriction zone of Tim23 that sorts ions, as was proposed for large, ion selective β -barrel channels²⁰²⁻²⁰⁴. It is tempting to speculate that the mode of ion filtering is shared at least with other large α -helical membrane channels, especially with homologs of the Tim17/22/23 family.

Most selectivity mutants also exhibited a growth defect when expressed in *tim23* Δ yeast cells. Unfortunately, apart from Tim23^{N150A}, the other ion filter mutants with a growth defect exhibited compromised mitochondrial steady state levels and consequently reduced TIM23 complex constitution, making it impossible to dissect contributions to their growth phenotype. Tim23^{G153A}, on the other hand, did not lead to impaired yeast growth despite showing a mediocre selectivity defect, indicating that a certain reduction in cation preference can be compensated for by the complex.

Tim23^{N150A} though showed the strongest reduction in ion selectivity, a growth phenotype at 37 °C, wild type-like protein levels and complex integrity and no other deviation from wild type Tim23 regarding electrophysiological properties. Import assays for wild type and N150A mutant with different TIM23 substrates revealed the reason for impaired cell growth, with Tim23^{N150A}-containing mitochondria exhibiting significantly reduced import capabilities for both matrix and sorted proteins, even more pronounced at non-permissive temperatures.

Titrating the Cox4 presequence to bilayer-incorporated channels lead to a highly reduced gating activity induction for mutant channels, from a relative increase in gating frequency of ≈ 50 for wild type, down to ≈ 5 for mutant channels in the presence of over 500 nM Cox4 presequence. We conclude that the reduced

5.3. *TIM23^{N150A} IS IMPAIRED IN PRESEQUENCE AND PREPROTEIN TRANSLOCATION* 95

cation preference of Tim23 renders the channel insensitive towards presequences, which in turn explains the reduced import rates of mitochondria.

It was unknown whether the increase in gating activity came from presequence binding to the IMS domain or the channel entry, or if it corresponds to presequence translocation, for which a transmembrane potential is sufficient. The mutated residue N150 lies at the very C-terminal end of TMS2, basically forming the channel exit towards the matrix. The effect it still has, on not only on import rates *in organello* but also on gating activity *in vitro*, strongly suggests that the flickering of Tim23 channels upon presequence incubation represents an actual translocation rather than pure binding on the IMS side.

Chapter 6

Summary and Conclusion

In eukaryotic cells, mitochondria are organelles that play an essential role in multiple physiological processes like energy metabolism, fatty acid oxidation or lipid synthesis. Mitochondria have a double-membrane envelope, dividing it into four different subcompartments, which are all targets of complex protein import machineries within the organelle. The most complex translocase in the organelle is the presequence translocase TIM23, importing over 70% of all mitochondrial proteins into the inner membrane or the matrix.

The eponymous subunit Tim23 forms a dynamic, water-filled pore within the complex, with a cation preference conserved among mitochondrial translocases. Tim23 interacts with presequences of import substrates, leading to increased channel activity, and with the receptor and voltage regulator Tim50 which induces channel closing at elevated membrane potentials.

In this thesis, combining single channel electrophysiology and site-directed mutagenesis, multiple pore-lining amino acid residues of Tim23 were identified as constituents of the channel's cation filter. Unlike proposed before, the ion fil-

ter can not be constituted by a localized constriction zone within the channel, but possibly by providing an energetically favorable or unfavorable surface pathway for ions, spanning the whole channel lumen. Combining electrophysiology and yeast biochemistry, we showed that the cation preference is a key property in recognizing and especially translocating positively charged presequences *in vitro* and preproteins *in organello*. High-resolution analysis of electrophysiology data further indicate that the presequence-induced fast-gating state of Tim23 presumably corresponds to a translocating state with peptides in transit.

Further, we investigated the domain origin for critical functions of the main receptor Tim50. We could show that both voltage regulation of, and presequence handover to Tim23 is independent of the essential presequence binding domain PBD but is localized in the soluble core domain of Tim50.

In conclusion, we provided the first experimental evidence that the cation preference of a mitochondrial protein translocase is linked to its ability to transport substrates with a positively charged presequence. We also elucidated the submolecular localization of essential interactions between receptor and channel of TIM23.

Bibliography

- [1] Bruce Alberts, Alexander Johnson, Julian Lewis, Martin Raff, Keith Roberts, and Peter Walter. *Molecular Biology of the Cell*. Garland Science, New York, 2002. ISBN 0-8153-3218-1.
- [2] Kim Bartlett and Simon Eaton. Mitochondrial beta-oxidation. *European journal of biochemistry*, 271(3):462–9, feb 2004. ISSN 0014-2956. URL <http://www.ncbi.nlm.nih.gov/pubmed/14728673>.
- [3] Johannes A. Mayr. Lipid metabolism in mitochondrial membranes. *Journal of Inherited Metabolic Disease*, 38(1):137–144, jan 2015. ISSN 0141-8955. doi: 10.1007/s10545-014-9748-x. URL <http://link.springer.com/10.1007/s10545-014-9748-x>.
- [4] Bruno Mesmin. Mitochondrial lipid transport and biosynthesis: A complex balance. *The Journal of Cell Biology*, 214(1):9–11, jul 2016. ISSN 0021-9525. doi: 10.1083/jcb.201606069. URL <http://www.jcb.org/lookup/doi/10.1083/jcb.201606069>.
- [5] Xuesong Liu, Caryn Naekyung Kim, Jie Yang, Ronald Jemmerson, and Xiaodong Wang. Induction of Apoptotic Program in Cell-Free Extracts: Requirement for dATP and Cytochrome c. *Cell*, 86(1):147–157, jul 1996. ISSN 00928674. doi: 10.1016/S0092-8674(00)80085-9. URL <http://linkinghub.elsevier.com/retrieve/pii/S0092867400800859>.
- [6] I. A. McNeish, S. Bell, T. McKay, T. Tenev, M. Marani, and N. R. Lemoine. Expression of Smac/DIABLO in ovarian carcinoma cells induces apoptosis via a caspase-9-mediated pathway. *Experimental Cell Research*, 286(2):186–198, jun 2003. ISSN 00144827. doi: 10.1016/S0014-4827(03)00073-9. URL <http://linkinghub.elsevier.com/retrieve/pii/S0014482703000739>.
- [7] Susan Elmore. Apoptosis: A Review of Programmed Cell Death. *Toxicologic Pathology*, 35(4):495–516, 2007. ISSN 01926233. doi: 10.1080/01926230701320337.
- [8] Daniel O. Daley, Keith L. Adams, Rachel Clifton, Svenja Qualmann, A. Harvey Millar, Jeffrey D. Palmer, Elke Pratje, and James Whelan. Gene transfer from mitochondrion to nucleus: Novel mechanisms for gene activation from Cox2. *Plant Journal*, 30(1):11–21, 2002. ISSN 09607412. doi: 10.1046/j.1365-313X.2002.01263.x.
- [9] Pavel Dolezal, Vladimir A. Likic, Jan Tachezy, and Trevor Lithgow. Evolution of the Molecular Machines for Protein Import into Mitochondria. *Science*, 313(5785):314–318, jul 2006. ISSN 0036-8075. doi: 10.1126/science.1127895. URL <http://www.ncbi.nlm.nih.gov/pubmed/16857931><http://www.sciencemag.org/cgi/doi/10.1126/science.1127895>.
- [10] S. Anderson, A. T. Bankier, B. G. Barrell, M. H. L. de Bruijn, A. R. Coulson, J. Drouin, I. C. Eperon, D. P. Nierlich, B. A. Roe, F. Sanger, P. H. Schreier, A. J. H. Smith, R. Staden, and I. G. Young. Sequence and organization of the human mitochondrial genome. *Nature*, 290(5806):457–465, apr 1981. ISSN 0028-0836. doi: 10.1038/290457a0. URL <http://www.nature.com/doi/10.1038/290457a0>.

- [11] M de Zamaroczy and Giorgio Bernardi. The primary structure of the mitochondrial genome of *Saccharomyces cerevisiae*—a review. *Gene*, 47(2-3):155–77, 1986. ISSN 0378-1119. URL <http://www.ncbi.nlm.nih.gov/pubmed/3549452>.
- [12] A Tzagoloff and a M Myers. Genetics of mitochondrial biogenesis. *Annual review of biochemistry*, 55: 249–285, 1986. ISSN 00664154. doi: 10.1146/annurev.biochem.55.1.249. URL <http://linkinghub.elsevier.com/retrieve/pii/S0092867400800859>.
- [13] Chris Meisinger, Albert Sickmann, and Nikolaus Pfanner. The Mitochondrial Proteome: From Inventory to Function. *Cell*, 134(1):22–24, jul 2008. ISSN 00928674. doi: 10.1016/j.cell.2008.06.043. URL <http://linkinghub.elsevier.com/retrieve/pii/S0092867408008301>.
- [14] Jan Dudek, Peter Rehling, and Martin van der Laan. Mitochondrial protein import: Common principles and physiological networks. *Biochimica et Biophysica Acta - Molecular Cell Research*, 1833(2): 274–285, 2013. ISSN 01674889. doi: 10.1016/j.bbamcr.2012.05.028. URL <http://dx.doi.org/10.1016/j.bbamcr.2012.05.028>.
- [15] Sanford M. Simon and Günter Blobel. A protein-conducting channel in the endoplasmic reticulum. *Cell*, 65(3):371–380, 1991. ISSN 00928674. doi: 10.1016/0092-8674(91)90455-8. URL <http://www.sciencedirect.com/science/article/pii/0092867491904558>.
- [16] Silke C. Hinnah, Kerstin Hill, Richard Wagner, Thomas Schlicher, and Jürgen Soll. Reconstitution of a chloroplast protein import channel. *EMBO Journal*, 16(24):7351–7360, 1997. ISSN 02614189. doi: 10.1093/emboj/16.24.7351.
- [17] Lisa Heins, Alexander Mehrle, Roland Hemmler, Richard Wagner, Michael Küchler, Friederike Hörmann, Dmitry Sveshnikov, and Jürgen Soll. The preprotein conducting channel at the inner envelope membrane of plastids. *EMBO Journal*, 21(11):2616–2625, 2002. ISSN 02614189. doi: 10.1093/emboj/21.11.2616.
- [18] Michael Meinecke, Christian Cizmowski, Wolfgang Schliebs, Vivien Krüger, Sabrina Beck, Richard Wagner, and Ralf Erdmann. The peroxisomal importomer constitutes a large and highly dynamic pore. *Nature Cell Biology*, 12(June 2009):273–277, feb 2010. ISSN 1465-7392. doi: 10.1038/ncb2027. URL <http://www.nature.com/doi/finder/10.1038/ncb2027>.
- [19] Sanford M. Simon and Günter Blobel. Signal peptides open protein-conducting channels in *E. coli*. *Cell*, 69:677–684, 1992. ISSN 00928674. doi: 10.1016/0092-8674(92)90231-Z.
- [20] O. Schneewind and D. M. Missiakas. Protein secretion and surface display in Gram-positive bacteria. *Philosophical Transactions of the Royal Society B: Biological Sciences*, 367(1592):1123–1139, 2012. ISSN 0962-8436. doi: 10.1098/rstb.2011.0210. URL <http://rstb.royalsocietypublishing.org/cgi/doi/10.1098/rstb.2011.0210>.
- [21] Michel Thieffry, Jean-Francois Chich, Denise Goldschmidt, and Jean-Pierre Henry. Incorporation in lipid bilayers of a large conductance cationic channel from mitochondrial membranes. *The EMBO journal*, 7(5):1449–54, 1988. ISSN 0261-4189. URL <http://www.pubmedcentral.nih.gov/articlerender.fcgi?artid=458395&tool=pmcentrez&rendertype=abstract>.
- [22] Klaus-Peter Künkele, Susanne Heins, Markus Dembowski, Frank E. Nargang, Roland Benz, Michel Thieffry, Jochen Walz, Roland Lill, Stephan Nussberger, and Walter Neupert. The preprotein translocation channel of the outer membrane of mitochondria. *Cell*, 93(6):1009–19, jun 1998. ISSN 0092-8674. URL <http://www.ncbi.nlm.nih.gov/pubmed/9635430>.
- [23] Kerstin Hill, Kirstin Model, Michael T. Ryan, Klaus Dietmeier, Falk Martin, Richard Wagner, and Nikolaus Pfanner. Tom40 forms the hydrophilic channel of the mitochondrial import pore for pre-proteins. *Nature*, 395(6701):516–521, oct 1998. ISSN 00280836. doi: 10.1038/26780. URL <http://www.ncbi.nlm.nih.gov/pubmed/9774109><http://www.nature.com/doi/finder/10.1038/26780>.

- [24] Peter J. T. Dekker, Petra Keil, Joachim Rassow, Ammy C. Maarse, Nikolaus Pfanner, and Michiel Meijer. Identification of MIM23, a putative component of the protein import machinery of the mitochondrial inner membrane. *FEBS Letters*, 330(1):66–70, 1993. ISSN 00145793. doi: 10.1016/0014-5793(93)80921-G.
- [25] A C Maarse, Jolanda Blom, Petra Keil, Nikolaus Pfanner, and Michiel Meijer. Identification of the essential yeast protein MIM17, an integral mitochondrial inner membrane protein involved in protein import. *FEBS Lett*, 349(2):215–221, 1994. URL <http://www.ncbi.nlm.nih.gov/pubmed/8050569>.
- [26] Michael Kübrich, Petra Keil, Joachim Rassow, Peter J. T. Dekker, Jolanda Blom, Michiel Meijer, and Nikolaus Pfanner. The polytopic mitochondrial inner membrane proteins MIM17 and MIM23 operate at the same preprotein import site. *FEBS Letters*, 349(2):222–228, aug 1994. ISSN 00145793. doi: 10.1016/0014-5793(94)00670-9. URL [http://doi.wiley.com/10.1016/0014-5793\(94\)00670-9](http://doi.wiley.com/10.1016/0014-5793(94)00670-9).
- [27] Jutta Berthold, Matthias F. Bauer, Hans-Christoph Schneider, Christian Klaus, Klaus Dietmeier, Walter Neupert, and Michael Brunner. The MIM complex mediates preprotein translocation across the mitochondrial inner membrane and couples it to the mt-Hsp70/ATP driving system. *Cell*, 81(7):1085–1093, 1995. ISSN 00928674. doi: 10.1016/S0092-8674(05)80013-3.
- [28] Matthias F. Bauer, Christian Sirrenberg, Walter Neupert, and Michael Brunner. Role of Tim23 as voltage sensor and presequence receptor in protein import into mitochondria. *Cell*, 87:33–41, 1996. ISSN 00928674. doi: 10.1016/S0092-8674(00)81320-3.
- [29] Christian Sirrenberg, Matthias F. Bauer, Bernard Guiard, Walter Neupert, and Michael Brunner. Import of carrier proteins into the mitochondrial inner membrane mediated by Tim22. *Nature*, 384(6609):582–5, 1996. ISSN 0028-0836. doi: 10.1038/384582a0. URL <http://www.ncbi.nlm.nih.gov/pubmed/8955274>.
- [30] Johannes M. Herrmann and Walter Neupert. Protein transport into mitochondria. *Current Opinion in Microbiology*, 3(2):210–214, 2000. ISSN 13695274. doi: 10.1016/S1369-5274(00)00077-1.
- [31] Doron Rapaport. Biogenesis of the mitochondrial TOM complex. *Trends in Biochemical Sciences*, 27(4):191–197, 2002. ISSN 09680004. doi: 10.1016/S0968-0004(02)02065-0.
- [32] Nils Wiedemann, Vera Kozjak, Agnieszka Chacinska, Birgit Schönfisch, Sabine Rospert, Michael T. Ryan, Nikolaus Pfanner, and Chris Meisinger. Machinery for protein sorting and assembly in the mitochondrial outer membrane. *Nature*, 424(6948):565–571, jul 2003. ISSN 00280836. doi: 10.1038/nature01753. URL <http://www.nature.com/doi/10.1038/nature01753>.
- [33] Vera Kozjak, Nils Wiedemann, Dusanka Milenkovic, Christiane Lohaus, Helmut E. Meyer, Bernard Guiard, Chris Meisinger, and Nikolaus Pfanner. An essential role of Sam50 in the protein sorting and assembly machinery of the mitochondrial outer membrane. *Journal of Biological Chemistry*, 278(49):48520–48523, 2003. ISSN 00219258. doi: 10.1074/jbc.C300442200.
- [34] Daigo Ishikawa, Hayashi Yamamoto, Yasushi Tamura, Kaori Moritoh, and Toshiya Endo. Two novel proteins in the mitochondrial outer membrane mediate β -barrel protein assembly. *The Journal of Cell Biology*, 166(5):621–627, aug 2004. ISSN 0021-9525. doi: 10.1083/jcb.200405138. URL <http://www.jcb.org/lookup/doi/10.1083/jcb.200405138>.
- [35] Thomas Waizenegger, Simone Schmitt, Jelena Zivkovic, Walter Neupert, and Doron Rapaport. Mim1, a protein required for the assembly of the TOM complex of mitochondria. *EMBO reports*, 6(1):57–62, 2005. ISSN 1469-221X. doi: 10.1038/sj.embor.7400318.
- [36] Jelena Popov-Čeleketić, Thomas Waizenegger, and Doron Rapaport. Mim1 Functions in an Oligomeric Form to Facilitate the Integration of Tom20 into the Mitochondrial Outer Membrane. *Journal of Molecular Biology*, 376(3):671–680, 2008. ISSN 00222836. doi: 10.1016/j.jmb.2007.12.006.

- [37] Joanne M. Hulett, Franziska Lueder, Nickie C. Chan, Andrew J. Perry, Peter Wolyneec, Vladimir A. Likic, Paul R. Gooley, and Trevor Lithgow. The Transmembrane Segment of Tom20 Is Recognized by Mim1 for Docking to the Mitochondrial TOM Complex. *Journal of Molecular Biology*, 376(3):694–704, 2008. ISSN 00222836. doi: 10.1016/j.jmb.2007.12.021.
- [38] Dražen Papić, Katrin Krumpe, Jovana Dukanovic, Kai S. Dimmer, and Doron Rapaport. Multispan mitochondrial outer membrane protein Ugo1 follows a unique Mim1-dependent import pathway. *Journal of Cell Biology*, 194(3):397–405, 2011. ISSN 00219525. doi: 10.1083/jcb.201102041.
- [39] Thomas Becker, Lena-Sophie Wenz, Vivien Krüger, Waltraut Lehmann, Judith M. Müller, Luise Goroncy, Nicole Zufall, Trevor Lithgow, Bernard Guiard, Agnieszka Chacinska, Richard Wagner, Chris Meisinger, and Nikolaus Pfanner. The mitochondrial import protein Mim1 promotes biogenesis of multispanning outer membrane proteins. *Journal of Cell Biology*, 194(3):387–395, 2011. ISSN 00219525. doi: 10.1083/jcb.201102044.
- [40] Dionisia P. Sideris, Nikos Petrakis, Nitsa Katrakili, Despina Mikropoulou, Angelo Gallo, Simone Ciofi-Baffoni, Lucia Banci, Ivano Bertini, and Kostas Tokatlidis. A novel intermembrane space-targeting signal docks cysteines onto Mia40 during mitochondrial oxidative folding. *Journal of Cell Biology*, 187(7):1007–1022, 2009. ISSN 00219525. doi: 10.1083/jcb.200905134.
- [41] Dusanka Milenkovic, Thomas Ramming, Judith M. Müller, Lena-Sophie Wenz, Natalia Gebert, Agnes Schulze-Specking, Diana Stojanovski, Sabine Rospert, and Agnieszka Chacinska. Identification of the Signal Directing Tim9 and Tim10 into the Intermembrane Space of Mitochondria. *Molecular Biology of the Cell*, 20(10):2530–2539, may 2009. ISSN 1059-1524. doi: 10.1091/mbc.E08-11-1108. URL <http://www.molbiolcell.org/cgi/doi/10.1091/mbc.E08-11-1108>.
- [42] Agnieszka Chacinska, Sylvia Pfannschmidt, Nils Wiedemann, Vera Kozjak, Luiza K Sanjuán Szklarz, Agnes Schulze-Specking, Kaye N. Truscott, Bernard Guiard, Chris Meisinger, and Nikolaus Pfanner. Essential role of Mia40 in import and assembly of mitochondrial intermembrane space proteins. *The EMBO Journal*, 23(19):3735–3746, sep 2004. ISSN 0261-4189. doi: 10.1038/sj.emboj.7600389. URL <http://www.pubmedcentral.nih.gov/articlerender.fcgi?artid=522791&tool=pmcentrez&rendertype=abstracthttp://emboj.emboipress.org/cgi/doi/10.1038/sj.emboj.7600389>.
- [43] Mari Naoe, Yukimasa Ohwa, Daigo Ishikawa, Chie Ohshima, Shuh-ichi Nishikawa, Hayashi Yamamoto, and Toshiya Endo. Identification of Tim40 That Mediates Protein Sorting to the Mitochondrial Intermembrane Space. *Journal of Biological Chemistry*, 279(46):47815–47821, nov 2004. ISSN 0021-9258. doi: 10.1074/jbc.M410272200. URL <http://www.jbc.org/cgi/doi/10.1074/jbc.M410272200>.
- [44] Nikola Mesecke, Nadia Terziyska, Christian Kozany, Frank Baumann, Walter Neupert, Kai Hell, and Johannes M. Herrmann. A disulfide relay system in the intermembrane space of mitochondria that mediates protein import. *Cell*, 121(7):1059–1069, 2005. ISSN 00928674. doi: 10.1016/j.cell.2005.04.011.
- [45] Kai Hell, Johannes M. Herrmann, Elke Pratje, Walter Neupert, and Rosemary A. Stuart. Oxalp, an essential component of the N-tail protein export machinery in mitochondria. *Proceedings of the National Academy of Sciences*, 95(5):2250–2255, mar 1998. ISSN 0027-8424. doi: 10.1073/pnas.95.5.2250. URL <http://www.pnas.org/content/95/5/2250><http://www.ncbi.nlm.nih.gov/pubmed/9482871><http://www.pnas.org/content/95/5/2250.full.pdf><http://www.pnas.org/content/95/5/2250.long><http://www.pnas.org/cgi/doi/10.1073/pnas.95.5.2250>.
- [46] Gregor Szyrach, Martin Ott, Nathalie Bonnefoy, Walter Neupert, and Johannes M. Herrmann. Ribosome binding to the Oxal complex facilitates co-translational protein insertion in mitochondria. *EMBO Journal*, 22(24):6448–6457, 2003. ISSN 02614189. doi: 10.1093/emboj/cdg623.

- [47] Maria Bohnert, Peter Rehling, Bernard Guiard, Johannes M. Herrmann, Nikolaus Pfanner, and Martin Van Der Laan. Cooperation of stop-transfer and conservative sorting mechanisms in mitochondrial protein transport. *Current Biology*, 20(13):1227–1232, 2010. ISSN 09609822. doi: 10.1016/j.cub.2010.05.058. URL <http://dx.doi.org/10.1016/j.cub.2010.05.058>.
- [48] Markus Hildenbeutel, Melanie Theis, Melanie Geier, Ilka Haferkamp, H. Ekkehard Neuhaus, Johannes M. Herrmann, and Martin Ott. The Membrane Insertase Oxal Is Required for Efficient Import of Carrier Proteins into Mitochondria. *Journal of Molecular Biology*, 423(4):590–599, nov 2012. ISSN 00222836. doi: 10.1016/j.jmb.2012.07.018. URL <http://dx.doi.org/10.1016/j.jmb.2012.07.018><http://linkinghub.elsevier.com/retrieve/pii/S0022283612005852>.
- [49] Uwe Ahting, Clemens Thun, Reiner Hegerl, Dieter Typke, Frank E. Nargang, Walter Neupert, and Stephan Nussberger. The Tom Core Complex. *The Journal of Cell Biology*, 147(5):959–968, nov 1999. ISSN 0021-9525. doi: 10.1083/jcb.147.5.959. URL <http://www.jcb.org/lookup/doi/10.1083/jcb.147.5.959>.
- [50] Kirstin Model, Thorsten Prinz, Teresa Ruiz, Michael Radermacher, Thomas Krimmer, Werner Kühlbrandt, Nikolaus Pfanner, and Chris Meisinger. Protein translocase of the outer mitochondrial membrane: role of import receptors in the structural organization of the TOM complex. *Journal of Molecular Biology*, 316(3):657–66, 2002. ISSN 0022-2836. doi: 10.1006/jmbi.2001.5365. URL <http://www.ncbi.nlm.nih.gov/pubmed/11866524>.
- [51] Agnieszka Chacinska, Carla M. Koehler, Dusanka Milenkovic, Trevor Lithgow, and Nikolaus Pfanner. Importing Mitochondrial Proteins: Machineries and Mechanisms. *Cell*, 138:628–644, 2009. ISSN 00928674. doi: 10.1016/j.cell.2009.08.005.
- [52] Jovana Dukanovic and Doron Rapaport. Multiple pathways in the integration of proteins into the mitochondrial outer membrane. *Biochimica et Biophysica Acta - Biomembranes*, 1808(3):971–980, 2011. ISSN 00052736. doi: 10.1016/j.bbamem.2010.06.021. URL <http://dx.doi.org/10.1016/j.bbamem.2010.06.021>.
- [53] Uwe Ahting, Michel Thieffry, Harald Engelhardt, Reiner Hegerl, Walter Neupert, and Stephan Nussberger. Tom40, the Pore-Forming Component of the Protein-Conducting Tom Channel in the Outer Membrane of Mitochondria. *The Journal of Cell Biology*, 153(6):1151–1160, jun 2001. ISSN 0021-9525. doi: 10.1083/jcb.153.6.1151. URL <http://www.jcb.org/lookup/doi/10.1083/jcb.153.6.1151>.
- [54] Kirstin Model, Chris Meisinger, and Werner Kühlbrandt. Cryo-Electron Microscopy Structure of a Yeast Mitochondrial Preprotein Translocase. *Journal of Molecular Biology*, 383(5):1049–1057, nov 2008. ISSN 00222836. doi: 10.1016/j.jmb.2008.07.087. URL <http://linkinghub.elsevier.com/retrieve/pii/S0022283608009674>.
- [55] Thomas Bausewein, Deryck J. Mills, Julian D. Langer, Beate Nitschke, Stephan Nussberger, and Werner Kühlbrandt. Cryo-EM Structure of the TOM Core Complex from *Neurospora crassa*. *Cell*, 170(4):693–700.e7, 2017. ISSN 10974172. doi: 10.1016/j.cell.2017.07.012.
- [56] Sandra van Wilpe, Michael T. Ryan, Kerstin Hill, Ammy C. Maarse, Chris Meisinger, Jan Brix, Peter J. T. Dekker, Martin Moczko, Richard Wagner, Michiel Meijer, Bernard Guiard, Angelika Hönlinger, and Nikolaus Pfanner. Tom22 is a multifunctional organizer of the mitochondrial preprotein translocase. *Nature*, 401(6752):485–489, sep 1999. ISSN 00280836. doi: 10.1038/46802. URL <http://www.ncbi.nlm.nih.gov/pubmed/10519552><http://www.nature.com/doi/finder/10.1038/46802>.
- [57] Takashi Saitoh, Mayumi Igura, Takayuki Obita, Toyoyuki Ose, Rieko Kojima, Katsumi Maenaka, Toshiya Endo, and Daisuke Kohda. Tom20 recognizes mitochondrial presequences through dynamic equilibrium among multiple bound states. *The EMBO journal*, 26(22):4777–4787, 2007. ISSN 0261-4189. doi: 10.1038/sj.emboj.7601888.

- [58] Nils Wiedemann, Nikolaus Pfanner, and Michael T. Ryan. The three modules of ADP/ATP carrier cooperate in receptor recruitment and translocation into mitochondria. *EMBO Journal*, 20(5):951–960, 2001. ISSN 02614189. doi: 10.1093/emboj/20.5.951.
- [59] Agnieszka Chacinska, Maria Lind, Ann E. Frazier, Jan Dudek, Chris Meisinger, Andreas Geissler, Albert Sickmann, Helmut E. Meyer, Kaye N. Truscott, Bernard Guiard, Nikolaus Pfanner, and Peter Rehling. Mitochondrial presequence translocase: Switching between TOM tethering and motor recruitment involves Tim21 and Tim17. *Cell*, 120(6):817–829, 2005. ISSN 00928674. doi: 10.1016/j.cell.2005.01.011. URL <http://dx.doi.org/10.1016/j.cell.2005.01.011>.
- [60] Jian Qiu, Lena-Sophie Wenz, Ralf M. Zerbes, Silke Oeljeklaus, Maria Bohnert, David A. Stroud, Christophe Wirth, Lars Ellenrieder, Nicolas Thornton, Stephan Kutik, Sebastian Wiese, Agnes Schulze-Specking, Nicole Zufall, Agnieszka Chacinska, Bernard Guiard, Carola Hunte, Bettina Warscheid, Martin Van Der Laan, Nikolaus Pfanner, Nils Wiedemann, and Thomas Becker. Coupling of mitochondrial import and export translocases by receptor-mediated supercomplex formation. *Cell*, 154(3):596–608, 2013. ISSN 00928674. doi: 10.1016/j.cell.2013.06.033. URL <http://dx.doi.org/10.1016/j.cell.2013.06.033>.
- [61] Lars Becker, Michael Bannwarth, Chris Meisinger, Kerstin Hill, Kirstin Model, Thomas Krimmer, Rita Casadio, Kaye N. Truscott, Georg E. Schulz, Nikolaus Pfanner, and Richard Wagner. Pre-protein translocase of the outer mitochondrial membrane: Reconstituted Tom40 forms a characteristic TOM pore. *Journal of Molecular Biology*, 353(5):1011–1020, 2005. ISSN 00222836. doi: 10.1016/j.jmb.2005.09.019.
- [62] Mercedes Romero-Ruiz, Kozhinjampara R. Mahendran, Reiner Eckert, Mathias Winterhalter, and Stephan Nussberger. Interactions of mitochondrial presequence peptides with the mitochondrial outer membrane preprotein translocase TOM. *Biophysical Journal*, 99(3):774–781, 2010. ISSN 00063495. doi: 10.1016/j.bpj.2010.05.010. URL <http://dx.doi.org/10.1016/j.bpj.2010.05.010>.
- [63] Kozhinjampara R. Mahendran, Mercedes Romero-Ruiz, Andrea Schlösinger, Mathias Winterhalter, and Stephan Nussberger. Protein translocation through Tom40: Kinetics of peptide release. *Biophysical Journal*, 102(1):39–47, 2012. ISSN 00063495. doi: 10.1016/j.bpj.2011.11.4003.
- [64] Kozhinjampara R. Mahendran, Usha Lamichhane, Mercedes Romero-Ruiz, Stephan Nussberger, and Mathias Winterhalter. Polypeptide translocation through the mitochondrial TOM channel: Temperature-dependent rates at the single-molecule level. *Journal of Physical Chemistry Letters*, 4(1):78–82, 2013. ISSN 19487185. doi: 10.1021/jz301790h.
- [65] Takuya Shiota, Kenichiro Imai, Jian Qiu, Victoria L. Hewitt, Kershing Tan, Hsin-Hui Shen, Noriyuki Sakiyama, Yoshinori Fukasawa, Sikander Hayat, Megumi Kamiya, Arne Elofsson, Kentaro Tomii, Paul Horton, Nils Wiedemann, Nikolaus Pfanner, Trevor Lithgow, and Toshiya Endo. Molecular architecture of the active mitochondrial protein gate. *Science reports*, 349(6255):1544–1548, 2015. doi: 10.5061/dryad.10278.
- [66] Nickie C. Chan and Trevor Lithgow. The Peripheral Membrane Subunits of the SAM Complex Function Codependently in Mitochondrial Outer Membrane Biogenesis. *Molecular Biology of the Cell*, 19(1):126–136, jan 2008. ISSN 1059-1524. doi: 10.1091/mbc.E07-08-0796. URL <http://www.molbiolcell.org/cgi/doi/10.1091/mbc.E07-08-0796>.
- [67] Astrid Klein, Lars Israel, Sebastian W. K. Lackey, Frank E. Nargang, Axel Imhof, Wolfgang Baumeister, Walter Neupert, and Dennis R. Thomas. Characterization of the insertase for β -barrel proteins of the outer mitochondrial membrane. *Journal of Cell Biology*, 199(4):599–611, 2012. ISSN 00219525. doi: 10.1083/jcb.201207161.
- [68] San Diego and La Jolla. Regulation of Mitochondrial Morphology and Inheritance by Mdm10p, a Protein of the Mitochondrial Outer Membrane. *The Journal of Cell Biology*, 126(6):1361–1373, 1994.

- [69] Benoît Kornmann, Erin Currie, Sean R. Collins, Maya Schuldiner, Jodi Nunnari, Jonathan S. Weissman, and Peter Walter. An ER-Mitochondria Tethering Complex Revealed by a Synthetic Biology Screen. *Science*, 325(5939):477–481, jul 2009. ISSN 0036-8075. doi: 10.1126/science.1175088. URL <http://www.sciencemag.org/cgi/doi/10.1126/science.1175088>.
- [70] Chris Meisinger, Michael Rissler, Agnieszka Chacinska, Luiza K. Sanjuán Szklarz, Dusanka Milenkovic, Vera Kozjak, Birgit Schönfisch, Christiane Lohaus, Helmut E. Meyer, Michael P. Yaffe, Bernard Guiard, Nils Wiedemann, and Nikolaus Pfanner. The Mitochondrial Morphology Protein Mdm10 Functions in Assembly of the Preprotein Translocase of the Outer Membrane. *Developmental Cell*, 7(1):61–71, jul 2004. ISSN 15345807. doi: 10.1016/j.devcel.2004.06.003. URL <http://linkinghub.elsevier.com/retrieve/pii/S0968000405000435><http://linkinghub.elsevier.com/retrieve/pii/S1534580704002047>.
- [71] Thomas Becker, Bernard Guiard, Nicolas Thornton, Nicole Zufall, David A. Stroud, Nils Wiedemann, and Nikolaus Pfanner. Assembly of the Mitochondrial Protein Import Channel: Role of Tom5 in Two-Stage Interaction of Tom40 with the SAM Complex. *Molecular Biology of the Cell*, 21(18):3106–3113, sep 2010. ISSN 1059-1524. doi: 10.1091/mbc.E10-06-0518. URL <http://www.molbiolcell.org/cgi/doi/10.1091/mbc.E10-06-0518>.
- [72] Thomas Becker, Sylvia Pfannschmidt, Bernard Guiard, Diana Stojanovski, Dusanka Milenkovic, Stephan Kutik, Nikolaus Pfanner, Chris Meisinger, and Nils Wiedemann. Biogenesis of the Mitochondrial TOM Complex: Mtm1 PROMOTES INSERTION AND ASSEMBLY OF SIGNAL-ANCHORED RECEPTORS. *Journal of Biological Chemistry*, 283(1):120–127, jan 2008. ISSN 0021-9258. doi: 10.1074/jbc.M706997200. URL <http://www.jbc.org/cgi/doi/10.1074/jbc.M706997200>.
- [73] Nicolas Thornton, David A. Stroud, Dusanka Milenkovic, Bernard Guiard, Nikolaus Pfanner, and Thomas Becker. Two Modular Forms of the Mitochondrial Sorting and Assembly Machinery Are Involved in Biogenesis of α -Helical Outer Membrane Proteins. *Journal of Molecular Biology*, 396(3):540–549, feb 2010. ISSN 00222836. doi: 10.1016/j.jmb.2009.12.026. URL <http://dx.doi.org/10.1016/j.jmb.2009.12.026><http://linkinghub.elsevier.com/retrieve/pii/S0022283609015319>.
- [74] Lars Ellenrieder, Łukasz Opaliński, Lars Becker, Vivien Krüger, Oliver Mirus, Sebastian P. Straub, Katharina Ebell, Nadine Flinner, Sebastian B. Stiller, Bernard Guiard, Chris Meisinger, Nils Wiedemann, Enrico Schleiff, Richard Wagner, Nikolaus Pfanner, and Thomas Becker. Separating mitochondrial protein assembly and endoplasmic reticulum tethering by selective coupling of Mdm10. *Nature Communications*, 7:13021, oct 2016. ISSN 2041-1723. doi: 10.1038/ncomms13021. URL <http://www.nature.com/doifinder/10.1038/ncomms13021>.
- [75] Stephan Kutik, Diana Stojanovski, Lars Becker, Thomas Becker, Michael Meinecke, Vivien Krüger, Claudia Prinz, Chris Meisinger, Bernard Guiard, Richard Wagner, Nikolaus Pfanner, and Nils Wiedemann. Dissecting Membrane Insertion of Mitochondrial β -Barrel Proteins. *Cell*, 132(6):1011–1024, 2008. ISSN 00928674. doi: 10.1016/j.cell.2008.01.028.
- [76] Hans de Cock, Marlies Struyvé, Michiel Kleerebezem, Theo van der Krift, and Jan Tommassen. Role of the carboxy-terminal phenylalanine in the biogenesis of outer membrane protein PhoE of *Escherichia coli* K-12. *Journal of Molecular Biology*, 269(4):473–478, jun 1997. ISSN 00222836. doi: 10.1006/jmbi.1997.1069. URL <http://linkinghub.elsevier.com/retrieve/pii/S002228369791069X>.
- [77] Tobias Jores, Anna Klinger, Lucia E. Groß, Shin Kawano, Nadine Flinner, Elke Duchardt-Ferner, Jens Wöhnert, Hubert Kalbacher, Toshiya Endo, Enrico Schleiff, and Doron Rapaport. Characterization of the targeting signal in mitochondrial β -barrel proteins. *Nature Communications*, 7(May):12036, jun 2016. ISSN 2041-1723. doi: 10.1038/ncomms12036. URL <http://www.nature.com/doifinder/10.1038/ncomms12036>.

- [78] Christian Sirrenberg, Maxi Endres, Heike Fölsch, Rosemary A. Stuart, Walter Neupert, and Michael Brunner. Carrier protein import into mitochondria mediated by the intermembrane proteins Tim10/Mrs11 and Tim12/Mrs5. *Nature*, 391(6670):912–915, 1998. ISSN 0028-0836. doi: 10.1038/36136.
- [79] Carla M. Koehler, Ernst Jarosch, Kostas Tokatlidis, Karl Schmid, Rudolf J. Schweyen, and Gottfried Schatz. Import of Mitochondrial Carriers Mediated by Essential Proteins of the Intermembrane Space. *Science*, 279(5349):369–373, jan 1998. ISSN 00368075. doi: 10.1126/science.279.5349.369. URL <http://www.sciencemag.org/cgi/doi/10.1126/science.279.5349.369>.
- [80] Shukry J. Habib, Thomas Waizenegger, Maciej Lech, Walter Neupert, and Doron Rapaport. Assembly of the TOB complex of mitochondria. *Journal of Biological Chemistry*, 280(8):6434–6440, 2005. ISSN 00219258. doi: 10.1074/jbc.M411510200.
- [81] Suzanne C. Hoppins and Frank E. Nargang. The Tim8-Tim13 Complex of *Neurospora crassa* Functions in the Assembly of Proteins into Both Mitochondrial Membranes. *Journal of Biological Chemistry*, 279(13):12396–12405, 2004. ISSN 00219258. doi: 10.1074/jbc.M313037200.
- [82] Kristen N. Beverly, Michael R. Sawaya, Einhard Schmid, and Carla M. Koehler. The Tim8-Tim13 Complex Has Multiple Substrate Binding Sites and Binds Cooperatively to Tim23. *Journal of Molecular Biology*, 382(5):1144–1156, 2008. ISSN 00222836. doi: 10.1016/j.jmb.2008.07.069.
- [83] Chaille T. Webb, Michael A. Gorman, Michael Lazarou, Michael T. Ryan, and Jacqueline M. Gulbis. Crystal Structure of the Mitochondrial Chaperone TIM9•10 Reveals a Six-Bladed α -Propeller. *Molecular Cell*, 21(1):123–133, jan 2006. ISSN 10972765. doi: 10.1016/j.molcel.2005.11.010. URL <http://linkinghub.elsevier.com/retrieve/pii/S1097276505017703>.
- [84] Dirk M. Walther, Doron Rapaport, and Jan Tommassen. Biogenesis of β -barrel membrane proteins in bacteria and eukaryotes: evolutionary conservation and divergence. *Cellular and Molecular Life Sciences*, 66(17):2789–2804, sep 2009. ISSN 1420-682X. doi: 10.1007/s00018-009-0029-z. URL <http://link.springer.com/10.1007/s00018-009-0029-z>.
- [85] Oliver Schmidt, Nikolaus Pfanner, and Chris Meisinger. Mitochondrial protein import: from proteomics to functional mechanisms. *Nature reviews. Molecular cell biology*, 11(9):655–667, 2010. ISSN 1471-0072. doi: 10.1038/nrm2959. URL <http://dx.doi.org/10.1038/nrm2959>.
- [86] Takuya Shiota, Miyuki Maruyama, Mami Miura, Yasushi Tamura, Koji Yamano, Masatoshi Esaki, and Toshiya Endo. The Tom40 assembly process probed using the attachment of different intramitochondrial sorting signals. *Molecular biology of the cell*, 23(20):3936–47, 2012. ISSN 1939-4586. doi: 10.1091/mbc.E12-03-0202. URL <http://www.pubmedcentral.nih.gov/articlerender.fcgi?artid=3469510&tool=pmcentrez&rendertype=abstract>.
- [87] Maria Bohnert, Lena-Sophie Wenz, Ralf M. Zerbes, Susanne E. Horvath, David A. Stroud, Karina von der Malsburg, Judith M. Müller, Silke Oeljeklaus, Inge Perschil, Bettina Warscheid, Agnieszka Chacinska, Marten Veenhuis, Ida J. van der Klei, Günther Daum, Nils Wiedemann, Thomas Becker, Nikolaus Pfanner, and Martin van der Laan. Role of mitochondrial inner membrane organizing system in protein biogenesis of the mitochondrial outer membrane. *Molecular Biology of the Cell*, 23(20):3948–3956, oct 2012. ISSN 1059-1524. doi: 10.1091/mbc.E12-04-0295. URL <http://www.scopus.com/inward/record.url?eid=2-s2.0-84867449307&partnerID=tZ0tx3y1http://www.molbiolcell.org/cgi/doi/10.1091/mbc.E12-04-0295>.
- [88] Max Harner, Christian Körner, Dirk M. Walther, Dejana Mokranjac, Johannes Kaesmacher, Ulrich Welsch, Janice Griffith, Matthias Mann, Fulvio Reggiori, and Walter Neupert. The mitochondrial contact site complex, a determinant of mitochondrial architecture. *The EMBO Journal*, 30(21):4356–4370, 2011. ISSN 0261-4189. doi: 10.1038/emboj.2011.379.

- [89] Karina von der Malsburg, Judith M. Müller, Maria Bohnert, Silke Oeljeklaus, Paulina Kwiatkowska, Thomas Becker, Adrianna Loniewska-Lwowska, Sebastian Wiese, Sanjana Rao, Dusanka Milenkovic, Dana P. Hutu, Ralf M. Zerbes, Agnes Schulze-Specking, Helmut E. Meyer, Jean-Claude Martinou, Sabine Rospert, Peter Rehling, Chris Meisinger, Marten Veenhuis, Bettina Warscheid, Ida J. van der Klei, Nikolaus Pfanner, Agnieszka Chacinska, and Martin van der Laan. Dual Role of Mitofilin in Mitochondrial Membrane Organization and Protein Biogenesis. *Developmental Cell*, 21(4):694–707, oct 2011. ISSN 15345807. doi: 10.1016/j.devcel.2011.08.026. URL <http://linkinghub.elsevier.com/retrieve/pii/S1534580711003649>.
- [90] Alwaleed K. Alkhaja, Daniel C. Jans, Miroslav Nikolov, Milena Vukotic, Oleksandr Lytovchenko, Fabian Ludewig, Wolfgang Schliebs, Dietmar Riedel, Henning Urlaub, Stefan Jakobs, and Markus Deckers. MINOSI is a conserved component of mitofilin complexes and required for mitochondrial function and cristae organization. *Molecular Biology of the Cell*, 23(2):247–257, jan 2012. ISSN 1059-1524. doi: 10.1091/mbc.E11-09-0774. URL <http://www.molbiolcell.org/cgi/doi/10.1091/mbc.E11-09-0774><http://www.pubmedcentral.nih.gov/articlerender.fcgi?artid=3258170&tool=pmcentrez&rendertype=abstract>.
- [91] Ralf M. Zerbes, Maria Bohnert, David A. Stroud, Karina von der Malsburg, Anita Kram, Silke Oeljeklaus, Bettina Warscheid, Thomas Becker, Nils Wiedemann, Marten Veenhuis, Ida J. van der Klei, Nikolaus Pfanner, and Martin van der Laan. Role of MINOS in Mitochondrial Membrane Architecture: Cristae Morphology and Outer Membrane Interactions Differentially Depend on Mitofilin Domains. *Journal of Molecular Biology*, 422(2):183–191, sep 2012. ISSN 00222836. doi: 10.1016/j.jmb.2012.05.004. URL <http://dx.doi.org/10.1016/j.jmb.2012.05.004><http://linkinghub.elsevier.com/retrieve/pii/S0022283612003786>.
- [92] C. Korner, Miguel Barrera, Jovana Dukanovic, Katharina Eydt, Max Harner, Regina Rabl, Frank Vogel, Doron Rapaport, Walter Neupert, and Andreas S Reichert. The C-terminal domain of Fcjl is required for formation of crista junctions and interacts with the TOB/SAM complex in mitochondria. *Molecular Biology of the Cell*, 23(11):2143–2155, jun 2012. ISSN 1059-1524. doi: 10.1091/mbc.E11-10-0831. URL <http://www.molbiolcell.org/cgi/doi/10.1091/mbc.E11-10-0831>.
- [93] Bernard Clantin, Anne-Sophie Delattre, Prakash Rucktooa, Nathalie Saint, Albano C. Méli, Camille Loch, Françoise Jacob-Dubuisson, and Vincent Villeret. Structure of the membrane protein FhaC: a member of the Omp85-TpsB transporter superfamily. *Science (New York, N.Y.)*, 317(5840):957–961, 2007. ISSN 0036-8075. doi: 10.1126/science.1143860. URL <http://www.ncbi.nlm.nih.gov/pubmed/17702945>.
- [94] Kornelius Zeth. Structure and evolution of mitochondrial outer membrane proteins of beta-barrel topology. *Biochimica et biophysica acta*, 1797(6-7):1292–1299, 2010. ISSN 0006-3002. doi: 10.1016/j.bbabi.2010.04.019. URL <http://dx.doi.org/10.1016/j.bbabi.2010.04.019>.
- [95] Luis Sánchez-Pulido, Damien Devos, Stéphanie Genevrois, Miguel Vicente, and Alfonso Valencia. POTRA: a conserved domain in the FtsQ family and a class of β -barrel outer membrane proteins. *Trends in Biochemical Sciences*, 28(10):523–526, oct 2003. ISSN 09680004. doi: 10.1016/j.tibs.2003.08.003. URL <http://linkinghub.elsevier.com/retrieve/pii/S096800040300197X><http://linkinghub.elsevier.com/retrieve/pii/S0968000403002123>.
- [96] Shukry J. Habib, Thomas Waizenegger, Agathe Niewienda, Stefan A. Paschen, Walter Neupert, and Doron Rapaport. The N-terminal domain of Tob55 has a receptor-like function in the biogenesis of mitochondrial β -barrel proteins. *Journal of Cell Biology*, 176(1):77–88, 2007. ISSN 00219525. doi: 10.1083/jcb.200602050.
- [97] Peter Rehling, Kirstin Model, Katrin Brandner, Peter Kovermann, Albert Sickmann, Helmut E. Meyer, Werner Kühlbrandt, Richard Wagner, Kaye N. Truscott, and Nikolaus Pfanner. Protein insertion into the mitochondrial inner membrane by a twin-pore translocase. *Science (New York, N.Y.)*, 299(5613):

- 1747–51, mar 2003. ISSN 1095-9203. doi: 10.1126/science.1080945. URL <http://www.sciencemag.org/cgi/doi/10.1126/science.1080945><http://www.ncbi.nlm.nih.gov/pubmed/12637749>.
- [98] Peter Kovermann, Kaye N. Truscott, Bernard Guiard, Peter Rehling, Naresh B. Sepuri, Hanne Müller, Robert E. Jensen, Richard Wagner, and Nikolaus Pfanner. Tim22, the Essential Core of the Mitochondrial Protein Insertion Complex, Forms a Voltage-Activated and Signal-Gated Channel. *Molecular Cell*, 9(2):363–373, feb 2002. ISSN 10972765. doi: 10.1016/S1097-2765(02)00446-X. URL <http://linkinghub.elsevier.com/retrieve/pii/S109727650200446X>.
- [99] Oliver Kerscher, Jason Holder, Maithreyan Srinivasan, Roxanne S. Leung, and Robert E. Jensen. The Tim54p-Tim22p complex mediates insertion of proteins into the mitochondrial inner membrane. *Journal of Cell Biology*, 139(7):1663–1675, 1997. ISSN 00219525. doi: 10.1083/jcb.139.7.1663.
- [100] O Kerscher, N B Sepuri, and Robert E. Jensen. Tim18p Is a New Component of the Tim54p-Tim22p Translocon in the Mitochondrial Inner Membrane. *Molecular Biology of the Cell*, 11(1):103–116, jan 2000. ISSN 1059-1524. doi: 10.1091/mbc.11.1.103. URL <http://www.molbiolcell.org/cgi/doi/10.1091/mbc.11.1.103>.
- [101] Carla M. Koehler, Michael P. Murphy, Nikolaus A. Bally, Danielle Leuenberger, Wolfgang Oppliger, Luisita Dolfini, Tina Junne, Gottfried Schatz, and Eran Or. Tim18p, a New Subunit of the TIM22 Complex That Mediates Insertion of Imported Proteins into the Yeast Mitochondrial Inner Membrane. *Molecular and Cellular Biology*, 20(4):1187–1193, feb 2000. ISSN 0270-7306. doi: 10.1128/MCB.20.4.1187-1193.2000. URL <http://mcb.asm.org/cgi/doi/10.1128/MCB.20.4.1187-1193.2000>.
- [102] Natalia Gebert, Michael Gebert, Silke Oeljeklaus, Karina von der Malsburg, David A. Stroud, Bogusz Kulawiak, Christophe Wirth, René P. Zahedi, Pavel Dolezal, Sebastian Wiese, Oliver Simon, Agnes Schulze-Specking, Kaye N. Truscott, Albert Sickmann, Peter Rehling, Bernard Guiard, Carola Hunte, Bettina Warscheid, Martin van der Laan, Nikolaus Pfanner, and Nils Wiedemann. Dual function of Sdh3 in the respiratory chain and TIM22 protein translocase of the mitochondrial inner membrane. *Molecular Cell*, 44(5):811–818, 2011. ISSN 10972765. doi: 10.1016/j.molcel.2011.09.025.
- [103] Catherine Baud, Carine de Marcos-Lousa, and Kostas Tokatlidis. Molecular Interactions of the Mitochondrial Tim12 Translocase Subunit. *Protein & Peptide Letters*, 14(6):597–600, jun 2007. ISSN 09298665. doi: 10.2174/092986607780990019. URL <http://www.eurekaselect.com/openurl/content.php?genre=article&issn=0929-8665&volume=14&issue=6&spage=597>.
- [104] Ian E. Gentle, Andrew J. Perry, Felicity H. Alcock, Vladimir A. Likic, Pavel Dolezal, Ee Ting Ng, Anthony W. Purcell, Malcolm McConville, Thomas Naderer, Anne-Laure Chanez, Fabien Charriere, Caroline Aschinger, André Schneider, Kostas Tokatlidis, and Trevor Lithgow. Conserved Motifs Reveal Details of Ancestry and Structure in the Small TIM Chaperones of the Mitochondrial Intermembrane Space. *Molecular Biology and Evolution*, 24(5):1149–1160, feb 2007. ISSN 0737-4038. doi: 10.1093/molbev/msm031. URL <https://academic.oup.com/mbe/article-lookup/doi/10.1093/molbev/msm031>.
- [105] Natalia Gebert, Agnieszka Chacinska, Karina Wagner, Bernard Guiard, Carla M. Koehler, Peter Rehling, Nikolaus Pfanner, and Nils Wiedemann. Assembly of the three small Tim proteins precedes docking to the mitochondrial carrier translocase. *EMBO reports*, 9(6):548–554, jun 2008. ISSN 1469-221X. doi: 10.1038/embor.2008.49. URL <http://embor.embopress.org/cgi/doi/10.1038/embor.2008.49>.
- [106] Alison J. Davis, Nathan N. Alder, Robert E. Jensen, and Arthur E. Johnson. The Tim9p/10p and Tim8p/13p Complexes Bind to Specific Sites on Tim23p during Mitochondrial Protein Import. *Molecular Biology of the Cell*, 18(2):475–486, nov 2006. ISSN 1059-1524. doi: 10.1091/mbc.E06-06-0546. URL <http://www.molbiolcell.org/cgi/doi/10.1091/mbc.E06-06-0546>.

- [107] Peter Rehling, Katrin Brandner, and Nikolaus Pfanner. Mitochondrial import and the twin-pore translocase. *Nature Reviews Molecular Cell Biology*, 5(7):519–530, jul 2004. ISSN 1471-0072. doi: 10.1038/nrml426. URL <http://www.nature.com/doi/finder/10.1038/nrml426>.
- [108] F.-Nora Vögtle, Stefanie Wortelkamp, René P. Zahedi, Dorothea Becker, Claudia Leidhold, Kris Gevaert, Josef Kellermann, Wolfgang Voos, Albert Sickmann, Nikolaus Pfanner, and Chris Meisinger. Global Analysis of the Mitochondrial N-Proteome Identifies a Processing Peptidase Critical for Protein Stability. *Cell*, 139(2):428–439, 2009. ISSN 00928674. doi: 10.1016/j.cell.2009.07.045.
- [109] Oleksandr Gakh, Patrizia Cavadini, and Grazia Isaya. Mitochondrial processing peptidases. *Biochimica et Biophysica Acta - Molecular Cell Research*, 1592(1):63–77, 2002. ISSN 01674889. doi: 10.1016/S0167-4889(02)00265-3.
- [110] Franz-Ulrich Hartl, Joachim Ostermann, Bernard Guiard, and Walter Neupert. Successive translocation into and out of the mitochondrial matrix: Targeting of proteins to the intermembrane space by a bipartite signal peptide. *Cell*, 51(6):1027–1037, 1987. ISSN 00928674. doi: 10.1016/0092-8674(87)90589-7.
- [111] Benjamin S. Glick, Anders Brandt, Kyle Cunningham, Sabina Müller, Richard L. Hallberg, and Gottfried Schatz. Cytochromes c1 and b2 are sorted to the intermembrane space of yeast mitochondria by a stop-transfer mechanism. *Cell*, 69(5):809–822, may 1992. ISSN 00928674. doi: 10.1016/0092-8674(92)90292-K. URL <http://linkinghub.elsevier.com/retrieve/pii/009286749290292K>.
- [112] Timothy A. Lohret, Robert E. Jensen, and Kathleen W. Kinnally. Tim23, a protein import component of the mitochondrial inner membrane, is required for normal activity of the multiple conductance channel, MCC. *The Journal of cell biology*, 137(2):377–86, apr 1997. ISSN 0021-9525. URL <http://www.ncbi.nlm.nih.gov/pubmed/9128249><http://www.pubmedcentral.nih.gov/articlerender.fcgi?artid=PMC2139772>.
- [113] Andreas Geissler, Agnieszka Chacinska, Kaye N. Truscott, Nils Wiedemann, Katrin Brandner, Albert Sickmann, Helmut E. Meyer, Chris Meisinger, Nikolaus Pfanner, and Peter Rehling. The mitochondrial presequence translocase: An essential role of Tim50 in directing preproteins to the import channel. *Cell*, 111(4):507–518, 2002. ISSN 00928674. doi: 10.1016/S0092-8674(02)01073-5.
- [114] Hayashi Yamamoto, Masatoshi Esaki, Takashi Kanamori, Yasushi Tamura, Shuh ichi Nishikawa, and Toshiya Endo. Tim50 is a subunit of the TIM23 complex that links protein translocation across the outer and inner mitochondrial membranes. *Cell*, 111(4):519–528, 2002. ISSN 00928674. doi: 10.1016/S0092-8674(02)01053-X.
- [115] Dejana Mokranjac, Stefan A. Paschen, Christian Kozany, Holger Prokisch, Suzanne C. Hoppins, Frank E. Nargang, Walter Neupert, and Kai Hell. Tim50, a novel component of the TIM23 pre-protein translocase of mitochondria. *EMBO Journal*, 22(4):816–825, 2003. ISSN 02614189. doi: 10.1093/emboj/cdg090.
- [116] Michael Gebert, Sandra G. Schrempp, Carola S. Mehnert, Anna K. Heißwolf, Silke Oeljeklaus, Raffaele Ieva, Maria Bohnert, Karina von der Malsburg, Sebastian Wiese, Thomas Kleinschroth, Carola Hunte, Helmut E. Meyer, Ilka Haferkamp, Bernard Guiard, Bettina Warscheid, Nikolaus Pfanner, and Martin van der Laan. Mgr2 promotes coupling of the mitochondrial presequence translocase to partner complexes. *Journal of Cell Biology*, 197(5):595–604, 2012. ISSN 00219525. doi: 10.1083/jcb.201110047.
- [117] Martin van der Laan, Michael Meinecke, Jan Dudek, Dana P. Hutu, Maria Lind, Inge Perschil, Bernard Guiard, Richard Wagner, Nikolaus Pfanner, and Peter Rehling. Motor-free mitochondrial presequence translocase drives membrane integration of preproteins. *Nature cell biology*, 9(10):1152–1159, 2007. ISSN 1465-7392. doi: 10.1038/ncbl635.

- [118] Martin Van Der Laan, Agnieszka Chacinska, Maria Lind, Albert Sickmann, Helmut E. Meyer, Chris Meisinger, Nikolaus Pfanner, Inge Perschil, Bernard Guiard, and Peter Rehling. Pam17 Is Required for Architecture and Translocation Activity of the Mitochondrial Protein Import Motor. *Molecular and cellular biology*, 25(17):7449–7458, 2005. doi: 10.1128/MCB.25.17.7449.
- [119] Mariel Donzeau, Krisztina Káldi, Alexander Adam, Stefan A. Paschen, Gerhard Wanner, Bernard Guiard, Matthias F. Bauer, Walter Neupert, and Michael Brunner. Tim23 Links the Inner and Outer Mitochondrial Membranes. *Cell*, 101(4):401–412, may 2000. ISSN 00928674. doi: 10.1016/S0092-8674(00)80850-8. URL <http://linkinghub.elsevier.com/retrieve/pii/S0092867400808508>.
- [120] Reinhard Albrecht, Peter Rehling, Agnieszka Chacinska, Jan Brix, Sergio A. Cadamuro, Rudolf Volkmer, Bernard Guiard, Nikolaus Pfanner, and Kornelius Zeth. The Tim21 binding domain connects the preprotein translocases of both mitochondrial membranes. *{EMBO} Rep.*, 7(12):1233–1238, 2006. ISSN 1469-221X. doi: 10.1038/sj.embor.7400828.
- [121] Christian Schulz, Oleksandr Lytovchenko, Jonathan Melin, Agnieszka Chacinska, Bernard Guiard, Piotr Neumann, Ralf Ficner, Olaf Jahn, Bernhard Schmidt, and Peter Rehling. Tim50's presequence receptor domain is essential for signal driven transport across the TIM23 complex. *Journal of Cell Biology*, 195(4):643–656, 2011. ISSN 00219525. doi: 10.1083/jcb.201105098.
- [122] Milit Marom, Dana Dayan, Keren Demishtein-Zohary, Dejana Mokranjac, Walter Neupert, and Abdusalam Azem. Direct interaction of mitochondrial targeting presequences with purified components of the TIM23 protein complex. *Journal of Biological Chemistry*, 286(51):43809–43815, 2011. ISSN 00219258. doi: 10.1074/jbc.M111.261040.
- [123] Oleksandr Lytovchenko, Jonathan Melin, Christian Schulz, Markus Kilisch, Dana P. Hutu, and Peter Rehling. Signal recognition initiates reorganization of the presequence translocase during protein import. *The EMBO journal*, 32(6):886–98, 2013. ISSN 1460-2075. doi: 10.1038/emboj.2013.23. URL <http://www.pubmedcentral.nih.gov/articlerender.fcgi?artid=3604718&tool=pmcentrez&rendertype=abstract>.
- [124] Bytul Rahman, Shin Kawano, Kaori Yunoki-Esaki, Takahiro Anzai, and Toshiya Endo. NMR analyses on the interactions of the yeast Tim50 C-terminal region with the presequence and Tim50 core domain. *FEBS Letters*, 588(5):678–684, 2014. ISSN 00145793. doi: 10.1016/j.febslet.2013.12.037. URL <http://dx.doi.org/10.1016/j.febslet.2013.12.037>.
- [125] Xinguo Qian, Michael Gebert, Jan Höpker, Ming Yan, Jingzhi Li, Nils Wiedemann, Martin Van Der Laan, Nikolaus Pfanner, and Bingdong Sha. Structural basis for the function of Tim50 in the mitochondrial presequence translocase. *Journal of Molecular Biology*, 411(3):513–519, 2011. ISSN 00222836. doi: 10.1016/j.jmb.2011.06.020. URL <http://dx.doi.org/10.1016/j.jmb.2011.06.020>.
- [126] Salomé Calado Botelho, Marie Österberg, Andreas S Reichert, Koji Yamano, Patrik Björkholm, Toshiya Endo, Gunnar von Heijne, and Hyun Kim. TIM23-mediated insertion of transmembrane α -helices into the mitochondrial inner membrane. *The EMBO Journal*, 30(6):1003–1011, 2011. ISSN 02614189. doi: 10.1038/emboj.2011.29. URL <http://emboj.embopress.org/cgi/doi/10.1038/emboj.2011.29>.
- [127] Y Gavel and G von Heijne. Cleavage-site motifs in mitochondrial targeting peptides. *Protein engineering*, 4(1):33–7, oct 1990. ISSN 0269-2139. URL <http://www.ncbi.nlm.nih.gov/pubmed/2290832>.
- [128] Joachim Rassow, Franz-Ulrich Hartl, Bernard Guiard, Nikolaus Pfanner, and Walter Neupert. Polypeptides traverse the mitochondrial envelope in an extended state. *FEBS Letters*, 275(1-2):190–194, nov 1990. ISSN 00145793. doi: 10.1016/0014-5793(90)81469-5. URL <http://www.sciencedirect.com/science/article/pii/0014579390814695http://doi.wiley.com/10.1016/0014-5793%2890%2981469-5>.

- [129] Raffaele Ieva, Sandra G. Schrempp, Łukasz Opaliński, Florian Wollweber, Philipp Höß, Anna K. Heißwolf, Michael Gebert, Ying Zhang, Bernard Guiard, Sabine Rospert, Thomas Becker, Agnieszka Chacinska, Nikolaus Pfanner, and Martin van der Laan. Mgr2 Functions as Lateral Gatekeeper for Preprotein Sorting in the Mitochondrial Inner Membrane. *Molecular Cell*, 56(5):641–652, dec 2014. ISSN 10972765. doi: 10.1016/j.molcel.2014.10.010. URL <http://www.ncbi.nlm.nih.gov/pubmed/25454944><http://linkinghub.elsevier.com/retrieve/pii/S1097276514007941>.
- [130] Stephan Meier, Walter Neupert, and Johannes M. Herrmann. Conserved N-terminal negative charges in the Tim17 subunit of the TIM23 translocase play a critical role in the import of preproteins into mitochondria. *Journal of Biological Chemistry*, 280(9):7777–7785, 2005. ISSN 00219258. doi: 10.1074/jbc.M412158200.
- [131] Christian Schulz, Alexander Benjamin Schendzielorz, and Peter Rehling. Unlocking the presequence import pathway. *Trends in Cell Biology*, 25(5):265–275, may 2015. ISSN 09628924. doi: 10.1016/j.tcb.2014.12.001. URL <http://dx.doi.org/10.1016/j.tcb.2014.12.001><http://linkinghub.elsevier.com/retrieve/pii/S0962892414002116>.
- [132] Martin van der Laan, Nils Wiedemann, David U. Mick, Bernard Guiard, Peter Rehling, and Nikolaus Pfanner. A Role for Tim21 in Membrane-Potential-Dependent Preprotein Sorting in Mitochondria. *Current Biology*, 16(22):2271–2276, 2006. ISSN 09609822. doi: 10.1016/j.cub.2006.10.025.
- [133] Nils Wiedemann, Martin Van Der Laan, Dana P. Hutu, Peter Rehling, and Nikolaus Pfanner. Sorting switch of mitochondrial presequence translocase involves coupling of motor module to respiratory chain. *Journal of Cell Biology*, 179(6):1115–1122, 2007. ISSN 00219525. doi: 10.1083/jcb.200709087.
- [134] Uma Turakhiya, Karina von der Malsburg, Vicki A. M. Gold, Bernard Guiard, Agnieszka Chacinska, Martin van der Laan, and Raffaele Ieva. Protein import by the mitochondrial presequence translocase in the absence of a membrane potential. *Journal of Molecular Biology*, 2016. ISSN 00222836. doi: 10.1016/j.jmb.2016.01.020. URL <http://linkinghub.elsevier.com/retrieve/pii/S0022283616000395>.
- [135] Keren Demishtein-Zohary, Umut Günsel, Milit Marom, Rupa Banerjee, Walter Neupert, Abdussalam Azem, and Dejana Mokranjac. Role of Tim17 in coupling the import motor to the translocation channel of the mitochondrial presequence translocase. *eLife*, 6:1–11, feb 2017. ISSN 2050-084X. doi: 10.7554/eLife.22696. URL <http://elifesciences.org/lookup/doi/10.7554/eLife.22696>.
- [136] Patrick D’Silva, Qinglian Liu, William Walter, and Elizabeth A. Craig. Regulated interactions of mtHsp70 with Tim44 at the translocon in the mitochondrial inner membrane. *Nature Structural & Molecular Biology*, 11(11):1084–1091, nov 2004. ISSN 1545-9993. doi: 10.1038/nsmb846. URL <http://www.ncbi.nlm.nih.gov/pubmed/15489862><http://www.nature.com/doi/10.1038/nsmb846>.
- [137] Dana P. Hutu, Bernard Guiard, Agnieszka Chacinska, Dorothea Becker, Nikolaus Pfanner, Peter Rehling, and Martin Van Der Laan. Mitochondrial Protein Import Motor: Differential Role of Tim44 in the Recruitment of Pam17 and J-Complex to the Presequence Translocase. *Molecular Biology of the Cell*, 19(6):2642–2649, jun 2008. ISSN 1059-1524. doi: 10.1091/mbc.E07-12-1226. URL <http://www.molbiolcell.org/cgi/doi/10.1091/mbc.E07-12-1226>.
- [138] Hans-Christoph Schneider, Jutta Berthold, Matthias F. Bauer, Klaus Dietmeier, Bernard Guiard, Michael Brunner, and Walter Neupert. Mitochondrial Hsp70/MIM44 complex facilitates protein import. *Nature*, 371(6500):768–774, oct 1994. ISSN 0028-0836. doi: 10.1038/371768a0. URL <http://www.nature.com/articles/371768a0>.
- [139] Peter Walsh, Dejan Bursać, Yin Chern Law, Douglas Cyr, and Trevor Lithgow. The J-protein family: modulating protein assembly, disassembly and translocation. *EMBO reports*, 5(6):567–571, 2004. ISSN 1469-221X. doi: 10.1038/sj.embor.7400172. URL <http://embor.embopress.org/cgi/doi/10.1038/sj.embor.7400172>.

- [140] Kaye N. Truscott, Wolfgang Voos, Ann E. Frazier, Maria Lind, Yanfeng Li, Andreas Geissler, Jan Dudek, Hanne Müller, Albert Sickmann, Helmut E. Meyer, Chris Meisinger, Bernard Guiard, Peter Rehling, and Nikolaus Pfanner. A J-protein is an essential subunit of the presequence translocase-associated protein import motor of mitochondria. *The Journal of Cell Biology*, 163(4):707–713, nov 2003. ISSN 0021-9525. doi: 10.1083/jcb.200308004. URL <http://www.jcb.org/lookup/doi/10.1083/jcb.200308004>.
- [141] Christian Kozany, Dejana Mokranjac, Martin Sichtung, Walter Neupert, and Kai Hell. The J domain-related cochaperone Tim16 is a constituent of the mitochondrial TIM23 preprotein translocase. *Nature Structural & Molecular Biology*, 11(3):234–241, mar 2004. ISSN 1545-9993. doi: 10.1038/nsmb734. URL <http://www.nature.com/doi/doi/10.1038/nsmb734>.
- [142] Koyeli Mapa, Martin Sikor, Volodymyr Kudryavtsev, Karin Waegemann, Stanislav Kalinin, Claus A.M. Seidel, Walter Neupert, Don C. Lamb, and Dejana Mokranjac. The Conformational Dynamics of the Mitochondrial Hsp70 Chaperone. *Molecular Cell*, 38(1):89–100, 2010. ISSN 10972765. doi: 10.1016/j.molcel.2010.03.010. URL <http://dx.doi.org/10.1016/j.molcel.2010.03.010>.
- [143] Christian Schulz and Peter Rehling. Remodelling of the active presequence translocase drives motor-dependent mitochondrial protein translocation. *Nature Communications*, 5:1–9, 2014. ISSN 2041-1723. doi: 10.1038/ncomms5349. URL <http://www.nature.com/doi/doi/10.1038/ncomms5349>.
- [144] Seth W. Hennon, Raunak Soman, Lu Zhu, and Ross E. Dalbey. YidC/Alb3/Oxal family of insertases. *Journal of Biological Chemistry*, 290(24):14866–14874, 2015. ISSN 1083351X. doi: 10.1074/jbc.R115.638171.
- [145] Martijn Rep and Leslie A. Grivell. Mba1 encodes a mitochondrial membrane-associated protein required for biogenesis of the respiratory chain. *FEBS Letters*, 388(2-3):185–188, jun 1996. ISSN 00145793. doi: 10.1016/0014-5793(96)00543-1. URL [http://doi.wiley.com/10.1016/0014-5793\(96\)00543-1](http://doi.wiley.com/10.1016/0014-5793(96)00543-1).
- [146] Ann E. Frazier, Rebecca D. Taylor, David U. Mick, Bettina Warscheid, Nadine Stoepel, Helmut E. Meyer, Michael T. Ryan, Bernard Guiard, and Peter Rehling. Mdm38 interacts with ribosomes and is a component of the mitochondrial protein export machinery. *Journal of Cell Biology*, 172(4):553–564, 2006. ISSN 00219525. doi: 10.1083/jcb.200505060.
- [147] Martin Ott, Martin Prestele, Heike Bauerschmitt, Soledad Funes, Nathalie Bonnefoy, and Johannes M. Herrmann. Mba1, a membrane-associated ribosome receptor in mitochondria. *The EMBO Journal*, 25(8):1603–1610, apr 2006. ISSN 0261-4189. doi: 10.1038/sj.emboj.7601070. URL <http://www.pubmedcentral.nih.gov/articlerender.fcgi?artid=1440829&tool=pmcentrez&rendertype=abstract><http://emboj.embopress.org/cgi/doi/10.1038/sj.emboj.7601070>.
- [148] Heike Bauerschmitt, David U. Mick, Markus Deckers, Christine Vollmer, Soledad Funes, K Kehrein, Martin Ott, Peter Rehling, and Johannes M. Herrmann. Ribosome-binding Proteins Mdm38 and Mba1 Display Overlapping Functions for Regulation of Mitochondrial Translation. *Molecular Biology of the Cell*, 21(12):1937–1944, jun 2010. ISSN 1059-1524. doi: 10.1091/mbc.E10-02-0101. URL <http://www.molbiolcell.org/cgi/doi/10.1091/mbc.E10-02-0101>.
- [149] Domenico Lupo, Christine Vollmer, Markus Deckers, David U. Mick, Ivo Tews, Irmgard Sinning, and Peter Rehling. Mdm38 is a 14-3-3-Like Receptor and Associates with the Protein Synthesis Machinery at the Inner Mitochondrial Membrane. *Traffic*, 12(10):1457–1466, oct 2011. ISSN 13989219. doi: 10.1111/j.1600-0854.2011.01239.x. URL <http://doi.wiley.com/10.1111/j.1600-0854.2011.01239.x>.
- [150] Marc Preuss, Klaus Leonhard, Kai Hell, Rosemary A. Stuart, Walter Neupert, and Johannes M. Herrmann. Mba1, a novel component of the mitochondrial protein export machinery of the yeast *Saccharomyces cerevisiae*. *The Journal of cell biology*, 153(5):1085–96, 2001. ISSN 0021-9525. doi: 10.1083/jcb.153.5.1085. URL <http://www.pubmedcentral.nih.gov/articlerender.fcgi?artid=2174334&tool=pmcentrez&rendertype=abstract>.

- [151] Stefan Pfeffer, Michael W. Woellhaf, Johannes M. Herrmann, and Friedrich Förster. Organization of the mitochondrial translation machinery studied in situ by cryoelectron tomography. *Nature Communications*, 6:6019, jan 2015. ISSN 2041-1723. doi: 10.1038/ncomms7019. URL <http://www.nature.com/doi/10.1038/ncomms7019>.
- [152] Karin Nowikovsky, Elisabeth M. Froschauer, Gabor Zsurka, Jozef Samaj, Siegfried Reipert, Martin Kolisek, Gerlinde Wiesenberger, and Rudolf J. Schweyen. The LETM1/YOLO27 Gene Family Encodes a Factor of the Mitochondrial K⁺ Homeostasis with a Potential Role in the Wolf-Hirschhorn Syndrome. *Journal of Biological Chemistry*, 279(29):30307–30315, jul 2004. ISSN 0021-9258. doi: 10.1074/jbc.M403607200. URL <http://www.jbc.org/cgi/doi/10.1074/jbc.M403607200>.
- [153] Elisabeth M. Froschauer, Karin Nowikovsky, and Rudolf J. Schweyen. Electroneutral K⁺/H⁺ exchange in mitochondrial membrane vesicles involves Yolo27/Letm1 proteins. *Biochimica et Biophysica Acta (BBA) - Biomembranes*, 1711(1):41–48, jun 2005. ISSN 00052736. doi: 10.1016/j.bbamem.2005.02.018. URL <http://linkinghub.elsevier.com/retrieve/pii/S0005273605000623>.
- [154] Dawei Jiang, Linlin Zhao, and David E Clapham. Genome-Wide RNAi Screen Identifies Letm1 as a Mitochondrial Ca²⁺/H⁺ Antiporter. *Science*, 326(5949):144–147, 2009. ISSN 0036-8075. doi: 10.1126/science.1175145. URL <http://www.sciencemag.org/cgi/content/abstract/326/5949/144>.
- [155] Vivien Krüger, Markus Deckers, Markus Hildenbeutel, Martin Van Der Laan, Maike Hellmers, Christina Dreker, Marc Preuss, Johannes M. Herrmann, Peter Rehling, Richard Wagner, and Michael Meinecke. The mitochondrial oxidase assembly protein1 (Oxal) insertase forms a membrane pore in lipid bilayers. *Journal of Biological Chemistry*, 287:33314–33326, 2012. ISSN 00219258. doi: 10.1074/jbc.M112.387563.
- [156] Walter Neupert and Johannes M. Herrmann. Translocation of proteins into mitochondria. *Annual review of biochemistry*, 76:723–749, 2007. ISSN 0066-4154. doi: 10.1146/annurev.biochem.76.052705.163409.
- [157] Kwangjin Park, Sung Jun Jung, Hyeonseong Kim, and Hyun Kim. Mode of membrane insertion of individual transmembrane segments in Mdl1 and Mdl2, multi-spanning mitochondrial ABC transporters. *FEBS Letters*, 588(18):3445–3453, 2014. ISSN 18733468. doi: 10.1016/j.febslet.2014.08.001. URL <http://dx.doi.org/10.1016/j.febslet.2014.08.001>.
- [158] Sebastian Reif, Olga Randelj, Grazyna Domańska, Elke A. Dian, Thomas Krimmer, Christian Motz, and Joachim Rassow. Conserved mechanism of Oxal insertion into the mitochondrial inner membrane. *Journal of Molecular Biology*, 354(3):520–528, 2005. ISSN 00222836. doi: 10.1016/j.jmb.2005.09.054.
- [159] Frank E. Nargang, Marc Preuss, Walter Neupert, and Johannes M. Herrmann. The Oxal protein forms a homooligomeric complex and is an essential part of the mitochondrial export translocase in *Neurospora crassa*. *Journal of Biological Chemistry*, 277(15):12846–12853, 2002. ISSN 00219258. doi: 10.1074/jbc.M112099200.
- [160] Kaoru Kumazaki, Shinobu Chiba, Mizuki Takemoto, Arata Furukawa, Ken-ichi Nishiyama, Yasunori Sugano, Takaharu Mori, Naoshi Dohmae, Kunio Hirata, Yoshiko Nakada-Nakura, Andrés D. Maturana, Yoshiki Tanaka, Hiroyuki Mori, Yuji Sugita, Fumio Arisaka, Koreaki Ito, Ryuichiro Ishitani, Tomoya Tsukazaki, and Osamu Nureki. Structural basis of Sec-independent membrane protein insertion by YidC. *Nature*, 509(7501):516–20, 2014. ISSN 1476-4687. doi: 10.1038/nature13167. URL <http://dx.doi.org/10.1038/nature13167>.
- [161] Kaoru Kumazaki, Toshiki Kishimoto, Arata Furukawa, Hiroyuki Mori, Yoshiki Tanaka, Naoshi Dohmae, Ryuichiro Ishitani, Tomoya Tsukazaki, and Osamu Nureki. Crystal structure of *Escherichia coli* YidC, a membrane protein chaperone and insertase. *Scientific reports*, 4:7299, 2014. ISSN 2045-2322. doi: 10.1038/srep07299. URL <http://www.nature.com/srep/2014/141203/srep07299/full/srep07299.html>.

- [162] Vera Kozjak-Pavlovic, Elke a. Dian-Lothrop, Michael Meinecke, Oliver Kepp, Katharina Ross, Krishnaraj Rajalingam, Anke Harsman, Eva Hauf, Volker Brinkmann, Dirk Günther, Ines Herrmann, Robert Hurwitz, Joachim Rassow, Richard Wagner, and Thomas Rudel. Bacterial porin disrupts mitochondrial membrane potential and sensitizes host cells to apoptosis. *PLoS Pathogens*, 5(10), 2009. ISSN 15537366. doi: 10.1371/journal.ppat.1000629.
- [163] Kornelius Zeth, Vera Kozjak-Pavlovic, Michaela Faulstich, Martin Fraunholz, Robert Hurwitz, Oliver Kepp, and Thomas Rudel. Structure and function of the PorB porin from disseminating *Neisseria gonorrhoeae*. *The Biochemical journal*, 449(3):631–42, feb 2013. ISSN 1470-8728. doi: 10.1042/BJ20121025. URL <http://www.ncbi.nlm.nih.gov/pubmed/23095086>.
- [164] Nathan N. Alder, Jennifer Sutherland, Ashley I. Buhring, Robert E. Jensen, and Arthur E. Johnson. Quaternary structure of the mitochondrial TIM23 complex reveals dynamic association between Tim23p and other subunits. *Molecular biology of the cell*, 19(1):159–170, 2008. ISSN 1059-1524. doi: 10.1091/mbc.E07-07-0669.
- [165] Laura De La Cruz, Rakhi Bajaj, Stefan Becker, and Markus Zweckstetter. The intermembrane space domain of Tim23 is intrinsically disordered with a distinct binding region for presequences. *Protein Science*, 19(11):2045–2054, 2010. ISSN 09618368. doi: 10.1002/pro.482.
- [166] Gautam Pareek, Vivekanandhan Krishnamoorthy, and Patrick D'Silva. Molecular Insights Revealing Interaction of Tim23 and Channel Subunits of Presequence Translocase. *Molecular and Cellular Biology*, 33(23):4641–4659, dec 2013. ISSN 0270-7306. doi: 10.1128/MCB.00876-13. URL <http://www.ncbi.nlm.nih.gov/pubmed/24061477><http://mcb.asm.org/cgi/doi/10.1128/MCB.00876-13>.
- [167] Kaye N. Truscott, Peter Kovermann, Andreas Geissler, Alessio Merlin, Michiel Meijer, Arnold J. M. Driessen, Joachim Rassow, Nikolaus Pfanner, and Richard Wagner. A presequence- and voltage-sensitive channel of the mitochondrial preprotein translocase formed by Tim23. *Nature structural biology*, 8(12):1074–1082, 2001. ISSN 1072-8368. doi: 10.1038/nsb726.
- [168] Sonia Martinez-Caballero, Sergey M. Grigoriev, Johannes M. Herrmann, María Luisa Campo, and Kathleen W. Kinnally. Tim17p regulates the twin pore structure and voltage gating of the mitochondrial protein import complex TIM23. *Journal of Biological Chemistry*, 282(6):3584–3593, 2007. ISSN 00219258. doi: 10.1074/jbc.M607551200.
- [169] Brian D. Hamman, Jui-Chang Chen, Edward E. Johnson, and Arthur E. Johnson. The Aqueous Pore through the Translocon Has a Diameter of 40–60 Å during Cotranslational Protein Translocation at the ER Membrane. *Cell*, 89(4):535–544, may 1997. ISSN 00928674. doi: 10.1016/S0092-8674(00)80235-4. URL <http://linkinghub.elsevier.com/retrieve/pii/S0030665708702269><http://linkinghub.elsevier.com/retrieve/pii/S0092867400802354>.
- [170] Michael Meinecke, Richard Wagner, Peter Kovermann, Bernard Guiard, David U. Mick, Dana P. Hutu, Wolfgang Voos, Kaye N. Truscott, Agnieszka Chacinska, Nikolaus Pfanner, and Peter Rehling. Tim50 maintains the permeability barrier of the mitochondrial inner membrane. *Science*, 312(5779):1523–1526, 2006. ISSN 0036-8075. doi: 10.1126/science.1127628.
- [171] Peter Kovermann. *Elektrophysiologische Charakterisierung des Proteinimports an der inneren Mitochondrienmembran*. PhD thesis, Universität Osnabrück, 2003.
- [172] Bertil Hille. *Ionic channels of excitable membranes*. Sinauer Associates, Inc., 3rd edition, 2001. ISBN 978-0878933211. URL <http://doi.wiley.com/10.1002/jnr.490130415>.
- [173] Nathan N. Alder, Robert E. Jensen, and Arthur E. Johnson. Fluorescence Mapping of Mitochondrial TIM23 Complex Reveals a Water-Facing, Substrate-Interacting Helix Surface. *Cell*, 134:439–450, 2008. ISSN 00928674. doi: 10.1016/j.cell.2008.06.007.

- [174] Ketan Malhotra, Murugappan Sathappa, Judith S. Landin, Arthur E. Johnson, and Nathan N. Alder. Structural changes in the mitochondrial Tim23 channel are coupled to the proton-motive force. *Nature Structural & Molecular Biology*, 20(8):965–972, jul 2013. ISSN 1545-9993. doi: 10.1038/nsmb.2613. URL <http://www.ncbi.nlm.nih.gov/pubmed/23832274><http://www.nature.com/doifinder/10.1038/nsmb.2613>.
- [175] Lilit Garibyan and Nidhi Avashia. Polymerase Chain Reaction. *Journal of Investigative Dermatology*, 133(3):1–4, mar 2013. ISSN 0022202X. doi: 10.1038/jid.2013.1. URL <http://linkinghub.elsevier.com/retrieve/pii/S0022202X1536139X>.
- [176] D Hanahan. Studies on transformation of *Escherichia coli* with plasmids. *Journal of molecular biology*, 166(4):557–80, jun 1983. ISSN 0022-2836. URL <http://www.ncbi.nlm.nih.gov/pubmed/6345791>.
- [177] Mariam Barbot, Daniel C. Jans, Christian Schulz, Niels Denkert, Benjamin Kroppen, Michael Hoppert, Stefan Jakobs, and Michael Meinecke. Mic10 Oligomerizes to Bend Mitochondrial Inner Membranes at Cristae Junctions. *Cell Metabolism*, 21(5):756–763, may 2015. ISSN 15504131. doi: 10.1016/j.cmet.2015.04.006. URL <http://linkinghub.elsevier.com/retrieve/pii/S1550413115001618>.
- [178] M. H. Zwietering, I. Jongenburger, F. M. Rombouts, and K van 't Riet. Modeling of the bacterial growth curve. *Applied and environmental microbiology*, 56(6):1875–81, jun 1990. ISSN 0099-2240. doi: 10.1111/j.1472-765X.2008.02537.x. URL <http://www.ncbi.nlm.nih.gov/pubmed/16348228><http://www.pubmedcentral.nih.gov/articlerender.fcgi?artid=PMC184525>.
- [179] E Hochuli, W Bannwarth, and H Döbeli. Genetic Approach to Facilitate Purification of Recombinant Proteins with a Novel Metal Chelate Adsorbent. *Nature Biotechnology*, 6:1321–1325, 1988. ISSN 0733-222X. doi: 10.1038/nbt1188-1321. URL <http://www.nature.com/nbt/journal/v6/n11/abs/nbt1188-1321.html>.
- [180] H G Barth, B E Boyes, and C Jackson. Size exclusion chromatography. *Analytical chemistry*, 66(12):595R–620R, jun 1994. ISSN 0003-2700. URL <http://www.ncbi.nlm.nih.gov/pubmed/8092479>.
- [181] Ulrich K. Laemmli. Cleavage of Structural Proteins during the Assembly of the Head of Bacteriophage T4. *Nature*, 227(5259):680–685, 1970. ISSN 0028-0836. doi: 10.1038/227680a0. URL <http://www.nature.com/doifinder/10.1038/227680a0>.
- [182] Alexander J. Ninfa, Avid P. Ballou, and Marilee Benore. Fundamental laboratory approaches for biochemistry and biotechnology. *Biochemistry and Molecular Biology Education*, 37(5):317–318, sep 2009. ISSN 14708175. doi: 10.1002/bmb.20321. URL <http://doi.wiley.com/10.1002/bmb.20321>.
- [183] Giovanni Candiano, Maurizio Bruschi, Luca Musante, Laura Santucci, Gian Marco Ghiggeri, Barbara Carnemolla, Paola Orecchia, Luciano Zardi, and Pier Giorgio Righetti. Blue silver: A very sensitive colloidal Coomassie G-250 staining for proteome analysis. *Electrophoresis*, 25(9):1327–1333, 2004. ISSN 01730835. doi: 10.1002/elps.200305844.
- [184] Yukio Fujiki, Ann L Hubbard, Stanley Fowler, and Paul B Lazarow. Isolation of Intracellular Membranes by Means of Sodium-Carbonate Treatment - Application to Endoplasmic-Reticulum. *Journal of Cell Biology*, 93(1):97–102, 1982. ISSN 0021-9525. doi: Doi10.1083/jcb.93.1.97.
- [185] Monika Naumowicz and Zbigniew Artur Figaszewski. Pore Formation in Lipid Bilayer Membranes made of Phosphatidylcholine and Cholesterol Followed by Means of Constant Current. *Cell Biochemistry and Biophysics*, 66(1):109–119, 2013. ISSN 10859195. doi: 10.1007/s12013-012-9459-6.
- [186] David Eliot Goldman. POTENTIAL, IMPEDANCE, AND RECTIFICATION IN MEMBRANES. *The Journal of general physiology*, 27(1):37–60, sep 1943. ISSN 0022-1295. doi: 10.1085/jgp.27.1.37. URL <http://jgp.rupress.org/content/27/1/37.abstract><http://www.ncbi.nlm.nih.gov/pubmed/19873371><http://www.pubmedcentral.nih.gov/articlerender.fcgi?artid=PMC2142582>.

- [187] Alan Lloyd Hodgkin and Bernard Katz. The effect of sodium ions on the electrical activity of giant axon of the squid. *The Journal of physiology*, 108(1):37–77, mar 1949. ISSN 0022-3751. URL <http://www.ncbi.nlm.nih.gov/pubmed/18128147><http://www.pubmedcentral.nih.gov/articlerender.fcgi?artid=PMC1392331>.
- [188] Oliver S. Smart, Jason Breed, Graham R. Smith, and Mark S. P. Sansom. A novel method for structure-based prediction of ion channel conductance properties. *Biophysical Journal*, 72(3):1109–1126, mar 1997. ISSN 00063495. doi: 10.1016/S0006-3495(97)78760-5. URL <http://linkinghub.elsevier.com/retrieve/pii/S0006349597787605>.
- [189] Anke Harsman, Vivien Krüger, Philipp Bartsch, Alf Honigmann, Oliver Schmidt, Sanjana Rao, Christof Meisinger, and Richard Wagner. Protein conducting nanopores. *Journal of physics. Condensed matter : an Institute of Physics journal*, 22(45):454102, 2010. ISSN 0953-8984. doi: 10.1088/0953-8984/22/45/454102.
- [190] Robert Reinhold, Vivien Krüger, Michael Meinecke, Christian Schulz, Bernhard Schmidt, Silke D. Grunau, Bernard Guiard, Nils Wiedemann, Martin van der Laan, Richard Wagner, Peter Rehling, and Jan Dudek. The channel-forming Sym1 protein is transported by the TIM23 complex in a presequence-independent manner. *Molecular and Cellular Biology*, 32(24):5009–5021, 2012. ISSN 0270-7306. doi: 10.1128/MCB.00843-12.
- [191] Philipp Bartsch, Anke Harsman, and Richard Wagner. Single Channel Analysis of Membrane Proteins in Artificial Bilayer Membranes. In Doron Rapaport and Johannes M. Herrmann, editors, *Membrane Biogenesis: Methods and Protocols*, volume 1033, chapter 22, pages 345–361. Springer Science+Business Media, 2013. ISBN 978-1-62703-486-9. doi: 10.1007/978-1-62703-487-6_22.
- [192] Frederic S Cohen, Joshua Zimmerberg, and Alan Finkelstein. Fusion of phospholipid vesicles with planar phospholipid bilayer membranes. *The Journal of general physiology*, 75:251–270, 1980. ISSN 0022-1295. URL <http://www.pubmedcentral.nih.gov/articlerender.fcgi?artid=2215255&tool=pmcentrez&rendertype=abstract>.
- [193] Frederic S. Cohen, Walter D. Niles, and Myles H. Akabas. Fusion of phospholipid vesicles with a planar membrane depends on the membrane permeability of the solute used to create the osmotic pressure. *The Journal of General Physiology*, 93(2):201–210, feb 1989. ISSN 0022-1295. doi: 10.1085/jgp.93.2.201. URL <http://www.jgp.org/cgi/doi/10.1085/jgp.93.2.201>.
- [194] Thomas Hotz, Ole M. Schutte, Hannes Sieling, Tatjana Polupanow, Ulf Diederichsen, Claudia Steinem, and Axel Munk. Idealizing ion channel recordings by a jump segmentation multiresolution filter. *IEEE Transactions on Nanobioscience*, 12(4):376–386, 2013. ISSN 15361241. doi: 10.1109/TNB.2013.2284063.
- [195] Florian Pein, Inder Tecuapetla-Gómez, Ole M. Schütte Claudia Steinem, and Axel Munk. Fully-Automatic Multiresolution Idealization for Filtered Ion Channel Recordings: Flickering Event Detection. *arXiv preprint*, jun 2017. URL <http://arxiv.org/abs/1706.03671>.
- [196] Joseph B. Patlak. Measuring kinetics of complex single ion channel data using mean-variance histograms. *Biophysical journal*, 65(July):29–42, 1993. ISSN 00063495. doi: 10.1016/S0006-3495(93)81041-5.
- [197] Keren Demishtein-Zohary, Milit Marom, Walter Neupert, Dejana Mokranjac, and Abdussalam Azem. GxxxG Motifs hold the TIM23 Complex Together. *FEBS Journal*, pages n/a–n/a, 2015. ISSN 1742464X. doi: 10.1111/febs.13266. URL <http://doi.wiley.com/10.1111/febs.13266>.
- [198] Niels Denkert, Alexander Benjamin Schendzielorz, Mariam Barbot, Lennart Versemann, Frank Richter, Peter Rehling, and Michael Meinecke. Cation selectivity of the presequence translocase channel Tim23 is crucial for efficient protein import. *eLife*, 6:1–16, aug 2017. ISSN 2050-084X. doi: 10.7554/eLife.28324. URL <http://elifesciences.org/lookup/doi/10.7554/eLife.28324>.

- [199] Jingzhi Li and Bingdong Sha. The structure of Tim50(164–361) suggests the mechanism by which Tim50 receives mitochondrial presequences. *Acta Crystallographica Section F Structural Biology Communications*, 71(9):1146–1151, 2015. ISSN 2053-230X. doi: 10.1107/S2053230X15013102. URL <http://scripts.iucr.org/cgi-bin/paper?S2053230X15013102>.
- [200] Jörg Martin, Kerstin Mahlke, and Nikolaus Pfanner. Role of an energized inner membrane in mitochondrial protein import: $\Delta\Psi$ Drives the movement of presequences. *Journal of Biological Chemistry*, 266(27):18051–18057, 1991. ISSN 00219258.
- [201] David Roise. Interaction of a synthetic mitochondrial presequence with isolated yeast mitochondria: mechanism of binding and kinetics of import. *Proc Natl Acad Sci USA*, 89(2):608–612, 1992. ISSN 00278424.
- [202] Wonpil Im and Benoît Roux. Ion Permeation and Selectivity of OmpF Porin: A Theoretical Study Based on Molecular Dynamics, Brownian Dynamics, and Continuum Electrodiffusion Theory. *Journal of Molecular Biology*, 322(4):851–869, sep 2002. ISSN 00222836. doi: 10.1016/S0022-2836(02)00778-7. URL <http://linkinghub.elsevier.com/retrieve/pii/S0022283602007787>.
- [203] Carsten Kutzner, Helmut Grubmüller, Bert L. De Groot, and Ulrich Zachariae. Computational electrophysiology: The molecular dynamics of ion channel permeation and selectivity in atomistic detail. *Biophysical Journal*, 101(4):809–817, 2011. ISSN 00063495. doi: 10.1016/j.bpj.2011.06.010.
- [204] Carsten Kutzner, David A. Köpfer, Jan-Philipp Machtens, Bert L. de Groot, Chen Song, and Ulrich Zachariae. Insights into the function of ion channels by computational electrophysiology simulations. *Biochimica et Biophysica Acta (BBA) - Biomembranes*, 1858(7):1741–1752, jul 2016. ISSN 00052736. doi: 10.1016/j.bbamem.2016.02.006. URL <http://linkinghub.elsevier.com/retrieve/pii/S0005273616300360>.

Appendix - R scripts

6.1 R: Reconstruction of .abf Using SMUCE

```
1 ls() # This is my default workspace from My
    Documents.
2 setwd(getwd()) # First change, if you haven't already.
3 rm(list=ls()) # Delete the default workspace.
4
5 .getNamespace <- function(name) .Internal(getRegisteredNamespace(as.name(name)
    )))
6 library(abf2)
7 library(gtools)
8 library(stats)
9 if(isNamespaceLoaded("stepR2")){detach("package:stepR2", unload=TRUE)} else
    {}
10 library(stepR)
11 # # # # # # #
12 # parameters to specify #
13 # record parameters
14 sampling<-5e4 #sampling frequency
15 cutoff<-5e3 #cutoff frequency of applied filter
16 # time window, when to apply fit
17 autotime<-FALSE #automatically specify time boundaries by checking voltage
    changes (time1=t(voltage1)+1s, time2=t(voltage2)-1s)
18 time1<-6 #voltage is usually changed at t=5s, at time1=6s the signal should
    be mostly stable
19 time2<-65 #voltage change at t=65s
20 # size of each fit-segment
21 LL<-15000 #segment of 15k points work nicely, can also try 20k or 25k, but
    the fits take longer
22 # threshold for gating detection
23 c0<-15 #minimum conductance change in pS for detection of a gating event
24 t0<-0 #minimum dwell time,
25 # setting for displaying plots
26 PLOT<-TRUE #decide if a plot of every segment (with length LL) should be
    displayed
27 # setting for saving gating events and dwell times to txt-files
28 SAVE<-TRUE
29 # # # # # # #
30
31
```

```

32 Find.Indices.False.Positive<-function(v){ # this function returns a matrix
    containing the clusters of indices of false positive events
33 v.aux<-c(v,v[length(v)])
34 l=length(v.aux)
35 if(l>0){
36   Matriz<-matrix(rep(0,(l-1)*(l-1)),nrow=(l-1))
37   temp<-c()
38   for(i in 1:(l-1)){
39     temp<-c(temp,v.aux[i])
40     if(abs(v.aux[i]-v.aux[(i+1)]) == 1){
41       temp<-c(temp,v.aux[(i+1)])
42     }
43     else{
44       temp<-unique(temp)
45       Matriz[i,1:length(temp)]<-temp[1:length(temp)];
46       temp<-c();
47     }
48   }
49 n.row<-sum(Matriz[,1] != 0)
50 M.aux<-matrix(rep(0,(l-1)*n.row),nrow=n.row)
51 ind.aux<-1:(l-1)
52 for(j in 1:n.row){
53   k<-ind.aux[Matriz[,1] != 0][j]
54   M.aux[j,]<-Matriz[k,]
55 }
56 } else{
57 M.aux<-matrix();
58 }
59 M.aux
60 }
61
62 indices.rep<-function(w){ #the parameter of this function, w, has to be the
    output of Find.Indices.False.Positive.
63 temp<-matrix(rep(0,nrow(w)*2),ncol=2) #each row contains: the index of the
    first gating event in a seq. of consecutive gating events; lenght of seq
    . of gating events
64 for(i in 1:nrow(w)){
65   temp[i,]<-c(w[i,1],length(w[i,w[i,]>0]))}
66 temp
67 }
68
69 #fit.idealization returns a list containing
70 #1) newFitValue, that is, after identifying false positive events, we removed
    them and replace their values accordingly.
71 #2) falsePositiveIndices, a vector containing the indices of all the false
    positive events.
72 #3) clustersIndices, a 2 x l matrix, first column contains the index of the
    first false positive event in a seq of consecutive false positive events,
73 # second column contains the lenght of the seq of the corresponding
    consecutive false positive events.
74 #4) values, a vector containing ONLY the values of the idealization.
75

```

```

76 fit.idealization<-function(fit , t1, t2){# fit is an object of the class fit(
      jsmurf or smuceR), t1 and t2 are thresholds
77   n=length(fit$value)
78   fit.leftEnd<-fit$leftEnd
79   fit.rightEnd<-fit$rightEnd
80
81   if(n>2){
82     ind1<-2:(n-1)
83     fit.value <- fit$value[ind1]
84     fit.value.fwd <- fit$value[3:n]
85     fit.value.bwd <- fit$value[1:(n-2)]
86
87     cri1 <- abs( fit.value-fit.value.fwd ) >= t1
88     cri2 <- abs( fit.value-fit.value.bwd ) >= t1
89     cri3 <- fit$rightEnd[ind1]-fit$leftEnd[ind1] < t2
90
91
92     x<-ind1[cri1 & cri2 & cri3] # indices of all false positive events
93     fit.leftEnd
94     gatings<-Find.Indices.False.Positive(x)
95     indices<-indices.rep(gatings)
96     Y.aux<-fit$value
97
98     for(i in 1:nrow(indices)){#here we update the vector fit$value, we remove
      the gating events and fill the gap accordingly
99       indice<-indices[i,1]
100      length<-indices[i,2]
101      ifelse(length == 1, Y.aux[indice]<-fit$value[(indice-1)], Y.aux[indice:(
        indice+length-1)] <- rep(fit$value[indice-1],length))
102      }
103
104      for(i in (n-1):1){ #delete subsequent identical levels
105        if(is.finite(Y.aux[i])){
106
107          if((Y.aux[i] - Y.aux[i+1])==0){
108            Y.aux<-Y.aux[-i]
109            fit.leftEnd<-fit.leftEnd[-(i+1)]
110            fit.rightEnd<-fit.rightEnd[-i]
111          } else {}
112          } else {}
113        }
114      }
115
116
117     f=length(Y.aux)
118     fit.value.new<-c()
119     for(j in 1:f){#here we simply update the fitted function, cf. fit.aux<-
      fitted(fit) above
120     l <- (fit.rightEnd[j]-fit.leftEnd[j]+1)
121     temp <- rep(Y.aux[j],l)
122     fit.value.new<-c(fit.value.new,temp)
123     }
124     } else {

```

```

125     x<-c(FALSE)
126     indices<-c()
127     Y.aux<-fit$value
128     f=length(fit$value)
129     fit.value.new<-c()
130     for(j in 1:f){#here we simply update the fitted function, cf. fit.aux<-
131         fitted(fit) above
132         l <- (fit$rightEnd[j]-fit$leftEnd[j]+1)
133         temp <- rep(Y.aux[j],l)
134         fit.value.new<-c(fit.value.new,temp)
135     }
136     List<-list("newFitValue"=fit.value.new,"falsePositiveIndices"=x,"
137         clustersIndices"=indices,"value"=Y.aux,"leftEnd"=fit.leftEnd,"
138         rightEnd"=fit.rightEnd)
139     return(List)
140 }
141 ### Gating Event Detection ###
142 # find transitions above t1, calculate the current changes and name them
143     gatingEvents
144 GatingEventDetection<-function(idealized.fit, t1, V, LL, sampling, time1, t0)
145     { #idealized.fit is the output of fit.idealization, t1 is the minimum
146         current change (in pA), V is the voltage applied in the trace, LL is the
147         length of the fit-segment, sampling is the sampling frequency, time1 is
148         the starting time of the idealization within the real trace (like time1=6
149         s if voltage change occurred at 5s) and h is the turn number, i.e. which
150         fit-segment is currently processed
151     nn <- length(idealized.fit$value)
152     if(nn>1){
153         ind2<-1:(nn-1)
154         ideal.value <- idealized.fit$value[ind2]
155         ideal.value.fwd <- idealized.fit$value[2:nn]
156         cri4 <- abs(ideal.value-ideal.value.fwd) >= t1
157         gatingEvents <- abs(idealized.fit$value[c(FALSE, cri4)] - idealized.fit$value[c(cri4, FALSE)])
158         conductance<-abs(gatingEvents/V*1000)
159         gatingTime<-((idealized.fit$leftEnd[c(FALSE, cri4)])/sampling)+time1
160         Gating.temp <- cbind(gatingTime, idealized.fit$value[c(cri4, FALSE)],
161             idealized.fit$value[c(FALSE, cri4)], gatingEvents, deparse.
162             level = 0)
163     } else { Gating.temp<-c() }
164     # tidy up, check 2nd threshold (minimum dwell time)
165     Gating<-Gating.temp
166     LG<-nrow(Gating)
167     if(LG>3){
168         Gating.t<-Gating
169         for(i in LG:4){
170             if(is.finite(as.numeric(Gating.t[i]))){
171                 diffG<- (as.numeric(Gating[i,1]) - as.numeric(Gating[(i-1),1]))*1000

```

```

165     if(diffG < t0){
166       Gating.t <- Gating.t[-i,]
167       LG.t <- nrow(Gating.t)
168       if(i < LG.t + 2){
169         if(i > 4){
170           diffG.bwd <- (as.numeric(Gating[i-1,1]) - as.numeric(Gating[(i-2),1])
171                        ) * 1000
172           ifelse(diffG.bwd > t0, Gating.t <- Gating.t[-(i-1),], "")
173         } else{ ifelse(i == 4, Gating.t <- Gating.t[-(i-1),]) }
174       } else{ }
175     } else{ }
176   }
177   Gating <- Gating.t
178 } else{ }
179
180 List <- list("Gating" = Gating)
181 return(List)
182 }
183
184
185 ### AFTER going through all trace-segments ###
186 # tidy up "ValuesDwell" and "Gating" to delete every entry below a set time
187 # minimum
188 # idealized.fit <- full.fit
189 # Gating <- Gatings$Gating
190 SmoothenIdeal <- function(idealized.fit, Gating, time1, time2, sampling, V, t1){
191   GatingPoints.t <- (as.double(Gating[,1][1:nrow(Gating)]) - time1) * sampling
192
193   GatingPoints <- append(GatingPoints.t, length(idealized.fit$newFitValue), after
194                        = length(GatingPoints.t))
195   GatingPoints <- append(GatingPoints, 0, after = 0)
196
197   for(i in 1:10){
198     L <- length(GatingPoints) - 1
199     Smooth.v <- c()
200     if(L > 1){
201       for(i in 1:L){
202         Smooth.v <- c(Smooth.v, as.double(summary(idealized.fit$newFitValue[(
203           GatingPoints[i]+1):(GatingPoints[i+1])])[4])) #mean value between
204           gating event "i" and "i+1"
205       }
206       for(i in length(Smooth.v):2){ #i <- 1
207         if((abs(Smooth.v[i] - Smooth.v[i-1])) < t1){
208           GatingPoints <- GatingPoints[-i]
209           GatingPoints.t <- GatingPoints.t[-(i-1)]
210         } else{ }
211       } } else{ }
212     }
213   }
214   L <- length(GatingPoints) - 1
215   Smooth.l <- c()
216   Smooth.r <- c()

```

```

213 Smooth.value<-c()
214 for(i in 1:L){
215   Smooth.value<-c(Smooth.value,as.double(summary(idealized.fit$newFitValue[(
      GatingPoints[i]+1):(GatingPoints[i+1]))[4])) #mean value between
      gating event "i" and "i+1"
216   Smooth.l<-c(Smooth.l,GatingPoints[i]+1) #leftEnd of each
      segmen
217   Smooth.r<-c(Smooth.r,GatingPoints[i+1]) #rightEnd of each
      segmen
218 }
219
220 L2<-length(GatingPoints)-1
221 Smooth.Gating<-c()
222 if(length(Smooth.value)>1){
223   Smooth.Gating<-cbind((GatingPoints.t/sampling)+timel,Smooth.value[1:(L2-1)
      ],Smooth.value[2:L2],abs(Smooth.value[1:(L2-1)]-Smooth.value[2:L2])
      ,abs(abs(Smooth.value[1:(L2-1)]-Smooth.value[2:L2])*1000/V),deparse
      .level=0)
224 } else {
225   Smooth.Gating<-cbind("-", "-", "-", "-", "-", deparse.level=0)
226 }
227
228 Smooth.DwellTime <- (Smooth.r - Smooth.l)/sampling
229 Smooth.DwellLevelC <- Smooth.value/V
230 Smooth.DwellLevelI <- Smooth.value
231 Smooth.Dwell<-c()
232 Smooth.Dwell<-cbind(Smooth.DwellTime,Smooth.DwellLevelI,Smooth.DwellLevelC,
      "", "", deparse.level=0)
233
234 List<-list("value"=Smooth.value,"leftEnd"=Smooth.l,"rightEnd"=Smooth.r,"
      Gating"=Smooth.Gating,"DwellTime"=Smooth.Dwell)
235
236 return(List)
237 }
238
239 # Loading datasets
240
241 files <- list.files(getwd(),pattern = "\\\\.abf$", all.files=TRUE,full.names=
      TRUE,ignore.case=TRUE,include.dirs=TRUE,recursive=TRUE)
242 files <- files[mixedorder(files)]
243 LF <- length(files)
244 files
245
246 for(f in 1:LF){ #go through all files that are present in the main folder
247
248   trace<- abfload(files[f])
249
250   if(nrow(trace$tags)>1){ #check if there has been a voltage applied
251     V<-trace$tags[2,2]
252
253     if(autotime){# if autotime==TRUE, set timel and time2 next to voltage changes
254       timel<-trace$tags[2,1]+1
255       if(nrow(trace$tags)>2){

```



```

256 time2<-trace$tags[3,1]-1
257 } else{ time2<-64 }
258 } else{ }
259
260 name <- basename( files[f] )
261 dir <- dirname( files[f] )
262 nameL <- nchar( basename( files[f] ) )
263 name <- substr( name,1,nameL-4) #reformat filename for data export later
264
265
266 lbound <- trace$s>time1;
267 ubound <- trace$s<time2;
268 traces <- trace$traces[ lbound & ubound ] # skim the trace to
269
270
271 t2 <- t0*sampling/1000 #threshold for dwell time in points
272 t1 <- abs(V*c0/1000) #threshold for gating events, scaled by voltage to
    account for smaller current-changes
273
274 LcountR <- ceiling( length( traces ) / LL ) #round up number of runs
275 if ( LcountR == 1 ) {
276 LL <- length( traces )
277 } else { }
278
279 full.fit <- c()
280 Gating <- c()
281 VD <- c()
282
283 for( h in 1:LcountR ) {
284 LB <- (h-1)*LL + 1
285 if ( h*LL <= length( traces ) ) {
286 RB <- h*LL
287 }
288 else { RB <- length( traces ) }
289 ion.chan <- traces[ LB:RB ]
290
291 # Setting the fit
292
293 # JSMURF for ion channel
294 dfil <- dfilter( "bessel", list( pole=4, cutoff = cutoff / sampling ) ) # define
    filter
295 fit.ion.chan <- jsmurf( ion.chan, param=dfil, r=1e2, confband=FALSE ) #
    reconstruction
296 fit.aux1 <- fitted( fit.ion.chan )
297 fit <- fit.ion.chan
298
299 ideal.ion.chan <- fit.idealization( fit.ion.chan, t1, t2 ) # idealization of
    reconstruction
300 full.fit$newFitValue <- c( full.fit$newFitValue, ideal.ion.chan$newFitValue )
301 full.fit$value <- c( full.fit$value, ideal.ion.chan$value )
302 full.fit$rightEnd <- c( full.fit$rightEnd, ( ideal.ion.chan$rightEnd + LL*(h-1) ) )
303 full.fit$leftEnd <- c( full.fit$leftEnd, ( ideal.ion.chan$leftEnd + LL*(h-1) ) )
304

```

```

305 }
306 }
307
308 Gatings<-c()
309 Smooth<-c()
310 Gatings<-GatingEventDetection( full.fit , t1 , V , LL , sampling , time1 , t0 ) # extract
      gating events from idealization
311 # Gating output is: Time[s] StartLevel[pA] EndLevel[pA] Difference[pA]
      Conductance[pS]
312 Smooth<-SmoothenIdeal( full.fit , Gatings$Gating , time1 , time2 , sampling , V , t1 ) #
      smoothen idealization data between detected gating events
313
314
315 # export matrices to txt , seperator is tab for easy import. no names to avoid
      "" which messes up with importIntoEnv
316 header<-cbind( paste( "Minimum Dwell Time:" , t0 , "ms ----" ) , paste( "Minimum Gating
      :" , c0 , "pS ----" ) , "" , "" , "" , deparse.level=0)
317 headerVD<-cbind( "Dwell Time (s)" , "Current (pA)" , "Conductance (nS)" , "" , "" ,
      deparse.level=0)
318 headerGating<-cbind( "Time (s)" , "From (pA)" , "To (pA)" , "Diff (pA)" , "Gating (pS)"
      , deparse.level=0)
319 Gating.final<-rbind( header , headerGating , Smooth$Gating , deparse.level=0)
320 VD<-rbind( header , headerVD , Smooth$DwellTime , deparse.level=0)
321
322
323 if(SAVE){ # export two files
324 write.table( Gating.final , file=paste( dir , "/" , V , "mV_" , name , "-SMUCE-gating.txt" ,
      sep="" ) , row.names=FALSE , col.names=FALSE , sep="\t" , quote=FALSE)
325 write.table( VD , file=paste( dir , "/" , V , "mV_" , name , "-SMUCE-dwell.txt" , sep="" ) , row
      .names=FALSE , col.names=FALSE , sep="\t" , quote=FALSE)
326 } else { }
327 } else { }
328
329 if(PLOT){ # plot the original trace , reconstruction , idealization and
      smoothened fit
330 SL<-LL/sampling
331 par(mfrow=c(1,1))
332 y=range(ion.chan)
333 dy=y[2]-y[1]; y=y+.1*dy*c(-1,1) # adjusting the y-axis
334 plot(ion.chan , type='p' , pch='.' , ylim=y , cex.lab=1.5 , cex.axis=1.25 , xaxt='
      n' , yaxt='n' , ylab='pA' , xlab='time (ms)')
335 mtext('A' , side=3 , adj=0 , line=1.2 , cex=2 , font=2)
336 axis(2 , las=1)
337 axis(1 , at=seq(0,LL , by=LL/3) , labels=c( time1+(h-1)*SL , time1+SL/3+(h-1)*SL ,
      time1+SL*2/3+(h-1)*SL , time1+SL+(h-1)*SL))
338 lines(1:length( fit.aux1 ) , fit.aux1 , type='l' , lwd=2.5 , lty=2 , col='green3')
339 lines(1:length( full.fit$newFitValue ) , full.fit$newFitValue , type='l' , lwd=5 , lty
      =3 , col='blue3')
340 lines(1:length( Smooth$newFit ) , Smooth$newFit , type='l' , lwd=3.5 , lty=4 , col='red3'
      )
341
342 legend("bottomright" , inset=.1 , legend=c("jsmurf-fit" , "Final Idealization" ,
      "Smooth Fit" ) , lty=c(2,3) , col=c("green3" , "blue3" , "red3") ,

```

```

343 horiz=F, pt.cex=0.8, cex=1)
344 } else{ }
345 }

```

./Rscripts/SMUCE.R

6.2 R: Reconstruction of .abf Using JULES

```

1 ls () # This is my
   default workspace from My Documents.
2 setwd(getwd()) # First change,
   if you haven't already.
3 load("DependencylonChannel-III.RData") # Load a
   previously saved workspace.
4 rm(list=ls()) # Delete the
   default workspace.
5 ls ()
6
7
8 library(tools)
9 library(gtools)
10 library(abf2)
11 if(isNamespaceLoaded("stepR")){
12   pkg <- "package:stepR"
13   detach(pkg, character.only=TRUE, unload=TRUE)
14 } else {}
15 library(stepR2)
16 library(dbacf)
17 time.start<-as.double(proc.time()[3])
18
19
20 GatingEventDetection<-function(idealized.fit, t1, V, sampling, t0){ #
   idealized.fit is the output of fit.idealization, t1 is the minimum
   conductance change (in pA), V is the voltage applied in the trace, LL is
   the length of the fit-segment, sampling is the sampling frequency, timel
   is the starting time of the idealization within the real trace (like
   timel=6s if voltage change occurred at 5s) and h is the turn number, i.e.
   which fit-segment is currently processed
21
22 ##### use as test environment #####
23 # idealized.fit<-postDeconv
24 # t1 <- c0
25 # V<-voltage
26 # sampling<-sr
27 # t0
28 #####
29
30 nn <- length(idealized.fit$value)
31 if(nn>1){
32   ideal.value <- idealized.fit$value[1:(nn-1)]
33   ideal.value.fwd <- idealized.fit$value[2:nn]

```

```

34 cri4 <- abs( ideal.value-ideal.value.fwd ) >= t1/1000 & ideal.value.fwd*
    abs(V) >= -4 & ideal.value*abs(V) >= -4 # filter out events that go
    far over zero (farer than 4pA)
35 for(i in 1:length(cri4)){
36   if(is.na(cri4[i])){
37     cri4[i]<-FALSE
38   } else {}
39 }
40
41 gatingEvents <- abs( idealized.fit$value[c(FALSE, cri4)]*V - idealized.
    fit$value[c(cri4, FALSE)]*V)
42 conductance<-gatingEvents/abs(V)*1000
43 gatingTime<- idealized.fit$leftEnd[c(FALSE, cri4)]
44 Gating.temp <- cbind(gatingTime, V*idealized.fit$value[c(cri4, FALSE)], V
    *idealized.fit$value[c(FALSE, cri4)], gatingEvents, conductance,
    deparse.level = 0)
45
46
47 # tidy up, check 2nd threshold (minimum dwell time)
48 Gating<-Gating.temp
49 LG<-nrow(Gating)
50 if(LG>3){
51   Gating.t<-Gating
52   for(i in LG:4){
53     if(is.finite(as.numeric(Gating.t[i]))){
54       diffG<- (as.numeric(Gating[i,1]) - as.numeric(Gating[(i-1),1]))*1000
55       if(diffG <t0){
56         Gating.t<-Gating.t[-i,]
57         LG.t<-nrow(Gating.t)
58         if(i<LG.t+2){
59           if(i>4){
60             diffG.bwd<-(as.numeric(Gating[i-1,1])-as.numeric(Gating[(i-2)
    ,1]))*1000
61             ifelse(diffG.bwd>t0, Gating.t<-Gating.t[-(i-1),], "")
62           } else { ifelse(i==4,Gating.t<-Gating.t[-(i-1),1])
63             } else { }
64           } else { }
65         } else { }
66       }
67     }
68     DwellTime <- c(Gating[,1], tail(idealized.fit$rightEnd, n=1)) - c(
    idealized.fit$leftEnd[1], Gating[,1])
69     DwellLevelI <- c(Gating[,2], tail(Gating[,3], n=1) )
70     DwellLevelC <- DwellLevelI/V
71   } else {
72     if(LG>0){
73       DwellTime <- c(Gating[,1], tail(idealized.fit$rightEnd, n=1)) - c(
    idealized.fit$leftEnd[1], Gating[,1])
74       DwellLevelI <- c(Gating[,2], tail(Gating[,3], n=1) )
75       DwellLevelC <- DwellLevelI/V
76     } else {
77       DwellTime <- c(Gating[,1], tail(idealized.fit$rightEnd, n=1)) - c(
    idealized.fit$leftEnd[1], Gating[,1])

```

```

78     avgC <-sum( (idealized.fit$value * (idealized.fit$rightEnd - idealized.
79               fit$leftEnd)) / (idealized.fit$rightEnd[nn] - idealized.fit$leftEnd
80               [1]))
81     DwellLevelC <- avgC
82     DwellLevelI <- avgC*V
83   }
84 }
85 FullDwellTimes <- cbind(DwellTime, DwellLevelI, DwellLevelC, "", "",
86                         deparse.level = 0)
87 } else {
88   Gating <- cbind(c(), c(), c(), c(), c(), deparse.level = 0)
89   FullDwellTimes <- cbind(idealized.fit$rightEnd - idealized.fit$leftEnd, V
90                           *idealized.fit$value, idealized.fit$value, "", "", deparse.level = 0)
91 }
92 List<-list("Gating"=Gating, "DwellTime"=FullDwellTimes)
93 return(List)
94 }
95
96 #-----PARAMETERS-----
97 #-----
98 sr <- 5e4 # sampling rate
99 cf <- 5e3 / 5e4 # cutoff factor, filter/sampling
100
101 #-----
102 m <- 30L
103 n_norm <- 5e5 # number of data points per fit segment
104 alpha <- 0.05 # quality parameter of fit
105 #-----GatingEventDetection-----
106 c0 <- 15 # gating threshold in pS
107 t0 <- 0 # dwell time threshold in ms
108 #-----
109 SingleFile <- FALSE # fit only one file?
110 FileNumber <- 13 # if yes, which?
111 FullTrace <- FALSE # consider full trace betw. V changes?
112 ManualStart <- 6 # starting point if above is FALSE
113 ManualEnd <- 65 # ending point if above is FALSE
114 PLOT <- TRUE # plot each 10s segment?
115 SAVE <- TRUE # save Gating Events and Dwell Times?
116 #-----
117
118 filter <- dfilter(type = "besselButter", param = list(poleBessel = 4,
119               cutoffBessel = 0.1, R = 500, C = 3300e-12), sr = 5e4, len = 30)
120 kern <- filter$kern
121 correlations <- filter$param$acf
122
123 files <- list.files(getwd(), "\\*.abfs", all.files=TRUE, full.names=TRUE, ignore
124                   .case=TRUE, include.dirs=TRUE, recursive=TRUE)
125 files <- files[mixedorder(files)]

```

```

125 files
126 if (SingleFile){LF<-1} else {LF <- length(files)}
127
128
129 for(f in 1:LF){           #reverse order
130 if (SingleFile){f<-FileNumber} else {}
131
132 name <- basename(files[f])
133 dir <- dirname(files[f])
134 nameL <- nchar(basename(files[f]))
135 name <- substr(name,1,nameL-4)
136
137 abf <- abfload(files[f])
138
139
140 if(FullTrace){
141 start <- ceiling(abf$tags[2,1] + 0.3)*sr
142 end <- floor(abf$tags[3,1] - 0.1)*sr
143 } else {
144   start <- ManualStart*sr
145   end <- ManualEnd*sr
146 }
147 startTime <- start/sr
148 endTime <- end/sr
149
150 L <- ceiling((end-start)/n_norm)
151 LastStep <- (end-start)/n_norm - floor((end-start)/n_norm)
152 FullTime <- abf$s
153 voltage <- abf$tags[2,2]
154 current <- abf$traces[1,]
155 FullData <- current / voltage
156 rm(abf)           #remove abf again, its huge!
157
158
159 GatingFinal =list()
160
161
162 for(i in 1:L){ #i<-1
163   time.quantiles1 <- as.double(proc.time()[3])
164   if(i==L & LastStep!=0){
165     n <- (LastStep*n_norm)
166     time <- FullTime[start + (i-1)*n_norm + 1:n]
167     data <- FullData[start + (i-1)*n_norm + 1:n]
168
169     stat <- t(readRDS(paste(getwd(), "/dyaLen/dyaLen", 2^ceiling(log2(n)), ".rds", sep = "")))
170     q <- critVal(stat = stat, n = n, family = "mDependentPS", alpha = alpha,
171               covariances = correlations, intervalSystem = "dyaLen", output = "vector")
172   } else {
173     stat <- t(readRDS(paste(getwd(), "/dyaLen/dyaLen", 2^ceiling(log2(n_norm)), ".rds", sep = "")))

```

```

173   q <- critVal(stat = stat, n = n_norm, family = "mDependentPS", alpha =
      alpha, covariances = correlations, intervalSystem = "dyaLen", output
      = "vector")
174   time <- FullTime[start + (i-1)*n_norm + 1:n_norm]
175   data <- FullData[start + (i-1)*n_norm + 1:n_norm]
176 }
177 time.quantiles<-as.double(proc.time()[3]) - time.quantiles1
178
179
180   time.Firstfit1<-as.double(proc.time()[3])
181 estSd <- stepR::sdrobnorm(data, lag = m + 1L)
182
183 fit <- stepFit(data, x = time, family = "mDependentPS", q = q, confband =
      TRUE,
184             covariances = estSd^2 * correlations, intervalSystem = "dyaLen
      ")
185 FirstFit <- fit
186 postIncr <- postFilterIncremental(fit, t0 = m)
187 time.Firstfit <- as.double(proc.time()[3]) - time.Firstfit1
188
189
190
191 # threshold to filter small jumps
192 # increasing sequences work better than computing just one round
193 time.iteration1<-as.double(proc.time()[3])
194 for(i in 1:(c0/1000/0.005 -1)){
195   postFpiterative <- postFilterFalsePositiveAbsoluteValue(postIncr, data,
      threshold = i*0.005)
196 }
197 postFpiterativeOld <- postFpiterative
198 postFpiterativeNew <- postFilterFalsePositiveAbsoluteValue(postFpiterativeOld
      , data, threshold = (c0/1000/0.005 -1)*0.005)
199
200 counter<-0
201 while (length(postFpiterativeNew$value) != length(postFpiterativeOld$value))
      {
202   postFpiterativeOld <- postFpiterativeNew
203   postFpiterativeNew <- postFilterFalsePositiveAbsoluteValue(
      postFpiterativeOld, data, threshold = (c0/1000/0.005 -1)*0.005)
204   counter<-counter+1
205 }
206
207 postFp <- postFpiterativeNew
208 time.iteration<- as.double(proc.time()[3]) - time.iteration1
209
210
211 time.deconv1<-as.double(proc.time()[3])
212 thresholdShortSegment <- 10 + m * 2
213 shiftStart <- m
214 shiftEnd <- m
215 messages <- TRUE
216

```

```

217 postDeconv <- deconvolveLocally(fit = postFp, data = data, x = time, filter =
      filter,
218                                     covariances = filter$param$acf * estSd^2,
219                                     thresholdShortSegment = thresholdShortSegment
220                                     ,
221                                     shiftStart = shiftStart, shiftEnd = shiftEnd,
222                                     messages = TRUE)
222 time.deconv<- as.double(proc.time()[3]) - time.deconvl
223 # output similar than with jsmurf: postDeconv$leftEnd ; postDeconv$value ;
      postDeconv$rightEnd
224
225 GatingFinal.t <-c()
226 GatingFinal.t <- GatingEventDetection(postDeconv, c0, voltage, sr, t0)
227 GatingFinal$Gating <- rbind(GatingFinal$Gating, GatingFinal.t$Gating, deparse
      .level=0)
228 GatingFinal$DwellTime <- rbind(GatingFinal$DwellTime, GatingFinal.t$DwellTime
      , deparse.level=0)
229
230 if(PLOT){
231   plot(time, data, type='p')
232   lines(FirstFit, col='blue3')
233   lines(postFp, col='red3')
234   lines(postDeconv, col='orange')
235 } else {}
236
237 } # end of the for-loop going through the whole data set of a
      single file
238
239
240 time.savel<- as.double(proc.time()[3])
241 header<-cbind(paste("Minimum Dwell Time:", t0, "ms ---"), paste("Minimum Gating
      :", c0, "pS ---"), "", "", "", deparse.level=0)
242 headerVD<-cbind("Dwell Time (s)", "Current (pA)", "Conductance (nS)", "", "",
      deparse.level=0)
243 headerGating<-cbind("Time (s)", "From (pA)", "To (pA)", "Diff (pA)", "Gating (pS)
      ", deparse.level=0)
244 Gating.final<-rbind(header, headerGating, GatingFinal$Gating, deparse.level=0)
245 VD<-rbind(header, headerVD, GatingFinal$DwellTime, deparse.level=0)
246
247
248 if(SAVE){
249   write.table(Gating.final, file=paste(dir, "/", voltage, "mV_", name, "_",
      startTime, "to", endTime, "-JULES-G.txt", sep=""), row.names=FALSE, col.
      names=FALSE, sep="\t", quote=FALSE)
250   write.table(VD, file=paste(dir, "/", voltage, "mV_", name, "_", startTime, "to",
      endTime, "-JULES-DT.txt", sep=""), row.names=FALSE, col.names=FALSE, sep="\
      t", quote=FALSE)
251 } else{ }
252
253
254 } # end of the for-loop going through all abf-files
255 time.full <- as.double(proc.time()[3]) - time.start
256 time.full

```

```
./Rscripts/JULES.R
```

6.3 R: Mean-Variance Analysis from Dwelltime-List

```

1 ls () # This is my default workspace from My
  Documents.
2 setwd(getwd()) # First change, if you haven't already.
3 rm(list=ls()) # Delete the default workspace.
4 ls ()
5 .getNamespace <- function(name) .Internal(getRegisteredNamespace(as.name(name
  )))
6 library(gtools)
7 library(stats)
8
9 #####
10 W.base <- 100 #window length for MV plot
11 freq.base<-50000
12 fil <- 1 #reduce number of datapoints and window length by factor <fil >
13 #####
14 freq <- freq.base / fil
15 W <- W.base / fil
16
17 files <- list.files(getwd(), pattern = "*dwell*\\.txt$", all.files=TRUE, full.
  names=TRUE, ignore.case=TRUE, include.dirs=TRUE, recursive=TRUE)
18 #files <- list.files(getwd(), pattern = "*DT*\\.txt$", all.files=TRUE, full.
  names=TRUE, ignore.case=TRUE, include.dirs=TRUE, recursive=TRUE)
19 files <- files[mixedorder(files)]
20 files
21 LF <- length(files)
22
23 MVtot<-c()
24
25 for(f in 1:LF){
26 data.orig <- read.table(files[f], header=FALSE, sep="\t", skip=2L, fill=TRUE
  , strip.white=TRUE, blank.lines.skip=TRUE)
27 data <- data.orig
28 data[1]<-round(data[1]*freq)
29 data<-data[-5]
30 data<-data[-4]
31 data<-data[-2]
32 data
33
34 for(i in 1:nrow(data)){
35 if(data[i,1]>W){
36 data[i,1] <- W
37 } else {}
38 }
39 data
40

```

```

41 fulldata <- c()
42 LL <- nrow(data[1])
43
44 for(i in 1:LL){
45   L <- data[i,1]
46   V <- data[i,2]
47   L
48   V
49   fulldata.t <- c()
50   n <- 1
51   while(n < (L+1)){
52     n.temp <- n
53     fulldata.t[n.temp] <- V
54     n <- n + 1
55   }
56   fulldata <- append(fulldata , fulldata.t)
57
58 }
59 Ltotal <- length(fulldata)
60
61 LW <- Ltotal - W
62
63 MV.M <- c()
64 MV.V <- c()
65
66 m<-1
67 while(m <(LW+1)){
68   mean.t<-c()
69   var.t<-c()
70   window <- fulldata[m:(m+W-1)]
71   mean.t <- mean(window)
72   var.t <- var(window)
73
74   MV.M[m] <- mean(window)
75   MV.V[m] <- var(window)
76   m <- m+1
77 }
78
79 name.t <- basename(files[f])
80 dir <- dirname(files[f])
81 nameL <- nchar(basename(files[f]))
82 name <- substr(name.t,1,nameL-4)
83
84 MV<-cbind(MV.M, MV.V, deparse.level = 0)
85 plot(MV[,1], MV[,2], type="l")
86
87 write.table(MV, file=paste(dir, "/", name, "_MV.txt", sep=""), row.names=FALSE, col.
  names=FALSE, sep="\t", quote=FALSE)
88
89 MVtot <- rbind(MVtot, MV, deparse.level = 0)
90 }
91 plot(MVtot[,1], MVtot[,2], type="l")

```

./Rscripts/MVanalysis.R

Acknowledgments

I would like to thank **Prof. Michael Meinecke**, my supervisor, for his outstanding guidance and for letting me work on this really cool project. Thank you for letting me follow ideas, for including me in multiple projects and collaborations and for trusting me and my decisions. Thank you for the discussions behind closed doors, behind open doors and also for having an open ear when you were already "on the hop" - but stayed to talk nonetheless. And thank you for the support in the rougher times of the years, I really appreciate that!

I would also like to thank **Prof. Claudia Steinem** and **Prof. Ralph Kehlenbach**, who were members of my thesis advisory committee, for their helpful discussions and comments during committee meetings.

I further want to thank ...

... **Alexander Benjamin Schendzielorz** not only for contributing yeast expertise and experiments to make the project even cooler, but also for the helpful discussions and for readily providing insights into yeast biochemistry.

... **Benjamin Kroppen**, **Dr. Mariam Barbot** and **Daryna Tarasenko** for the nice lab atmosphere and many nice discussions and help. Ben especially for being the best desk partner, for just being a friend and for prompting me to think of cool biophysical stuff unrelated to electrophysiology. Mari especially for sometimes intense discussions, lots of help and for showing me the ropes in the lab and the institute some years ago, and Daryna especially for stimulating discussions and for readily helping when needed.

... **Lennart Versemann** and **Meike Wiegand**, whom I supervised during their lab rotations and their bachelor resp. master thesis and who also contributed to this project.

... the **GGNB** and the **Biomolecules** program for providing a great research environment and very nice retreats with stimulating discussions.

... the **DFG** and especially the Research Unit 1905 "**PerTrans**" for financial

support.

... my parents **Tine** and **Uwe** and my sisters **Annika** and **Maike** for the trust and support and for being a great family.

... my wife **Wibke** and our kids **Maja**, **Fritz** and **Karl** for giving me something to look forward to after work, for supporting me and for always cheering me up. Wibke, danke für die Unterstützung, für den-Rücken-frei-halten, für das Zuhören und für das Antreiben. Ohne Dich wäre ich heute vieles nicht. Ehemann, Vater, Physiker, Doktor, glücklich...

... whomever I might have forgotten in this list but thinks she or he deserves acknowledgment. Thank you as well!

Curriculum Vitae

Personal

Name Niels Denkert
Data of birth 24.01.1986
Place of birth Kiel, Germany
Nationality German
E-Mail n.denkert@gmx.de

Education

- 2013 - 2017** **PhD student** at the Georg-August University, Göttingen in the "Biomolecules" doctoral program of the Göttingen Graduate School for Neurosciences and Molecular Biosciences (GGNB)
Supervisor: Prof. Dr. Michael Meinecke
Title: "Molecular Characterization of the Mitochondrial Presequence Translocase"
- 2012 - 2013** **Diploma thesis** in the "Biophysics" department of the Research-Center Borstel
Supervisor: Prof. Dr. Thomas Gutschmann
Title: "Horizontal and lateral characterization of glycolipid layers"
- 2006 - 2013** **Diploma student of Physics** at the Christian-Albrechts-University of Kiel
Major: Solid state physics. Minor: Biophysics.
- 2005 - 2006** Alternative civilian service at Johanniter e.V., Rendsburg, Germany

1996 - 2005 School education at Hebbelschule Kiel. Graduated with Abitur.

Publication List

- 2017** **Niels Denkert***, Alexander Benjamin Schendzielorz*, Mariam Barbot, Lennart Verseemann, Frank Richter, Peter Rehling and Michael Meinecke. 2017. Cation selectivity of the presequence translocase channel Tim23 is crucial for efficient protein import. *eLife* 6:e28324
- 2015** Mariam Barbot, Daniel C. Jans, Christian Schulz, **Niels Denkert**, Benjamin Kroppen, Michael Hoppert, Stefan Jakobs and Michael Meinecke. 2015. Mic10 Oligomerizes to Bend Mitochondrial Inner Membranes at Cristae Junctions. *Cell Metabolism* 21, 756–763

Conference Participations

- 2014** Poster: **Niels Denkert**, Jessica Klümper, Wolfgang Schliebs, Ralf Erdmann and Michael Meinecke. 2014. The human peroxisomal translocon contains a dynamic pore. 2014. *Open European Peroxisome Meeting*.